POWER REACTOR TECHNOLOGY

A Quarterly Technical Progress Review

Prepared for DIVISION OF TECHNICAL INFORMATION, USAEC, by
W. H. ZINN and J. R. DIETRICH, GENERAL NUCLEAR ENGINEERING CORPORATION

September 1962

VOLUME 5

NUMBER 4

TECHNICAL PROGRESS REVIEWS

To meet the needs of industry for concise summaries of current atomic developments, the Atomic Energy Commission is publishing this series, Technical Progress Reviews. Issued quarterly, each of the reviews digests and evaluates the latest findings in a specific area of nuclear technology and science.

The four journals published in this series are:

Nuclear Safety, Wm. B. Cottrell, W. H. Jordan, and associates, Oak Ridge National Laboratory

Power Reactor Technology, W. H. Zinn and J. R. Dietrich, General Nuclear Engineering Corporation

Reactor Materials, R. W. Dayton, E. M. Simons, and associates, Battelle Memorial Institute

Reactor Fuel Processing, Stephen Lawroski and associates, Chemical Engineering Division, Argonne National Laboratory

Each journal may be purchased ($2.00 per year for subscription and individual issues $0.55) from the Superintendent of Documents, U. S. Government Printing Office, Washington 25, D. C. See back cover for remittance instructions and foreign postage requirements.

Availability of Reports Cited in This Review

Unclassified AEC reports are available for inspection at AEC depository libraries and are sold by the Office of Technical Services, Department of Commerce, Washington 25, D. C. Some of the reports cited are not available owing to their preliminary nature; however, the information contained in them will eventually be made available in formal progress or topical reports.

Unclassified reports issued by other Government agencies or private organizations should be requested from the originator.

Unclassified British and Canadian reports may be inspected at AEC depository libraries. British reports are sold by the British Information Service, 45 Rockefeller Plaza, New York, N. Y.; Canadian reports (AECL series) are sold by the Scientific Document Distribution Office, Atomic Energy of Canada, Ltd., Chalk River, Ontario, Canada.

Classified U. S. and foreign reports identified in this journal as Classified may be purchased by properly cleared Access Permit Holders from the Division of Technical Information Extension, U. S. Atomic Energy Commission, P. O. Box 1001, Oak Ridge, Tenn. Such reports may be inspected at classified AEC depository libraries.

POWER REACTOR TECHNOLOGY

A REVIEW OF RECENT DEVELOPMENTS

Prepared for DIVISION OF TECHNICAL INFORMATION, USAEC,
by W. H. ZINN and J. R. DIETRICH,
GENERAL NUCLEAR ENGINEERING CORPORATION

● SEPT. 1962
● VOLUME 5
● NUMBER 4

Foreword

This quarterly review of reactor development has been prepared at the request of the Division of Technical Information of the U. S. Atomic Energy Commission. Its purpose is to assist interested organizations in the task of keeping abreast of new results in reactor technology for civilian application.

Power Reactor Technology contains reviews of selected recently published reports that are judged noteworthy, in the fields of power-reactor research and development, power-reactor applications, design practice, and operating experience. It is not meant to be a comprehensive abstract of all material published during the quarter, nor is it meant to be a treatise on any part of the subject. However, related articles are often treated together to yield reviews having some breadth of scope, and from time to time background material is added to place recent developments in perspective.

The intention is to cover the various areas of reactor development from the general viewpoint of the reactor designer rather than from the more detailed points of view of specialists in the individual areas. To whatever extent the coverage of *Power Reactor Technology* may occasionally overlap the fields of the other Technical Progress Reviews, the overlaps will be motivated by this objective of viewing current progress through the eyes of the reactor designer.

A degree of critical appraisal and some interpretation of results are often necessary to define the significance of reported work. Any such appraisals or interpretations represent only the opinions of the reviewers and the editor of *Power Reactor Technology*, who are General Nuclear Engineering Corporation personnel. Readers are urged to consult the original references in order to obtain all the background of the work reported and to obtain the interpretation of the results given by the original authors.

W. H. ZINN, President
J. R. DIETRICH, Vice President and Editor
General Nuclear Engineering Corporation

Issued quarterly by the U. S. Atomic Energy Commission. Use of funds for printing this publication approved by the Director of the Bureau of the Budget on November 1, 1960.

Contents

Section

I

Power Reactor Technology

Economics

D_2O Production Costs

A report on design studies, by Proctor and Thayer[1] of Du Pont Company's Atomic Energy Division, indicates that future large-scale D_2O production units should be capable of producing D_2O at a cost of approximately $17 per pound. As shown in Table I-1,* this is only about 60% of the current cost of production at the Savannah River facility, even though the projected costs are based on the 14% annual capital charges that are typical of the utility industry rather than on the 10% capital charges that are consistent with the current D_2O cost of $28 per pound. These estimates are particularly interesting in the light of the extensive work of Barr and Drews,[2] of Esso Research and Engineering Company, who explored some 100 alternate methods of obtaining D_2O and found none that were economically competitive with the H_2S-H_2O dual-temperature (GS) process currently in use at Savannah River Plant (SRP).

The cost of D_2O is an important factor in the cost of power from heavy-water reactors, as has been discussed previously in the September 1958 issue of *Power Reactor Technology*, Vol. 1, No. 4, pages 59 to 61, and the March 1960 issue of *Power Reactor Technology*, Vol. 3, No. 2, pages 52 to 55. The heavy-water inventory of a typical 300-Mw(e) D_2O-moderated power reactor is projected in reference 3 as about 1 ton/Mw(e). With heavy water valued at $28 per pound and treated as a nondepreciable capital investment, the capital charges (at 12.5%) and operating costs attributable directly to D_2O amount to 1.2 and 0.3 mills/kw-hr, respectively, or almost 18% of the 8.5 mills/kw-hr total cost of export power. Reducing the cost of D_2O to $17 per pound should reduce the total power cost from such a plant by 0.6 mill.[3]

As of September 1959, approximately eight of the 24 two-stage GS units at SRP were in full production, giving an annual production of 180 tons of D_2O per year. All six of the five-stage GS units at the Dana, Ind., plant were completely shut down early in 1957, and their D_2O inventory was transferred to SRP.[4] The reserve capacity of the SRP units is currently sufficient to provide D_2O for one 300-Mw(e) power reactor per year (approximately the same as in September 1959). If a continuing demand for D_2O in excess of this reserve capacity should develop, the predicted advantages of third-generation production facilities might be realized.

The recovery of tonnage quantities of D_2O from natural sources requires large-scale operations because deuterium oxide constitutes only one part in 7000 in normal water and only 20% of this deuterium is economically recoverable with the GS process.

The basic unit quantities of materials and services required by the GS process[4] are given in Table I-2.*

Although the details of the GS process have been published elsewhere,[4-7] a brief review of the process is needed for understanding of the changes recommended[1] for a third-generation facility. The GS process is a dual-temperature H_2S/H_2O exchange process that produces water containing 15 mole % D_2O using treated natural water as feed. For proper operation the gas and liquid flow rates must be precisely regulated; methods have been devised for detecting and correcting changes in gas or liquid flow[4] of the order of 0.5%.

*Table I-1 and Figs. I-1 to I-4 are reprinted here by permission from *Chemical Engineering Progress*.[1]

*Tables I-2 and I-3 are reprinted here by permission from *Chemical Engineering Progress*.[4]

Table I-1 COMPARISON OF COSTS PER POUND OF HEAVY WATER PRODUCED[1]

	Savannah River at 500 tons/year	New plants 50 tons/year	New plants 200 tons/year
Operating Costs			
Feedwater	$ 0.40	$ 0.60	$0.55
H_2S makeup gas	0.30	0.05	0.05
Total materials	$ 0.70	$ 0.65	$0.60
Salaries and operating labor	$ 1.30	$ 2.60	$1.00
Maintenance:			
Labor	$ 1.33	$ 2.45	$1.30
Materials	0.52	0.30	0.25
Total direct maintenance	$ 1.85	$ 2.75	$1.55
Utilities:			
Steam or natural gas	$ 4.35	$ 2.00	$1.85
Electric power	1.35	1.00	0.85
Cooling water	0.20	0.15	0.15
Total utilities	$ 5.90	$ 3.15	$2.85
Miscellaneous	$ 0.15	$ 0.15	$0.15
Total direct cost	$ 9.90	$ 9.30	$6.15
Administrative and general expense	3.60	3.45	1.75
Operating cost (excluding capital charges)	$13.50	$12.75	$7.90
Capital Charge (14% per Annum)			
GS process:			
Piping	$ 5.20	$ 1.70	$1.65
Towers	4.05	1.95	1.90
Heat exchangers	1.95	1.85	1.95
Structure	1.55	0.40	0.20
Instrumentation	0.85	0.75	0.55
Switchgear and control buildings	0.40		
Turbines		0.50	0.60
Other	1.40	0.40	0.40
Total	$15.40	$ 7.55	$7.25
Vacuum distillation plant	$ 0.35	$ 1.15	$0.55
Electrolytic plant	0.20		
Steam and electric power plant	2.10	0.55	0.30
Water treatment and distribution	1.00	0.60	0.35
H_2S manufacturing plant	0.15		
Gas-storage facilities and flare	0.25	0.80	0.30
General facilities	0.85	1.25	0.60
H_2S inventory at $0.50/lb delivered		0.10	0.10
Total capital charge at 14%	$20.30	$12.00	$9.45
(Capital charges at 10%)	($14.50)	($ 8.60)	($6.80)
Total Production Cost per Pound of D_2O			
Operating cost and capital charges at 14%	$33.80	$24.75	$17.35
Operating cost and capital charges at 10%	($28.00)	($21.35)	($14.70)

Table I-2 UNIT QUANTITIES OF INGREDIENTS AND SERVICES[4]

	Quantity per pound of D_2O
Treated feedwater, gal	3,500
Hydrogen sulfide, lb	0.94
Electrical energy, kw-hr	310
Process steam, lb (equivalent to 900 psi)	5,600
Cooling water, gal	12,000

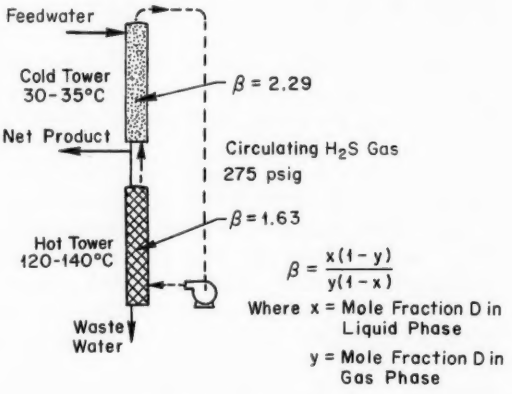

Fig. I-1 Simplified flow diagram for the GS heavy-water process.[1]

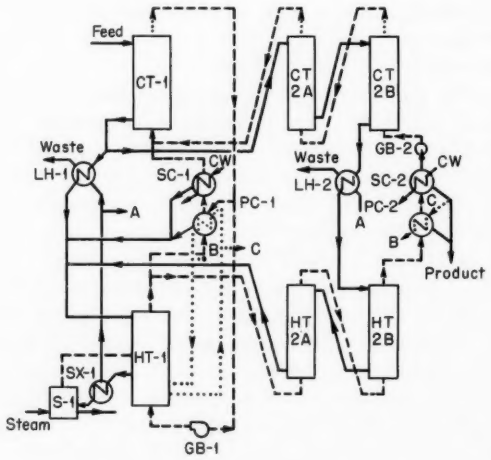

Fig. I-2 Diagram of the Savannah River GS process in commercial operation.[1] ——, liquid. - - -, gas and vapor. . . . , heat recovery. Code: CT, cold tower; HT, hot tower; LH, liquor heater; PC, primary condenser; SC, second condenser; SX, stripper exchanger; GB, gas blower; S, stripper; suffix 1 denotes first stage; suffix 2 denotes second stage.

A simplified schematic diagram of the SRP GS unit is shown in Fig. I-1, with the heat recovery systems omitted for simplicity. The two towers shown make up a "stage," and heavy water is concentrated by passing a feed stream countercurrent to a stream of hydrogen sulfide gas. The separation is based on the effect of temperature on the following reaction:

$$H_2S + HDO \underset{\text{cold}}{\overset{\text{hot}}{\rightleftharpoons}} H_2O + HDS$$

The water is enriched in deuterium while passing through the cold tower and stripped while passing through the hot tower, emerging from the hot tower at a deuterium concentration less than that in the feed stream. The product stream then becomes the feed stream for another stage; at SRP a two-stage cascade is used, and the total capacity of 500 tons/year is attained by 24 two-stage units operating in parallel. Figure I-2 shows the schematic diagram for one SRP two-stage unit. The product is about 15 mole % D_2O. Concentration to 90% is done by vacuum distillation, and an electrolytic process is used for the final concentration to 99.75% ("reactor grade"). The new facility proposed by Proctor and Thayer[1] uses a three-stage cascade with improved heat-recovery systems and employs a few very large contacting units all interconnected to form a single large production unit. A schematic of this facility is shown in Fig. I-3. In comparing Fig. I-3 with Fig. I-2, it should be noted that Fig. I-2 shows only one of 24 identical units for a 500 ton/year

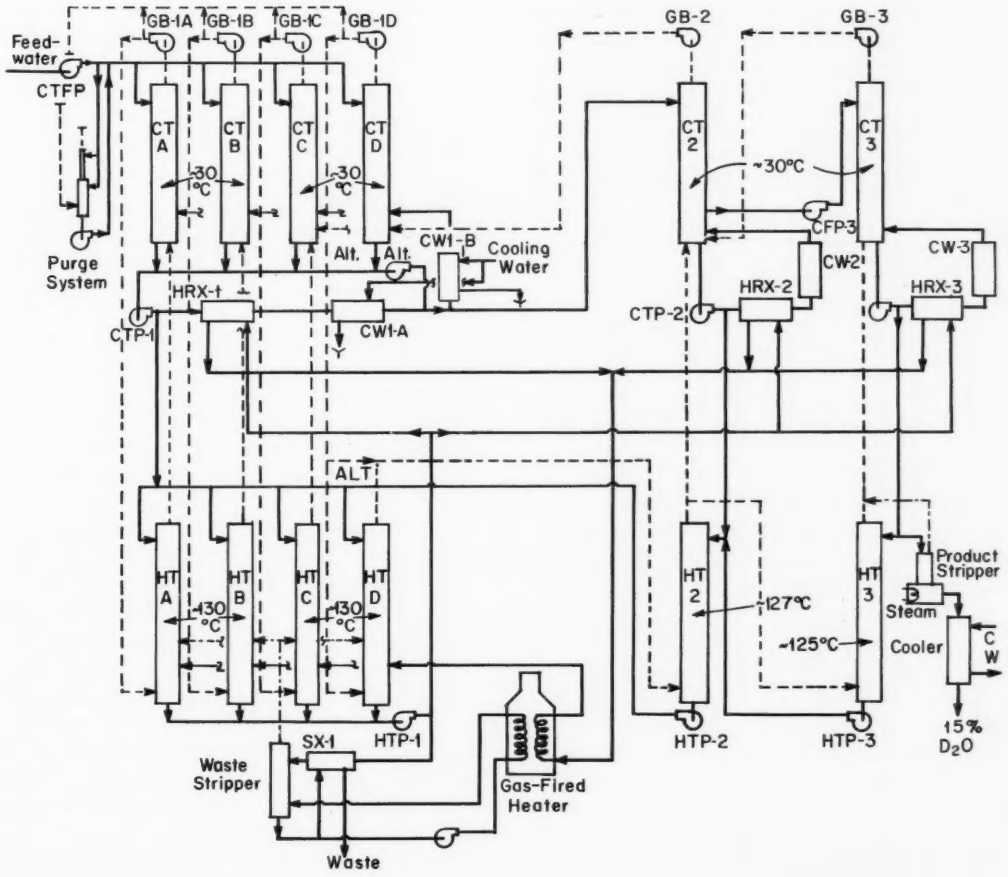

Fig. I-3 Flow diagram for a proposed 200 ton/year GS-process heavy-water unit.[1] ——, water. - - -, H_2S. —·—, steam. ALT. = alternate route.

facility, whereas Fig. I-3 shows all the contactors used in the 200-ton facility.

The specific changes proposed[1] for third-generation facilities are outlined briefly below.

1. Direct-fired natural-gas heaters are substituted for extraction steam from a coal-fired central power station as a source of process heat. With optimum plant location, this is expected to reduce the cost of process heat

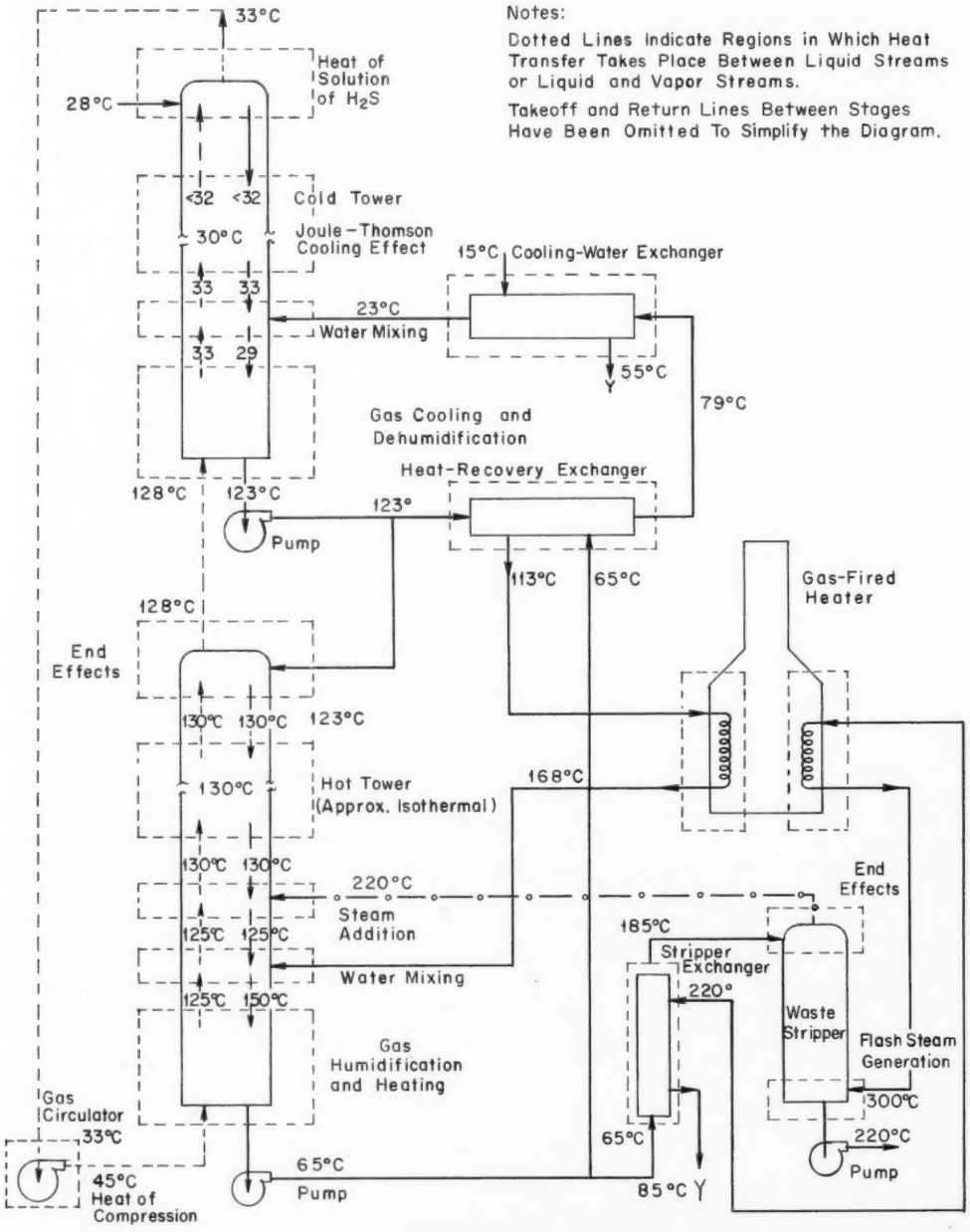

Fig. I-4 Modified heat-recovery circuit for the GS process.[1]

from $0.36 per million Btu to $0.17 to $0.21 per million Btu, exclusive of capital charges for the gas heaters which are included in process equipment. Natural gas also permits the use of gas-turbine drives on H_2S circulators with turbine exhaust gas contributing to process heating.

2. More economical heat-recovery systems are obtained in the new facility through the extensive use of direct-contact heat exchange and the substitution of liquid-liquid heat exchangers [$U = \sim 175$ pcu/(hr)(sq ft)(°C)] for gas-liquid exchangers ($U = 75$) such as PC-1, PC-2, SC-1, and SC-2 in Fig. I-2. Although the SRP GS-system heat-recovery efficiency approaches 65%, approximately 13% of the capital invested in the plant was expended on heat exchangers to obtain this efficiency, and an additional 15% was spent on associated heat-exchanger piping. The reference[1] does not attempt to identify the fraction of the overall savings attributable to the improved system but does indicate that the heat recovery achieved with the new arrangement will be about 60%. The temperature and flow diagram for the new system is shown in Fig. I-4.

3. Requirements for rail shipment limited the diameter of the first-stage SRP contacting towers to 12 ft. For the new plants, shipment by water is proposed and an upper limit of 17 ft on the diameter is used. The larger individual towers are less costly per unit of capacity, and the cost of piping is significantly reduced because the total number of towers is reduced. The use of large units is also extended to the second- and third-stage towers; the combined flow from four first-stage units is fed to a single second-stage tower.

4. Sieve-plate towers are used in the new design instead of bubble plates because they allow 15 to 20% greater throughput, 10% better plate efficiency, and 20% less pressure drop. In addition, for type 304 stainless-steel plate construction, the sieve-plate towers are estimated to be 20% less expensive than the bubble-cap towers.

5. Since the operation of the SRP and Dana plants has shown that satisfactory final product concentration can be obtained by vacuum distillation, the electrolytic refining process has been eliminated in the new plant. Similarly, separate H_2S generation facilities have been eliminated, and H_2S needed for makeup is obtained by adding sodium hydrosulfide to the feedwater. The initial 300-ton charge of H_2S would be purchased from an off-site source.

Table I-3 DANA PLANT OPERATING FORCE[4]

	Supervisory	Nonsupervisory
Operation of process facilities	50	180
Maintenance	48	357
Utilities	14	60
Technical (plant control and technical assistance)	25	38
Services (medical, patrol, accounting, transportation, etc.)	25	114
Administration	8	1
Total	170	750

6. Reduction in the number of units would reduce personnel requirements. Estimated personnel requirements are 210 for the new 200-ton plant and 115 for the 50-ton plant, of which 17 to 20% would be supervisory personnel. For comparison the staff requirements for the six five-stage units at Dana are shown[4] in Table I-3.

This analysis by Proctor and Thayer[1] is particularly interesting since its technological data and cost estimates are based on extensive operating experience at Dana and Savannah River. A further conclusion of the study,[1] that costs significantly lower than $17 per pound are not likely to be obtained without a major breakthrough in D_2O production technology, is also significant.

New Uranium Prices

On July 1, 1961, the Atomic Energy Commission announced a reduction in the price of enriched and depleted uranium to be consistent with a price reduction in natural-uranium concentrate. This was reviewed in the September 1961 issue of *Power Reactor Technology*, Vol. 4, No. 4, page 1. Another price change was recently announced by AEC and was to become effective[8,9] on July 1, 1962. This change reflects a reduction in the charge for separative work resulting from economies in operation of the gaseous diffusion plants at Oak Ridge, Paducah, and Portsmouth. The reduction in the cost of separative work was from $37 to $30 per kilogram of uranium. Table I-4 gives examples of the base charges for enriched and depleted UF_6. The decrease in enriched-uranium charges has been estimated[9] to be

worth about 0.15 to 0.20 mill/kw-hr in the cost of nuclear power.

Although the decrease in the price of enriched uranium resulting from a lower value of separative work is intuitively correct, it is not immediately obvious why the price of depleted uranium should increase. This question can be examined further in the light of the discussion presented in the December 1960 issue of *Power Reactor Technology*, Vol. 4, No. 1, pages 3 to 5. The tails assay for minimum product cost is a function of the assay of feed and the ratio of the feed and separative-work costs. As the ratio of the unit costs of feed and separative work decreases, the tails assay for minimum unit cost of the product increases; this is shown in Fig. 1, page 4 of the September 1960 issue of *Power Reactor Technology*. These ratios and the tails assay for minimum product unit cost are shown in Table I-5 for various time periods.

Table I-4 EXAMPLES OF BASE CHARGES FOR ENRICHED AND DEPLETED URANIUM AS URANIUM HEXAFLUORIDE[8]

U^{235} assay, wt.%	New charges		Previous charges,	
	$/kg of contained uranium*	$/g of contained U^{235}	$/g of contained U^{235}	
Enriched uranium				Reduction, %
90	10,808.00	12.01	13.65	12
20	2,252.00	11.26	12.74	12
10	1,062.00	10.62	11.95	11
5	479.40	9.59	10.71	10
3	254.30	8.48	9.37	10
2	146.50	7.33	8.00	8
1.5	95.30	6.35	6.84	7
1.0	47.70	4.77	4.99	4
Depleted uranium				Increase, %
0.7	22.60	3.23	3.23	0
0.6	15.35	2.56	2.47	4
0.5	8.90	1.78	1.61	10
0.4	3.70	0.93	0.75	24
0.38	3.00	0.79	0.79	0

If a user specifies a U^{235} assay between 0.38 and 0.22 wt.%, the charge will be $3 per kilogram of contained uranium. However, if the U^{235} assay is not specified by the user, AEC will supply uranium having a U^{235} assay to be determined by AEC in the range below 0.38% and will charge $2.50 per kilogram of uranium.

*Official base charges.

The cost, C_p, of material of composition x_p produced in an ideal cascade making waste of the optimum composition x_0 is as follows:[10]

$$C_p = C_E \left[(2x_p - 1) \ln \frac{x_p (1-x_0)}{x_0 (1-x_p)} + \frac{(x_p - x_0)(1-2x_0)}{x_0 (1-x_0)} \right] \quad (1)$$

This equation assigns zero cost to a product having composition x_0 equal to the waste composition; however, it is not reasonable to assign zero value to the actual depleted tails from the diffusion plants. The procedure for setting the uranium prices appears, at least approximately, to be to set a fixed base price ($2.50 or $3.00 per kilogram; see Table I-4) for uranium of nominal tails assay and to use the ideal cost (Eq. 1) as the price for all assays yielding an ideal cost higher than the base.

It has been shown[10,11] that this equation reproduces the pre-July 1961 charges for enriched and depleted uranium hexafluoride, using the data shown in Table I-5. Spot checks of the equation for the post-July 1962 charges indicate agreement within about 5%, again using the data given in Table I-5, with product enrichments of 0.5 and 90%. Examination of Eq. 1 shows qualitatively that, when x_p and x_0 are of the same order of magnitude, as they are for depleted uranium as a product, changing x_0 has a large effect on the product cost. How-

Table I-5 COST DATA FOR DIFFUSION CASCADES

Time period	Cost of feed, C_F, $/kg	Cost of separative work, C_E, $	Ratio, C_F/C_E	Approximate tails assay for minimum unit product cost, x_0, wt.%
Pre-July 1961	39.27	37.29	1.05	0.22
July 1961 – July 1962	23.50	37.29	0.63	0.28
Post-July 1962	23.50	30.00	0.78	0.25

ever, when enriched uranium is produced, the cost of the product is relatively insensitive to small changes in x_0. Another way of saying this is that relatively highly enriched uranium benefits from the reduction of the cost of separative work because a large part of its cost is due to the isotope-separation costs. Depleted uranium also benefits from the reduction of the cost of separative work, but if the cascade is optimized for minimum unit product cost, the increased separative work more than makes up for the reduction in the cost of separative work. The increased separative work comes about because the optimizing procedure results in a reduction in the tails assay.

References

1. J. F. Proctor and V. R. Thayer, Economics of Heavy Water Production, *Chem. Eng. Progr.*, 58(4): 53–61 (April 1962).
2. F. T. Barr and W. P. Drews, The Future for Cheap Heavy Water, *Chem. Eng. Progr.*, 56(3): 49–56 (March 1960).
3. L. Isakoff, Economic Potential for D_2O Power Reactors, USAEC Report DP-570, E. I. du Pont de Nemours & Co., Technical Div., February 1961.
4. W. P. Bebbington and V. R. Thayer, Production of Heavy Water, *Chem. Eng. Progr.*, 55(9): 70–78 (September 1959).
5. W. P. Bebbington et al., Production of Heavy Water, Savannah River and Dana Plants, Technical Manual, USAEC Report DP-400, Savannah River Laboratory, July 1959.
6. M. Benedict, Survey of Heavy Water Production Processes, *Proceedings of the International Conference on the Peaceful Uses of Atomic Energy, Geneva, 1955*, Vol. 8, pp. 377–405, United Nations, New York, 1956.
7. V. R. Thayer, Heavy Water Production in the U.S.A., *Nucl. Power*, 5(46): 108–111 (February 1960).
8. AEC To Revise Charges for Enriched and Depleted Uranium, AEC News Release, May 29, 1962.
9. New AEC Fuel Charge Reductions, *The Forum Memo to Members*, Atomic Industrial Forum, Inc., 9(6): 12 (June 1962).
10. M. Benedict and T. H. Pigford, *Nuclear Chemical Engineering*, p. 403, McGraw-Hill Book Company, Inc., New York, 1957.
11. H. L. Hollister and Artha Jean Burington, Pricing Enriched Uranium, *Nucleonics*, 16(1): 54–57 (January 1958).

Section

II

Power Reactor Technology

Fuel Cycles: Plutonium Recycle

In evaluations of plutonium recycle, there are two areas of interest: the conservational and the economic. The central concern of the former is how much the recycle of plutonium can extend the nuclear fuel reserves, whereas that of the latter is what effect the recycle of plutonium will have on the cost of nuclear-power generation. These two considerations are closely related, for the incentive for conservation of nuclear fuels may always be expressed in economic terms; but, whereas conservation must inherently be concerned with the long-term future, it is possible to examine the economics of a fuel cycle using the "ground rules" appropriate to any point in time which may be of interest, including the present. If one does want to evaluate the economics of plutonium recycle for the present or near future, without including the effect of an arbitrarily fixed plutonium price, one may rephrase the economic question to ask what the price of plutonium would have to be to make plutonium just competitive with U^{235} as a reactor fuel. A considerable amount of AEC-sponsored work is under way to find the answer to this question. Presumably the answer will be one factor that is taken into account in arriving at a long-term policy for plutonium pricing. One would expect that questions of longer-range economics, or conservation, would also play an important part in determining such a policy. In any event the studies of the relative worth of plutonium as a reactor fuel can establish the basic technical relations, and illuminate many of the subtleties, of the complex subject of plutonium recycle.

It is an elementary observation that no single number can express the value of plutonium in different specific applications. Plutonium comes in a range of isotopic mixtures, and the value (positive or negative) of each isotope will vary with the reactor type and with the characteristics of individual reactors of each type. An interesting and recently issued report[1] of analytical work at Hanford covers physics studies of plutonium values in five reactors of different types. Although a comprehensive summary of the report cannot be given here because of the complexity of the subject and because of the many technical choices and approximations that were necessary with respect to reactor characteristics, cross sections, and related quantities, it is nevertheless worthwhile to note some of the results.

The reactors considered are an advanced pressurized-water reactor, a boiling-water reactor, an organic-moderated reactor, a pressure-tube heavy-water reactor, and a gas-cooled graphite-moderated reactor. The characteristics of these were not selected to be optimum for plutonium recycle but, rather, to be representative of current or slightly advanced design practice. The pressurized-water reactor, for example, is based on the design developed in the Combustion Engineering–Stone and Webster study[2] of advanced pressurized-water reactors; the gas-cooled reactor is of the Bradwell type, and the D_2O-reactor characteristics are based on those of the Plutonium Recycle Test Reactor (PRTR).

The central objective of the study[1] was to arrive at plutonium values for each reactor; the plutonium value is defined as the price of plutonium that would cause the net reactor fuel cost to be independent of whether the plutonium were recycled or sold. The reference points out that this value can be a function of many factors, such as fuel exposure between recycles, and control-rod limits. In the study a definite and significant point for the evaluation was therefore found by determining, for each case, the enrichment (and resulting exposure) that would yield the lowest fuel cost. The evalu-

Table II-1 PLUTONIUM VALUES AND RECYCLE STEPS COMPUTED BY MELEAGER CHAIN* FOR THE SIMULATED APWR-II (BATCH) REACTOR[1]

Step No.	Exposure, Mwd/ton	Initial enrichments, weight fraction		Weight fraction of total plutonium				Fuel cost, mills/kw(e)-hr	Plutonium values	
		Total	Uranium	Pu^{239}	Pu^{240}	Pu^{241}	Pu^{242}		$/g, fissile	$/g, total
1	14,070	0.0304	0.0304	0	0	0	0	2.56		
2	14,938	0.0313	0.0276	0.707	0.181	0.094	0.018	2.56	12.30	9.90
3	14,947	0.0316	0.0265	0.600	0.209	0.136	0.055	2.56	11.60	8.50
4†	15,600	0.0325	0.0269	0.549	0.212	0.148	0.091	2.56	11.30	7.90
5†	16,546	0.0336	0.0277	0.520	0.208	0.151	0.121	2.56	10.90	7.30
6†	16,722	0.0339	0.0279	0.502	0.201	0.150	0.147	2.56	9.90	6.50

*MELEAGER CHAIN is the name of the computer code used[3] (IBM-7090).

†The plutonium discharged at the end of any given cycle has some value that can be determined only by its performance in succeeding cycles; hence the fuel cost and the plutonium value in any given cycle can be determined, rigorously, only by extending the calculation to succeeding cycles until equilibrium is reached. Reference 1 employs a method by which adequate accuracy is attained by extending the calculation for only a few cycles beyond the cycle of interest. The calculations of cycles 4, 5, and 6, above, served this purpose of defining the "plutonium credit" for the earlier cycles. The authors[1] point out that the results for cycles 4, 5, and 6 should therefore not be considered to have significance; they are included only to give a comprehensive picture of the computational scheme. — *The Editor*

Table II-2 CASES ANALYZED FOR PLUTONIUM VALUE STUDY[1]

Reactor* run identification	Refueling strategy		Pu zoned	Interest rate, %		Remarks
	Batch	Graded		4.75	12.5	
APWR-I†	X			X		Initial Pu prices estimated
APWR-II	X			X		Improved Pu prices from APWR-I
APWR-III	X				X	
APWR-IV	X		X	X		Extra process costs with Pu enrichment = $30/lb of U
BWR-I	X			X		
BWR graded		X		X		
D_2O	X				X	
D_2O graded		X		X		
GCR	X			X		
OMR	X			X		
OMR prime	X			X		

*APWR = advanced pressurized-water reactor; BWR = boiling-water reactor; D_2O = heavy-water reactor; GCR = gas-cooled reactor; OMR = organic-moderated reactor.

†Since the plutonium discharged at the end of any irradiation step has a value that is determined by its economic performance in subsequent steps, the results of any given step cannot be calculated independently. The results for a series of steps, such as those shown in Table II-1, must be arrived at by an iteration process that converges on a consistent set of values. The significance of APWR-I case is that it did not have the benefit of this reiteration: the calculated recycle values of plutonium at each step depended on estimates of plutonium product values in subsequent steps. All other cases listed in this table were calculated by the iterative procedure.

ation was then made at or near that enrichment value.

For the case in which a reactor is initially fueled with uranium, and plutonium is recycled in successive fuel-reload batches, the value of the plutonium will decrease with each successive recycle as the content of nonfissionable plutonium isotopes (240 and 242) builds up. The value should approach a constant level after many recycles, as the isotopic composition approaches an equilibrium. The Pu^{240}, a fertile isotope which in some respects is superior to U^{238}, does not degrade the value of the fissile isotopes of plutonium with which it is mixed, but it does, of course, lower the value of the total plutonium mixture because it dilutes the content

Table II-3 REACTOR CHARACTERISTICS AND CALCULATED PLUTONIUM VALUES FOR SEVERAL CASES[1]

[Inventory Charge Is 4.75% per Year in All Cases; Fuel Fabrication Cost Is $40 per Pound of Uranium in All Cases (No Extra Charges for Plutonium Fabrication)]

	D_2O graded	D_2O batch	GCR batch	BWR graded	BWR batch	APWR-II batch	OMR batch
Cladding material	Zircaloy	Zircaloy	Magnox	Zircaloy	Zircaloy	Stainless steel	Aluminum
Effective nonfuel absorption cross section per unit fuel volume	0.020	0.020	0.038	0.029	0.029	0.096	0.075
Effective slowing down power per unit fuel volume	2.17	2.17	5.06	2.113	2.113	2.88	2.113
Spectral index (r) at beginning of first step*	0.14	0.14	0.04	0.17	0.17	0.15	0.24
Spectral index (r) at end of fifth step*	0.20	0.20	0.05	0.27	0.27	0.20	0.38
Effective neutron temperature, °C	127	127	600	470	470	450	450
α (Pu^{239}):							
At beginning of first step	0.525	0.525	0.595	0.581	0.581	0.580	0.587
At end of fifth step	0.523	0.523	0.582	0.570	0.570	0.566	0.577
α (Pu^{241}) (for all steps)	0.376	0.376	0.376	0.376	0.376	0.376	0.376
Fuel cost, mills/kw-hr	1.41	1.96	2.17	1.90	2.09	2.56	2.53
Fuel enrichments, %:							
First step, total and U^{235}	1.33	1.48	1.65	1.63	2.18	3.04	3.15
Second step, total	1.44	1.63	1.58	1.84	2.32	3.13	3.37
Second step, U^{235}	1.04	1.27	1.41	1.40	1.86	2.76	2.87
Third step, total	1.45	1.71	1.65	1.99	2.42	3.16	3.56
Third step, U^{235}	0.99	1.26	1.45	1.39	1.78	2.65	2.82
Fuel exposure, Mwd/ton:							
First step	16,804	11,490	12,115	12,330	13,526	14,070	13,535
Second step	17,993	12,955	11,613	14,275	14,882	14,938	14,985
Third step	16,883	13,635	12,541	15,564	15,439	14,947	15,923
Plutonium values, $/g:							
Second step, fissile	9.30	11.90	11.50	11.40	12.40	12.30	11.80
Second step, total	6.40	9.10	6.70	8.80	9.80	9.90	10.00
Third step, fissile	7.70	11.20	13.20	9.70	11.20	11.60	10.60
Third step, total	4.60	7.30	6.30	7.00	8.40	8.50	8.60

*The first step is the initial operation, with only U^{235} initially present as fissionable isotope; the second step is the first plutonium recycle, etc. Compare Table II-1.

of fissile isotope. Since Pu^{240} has a rather high absorption cross section, in both the thermal and resonance energy regions, its concentration in the plutonium mixture usually approaches an equilibrium value after one or two recycles. The Pu^{242} is not fertile: it acts as a parasitic absorber and degrades the value of both the plutonium mixture and the fissile isotopes. Its cross section is relatively small, and its concentration approaches equilibrium only slowly unless there is some external loss as, for example, through fuel-processing losses.* As secondary effects of these changes, the total enrichment value for minimum fuel cost and the corresponding fuel batch exposure change from one recycle step to the next but not greatly. These characteristics are illustrated in Table II-1, which gives the calculated results for six successive recycle steps in the simulated advanced pressurized-water reactor (APWR) when it is operated with a single-batch reloading scheme.

Variations in operating and economic conditions were investigated with some of the reactors. These included variations in refueling strategy, which covered single-batch reloading and graded irradiation (continuous reloading); the zoning of plutonium to reduce the number of plutonium-containing fuel elements in the reactor; a variation in the interest rate on fuel in inventory; and a variation in the cost of producing plutonium-bearing fuel elements. The variations investigated for the different reac-

*In reference 1 the losses assumed were 3% per recycle for all isotopes except Pu^{241}; for the latter the effective loss was increased to 8% to account for radioactive decay.

tors are indicated in Table II-2. Table II-3 lists some of the important reactor-physics characteristics of the reactors and gives the calculated plutonium values, for the first and second recycles (e.g., steps 2 and 3 of Table II-1), in several of the more interesting cases. The analysis showed that, for all reactors except the gas-cooled reactor, the value of plutonium, in dollars per gram of fissile isotope, decreased approximately linearly with the Pu^{242} content; the rate of decrease varied, however, from reactor to reactor. Table II-4 shows the values of the constants A_0 and A_1 for the various cases when the plutonium value X is represented by an empirical equation of the form: $X = A_0 + A_1 p_{42}$ dollars per gram of fissile isotope, where p_{42} is the Pu^{242} content, in grams of Pu^{242} per gram of plutonium.

The analysis showed that the plutonium values (and, of course, the fuel costs) are highest in the fuel cycles employing single-batch reloading. The plutonium values were relatively insensitive to the interest rate on the fuel in inventory. The effect of an assumed additional fabrication cost of plutonium-bearing elements (above that of uranium elements) is shown in Table II-5. Note that this table applies to a zoned case in which only a fraction of the fuel elements contain recycled plutonium. The plutonium is used to enrich uranium that has a U^{235} content equal to the diffusion-plant tails assay; with this approach only about 20% of the fuel elements contain recycled plutonium.

Table II-4 COEFFICIENTS FOR THE EMPIRICAL EQUATIONS* THAT RELATE PLUTONIUM VALUE TO Pu^{242} CONTENT IN THE SIMULATED REACTORS[1]

Reactor	A_0	A_1	A_2
APWR-I	12.65	−16.7	
APWR-III	11.44	−40.3	
APWR-IV	10.32	−10.1	
OMR	8.31	−103.5	
GCR†	10	56.7	(−275.1)
BWR	13.27	−31.5	
D_2O-I	11.05	−22.5	
D_2O-II	12.43	−19.9	
D_2O graded	10.23	−14.4	
BWR graded	13.54	−55.0	

* Empirical equation of the form $X = A_0 + A_1 p_{42}$, where X is the plutonium value, in dollars per gram (fissile), and p_{42} is the Pu^{242} content, in grams of Pu^{242} per gram of plutonium.

† Second-order equation of the form $X = A_0 + A_1 p_{42} + A_2 p_{42}$ was necessary for this reactor.

Table II-5 COMPUTED PLUTONIUM VALUES SHOWING EFFECT OF EXTRA PROCESSING COSTS* WITH PLUTONIUM ENRICHMENT FOR A ZONED BATCH CYCLE IN SIMULATED APWR REACTOR[1]

Cumulative exposure of recycled fuel, Mwd/ton	Plutonium values, $/g (fissile)	
	No extra processing costs	Extra processing costs
15,000	12.30	9.85
30,000	11.60	10.00
45,000	11.30	9.50†

* Feed use charge is 4.75%. Fabrication charge is $40 per pound of uranium plus extra processing costs, if any; the extra cost for plutonium-bearing fuel is taken as $30 per pound of uranium. For any given cumulative exposure, plutonium compositions are essentially unaffected by change in processing cost.

†Reference 1 contained a typographical error in these figures; it has been corrected here by a private communication from the authors.

The value computed for plutonium is, of course, directly dependent on the uranium price scale used. The scale used in the study is that which was in effect from July 1, 1961, to July 1, 1962. The reference[1] points out that, if the uranium price scale is changed, the plutonium values should change in proportion to the price of fully enriched U^{235}, not in proportion to the price of the U^{235} that the plutonium replaces in a partially enriched fuel. It is stated[1] that this dependence has been confirmed by a general analysis.

It is worthwhile to examine those results of the analysis which have a bearing on the efficiency of utilization of the original fissile isotope (U^{235}); this is a basic factor in any consideration of the rate at which the high-quality nuclear fuel reserves might be depleted by a large-scale nuclear-power industry. In making such an examination, it is important to remember that the objective of the analysis[1] was to determine plutonium values in reactors representative of current practice; it was not to determine the efficiency of fuel utilization. An optimization of either the reactors or their fuel cycles for maximum fuel utilization would not have been consistent with the objective. Consequently, the results should not be considered indicative of potential efficiencies of utilization, but, rather, they are more representative of the fuel utilizations that might characterize reactors of current or slightly advanced types,

with plutonium recycle, when their designs and operating characteristics are determined by current economic pressures.

Table II-6* gives, for each successive cycle in the various reactors, the energy produced per gram of U^{235} destroyed in the reactor. If pure U^{235} produced all the energy, the energy production per gram of U^{235} destroyed (by fission and neutron capture) would be about 0.8 Mwd. The amounts by which the values in Table II-6 exceed this value of 0.8 Mwd/g represent the amount of additional energy produced by the fission of plutonium. In step 1 the additional energy is produced by fissioning of the plutonium *in situ* in the reactor, before any recycling is done. The amount of extra energy produced increases in the next few steps, as more and more plutonium builds up and is recycled. Eventually an equilibrium will be approached, in which the amount and composition of recycled material remains constant from step to step, and the energy production per gram of U^{235} destroyed becomes constant. This value represents the maximum utilization of the natural fissile isotope (U^{235}) that will be attained with the reactor and the recycling schedule under consideration. It appears from Table II-6 that, for practical purposes, this equilibrium value of utilization may be considered to be reached after the third or fourth recycle (steps 4 or 5). It may be seen from the table that with plutonium recycle the amount of energy obtained per gram of U^{235} is higher than that which would result from the "burning" of pure U^{235} by a factor that ranges from about 1.8 (= 1.46/0.8) for the APWR to slightly more than 3 (= 2.4+/0.8) for the D_2O and boiling-H_2O reactors.

In the computations discussed to this point, the fuel enrichment used has always been that which yields minimum fuel cost. The fuel-cost minimum results from a balance of several opposing factors. As enrichment is increased, the fuel exposure per cycle increases and the fuel-cost components due to processing and fabrication costs decrease. Roughly, it may be said that, as enrichment is increased, the minimum fuel cost occurs when the effects of these cost reductions are just balanced by the increases in net burnup and inventory costs which accompany the enrichment increase. The fuel enrichment that yields the maximum utilization of fissile isotope is determined by different factors and may be quite different from that which yields minimum fuel cost. The longer exposure resulting from higher enrichment reduces, of course, the effect of processing losses. Most of the reactor physics effects tend to decrease the utilization as enrichment is increased (in reactors with fixed fuel and moderator lattices, as are considered here). The two major effects are the increase, with enrichment, of the average fission-product burden in the reactor and the "hardening" of the neutron spectrum. The result of these factors appears to be that, with "equilibrum" plutonium recycle, the utilization is either relatively insensitive to enrichment or, in most cases, decreases steadily as the enrichment is increased (Table II-7). If pluto-

Table II-6* MEGAWATT-DAYS PER GRAM OF U^{235} DESTROYED†

Step No.	APWR simulation‡ I (batch)	APWR simulation‡ II (batch)	APWR simulation‡ III (batch)	APWR simulation‡ IV (batch)	D_2O simulation‡ I (batch)	D_2O simulation‡ II (batch)	D_2O simulation‡ III (graded)	BWR simulation Batch	BWR simulation Graded	OMR simulation (batch)	GCR simulation (batch)
1	1.07	1.06	1.05	1.06	1.28	1.30	1.65	1.25	1.39	1.05	1.21
2	1.31	1.31	1.30	1.31	1.80	1.78	2.39	1.76	2.04	1.33	1.45
3	1.40	1.41	1.41	1.41	1.99	1.95	2.45	1.98	2.29	1.47	1.50
4	1.44	1.44	1.47	1.45	2.02	2.00	2.48	2.07	2.39	1.55	1.51
5	1.47	1.46	1.49	1.45	2.02	1.98	2.43	2.14	2.42	1.53	1.50
6		1.46	1.49	1.46	2.07	1.97	2.44	2.15	2.44		1.52

*The material in this table is from the analyses reported in reference 1, but some of the material does not appear in the reference. The table was furnished by E. A. Eschbach.

†Note that this refers to destruction of U^{235}, including the formation of U^{236}. This is approximately 20% less than the formulation per gram of U^{235} fissioned.

‡The Roman numerals refer to the various cases specified in Table II-2.

*We are indebted to E. A. Eschbach for Tables II-6 and II-7. — *The Editor*

Table II-7* VARIATION OF MEGAWATT-DAYS PER GRAM OF U^{235} DESTROYED AND FUEL COST WITH ENRICHMENT

(Exposure Increasing with Enrichment)

Enrichment level	APWR-I (batch)				D_2O-I (graded)				BWR (graded)			
	First step with no plutonium feed		Fourth step		First step with no plutonium feed		Fourth step		First step with no plutonium feed		Fourth step	
	Mwd/g of U^{235} destroyed	Fuel cost, mills/kw-hr	Mwd/g of U^{235} destroyed	Fuel cost, mills/kw-hr	Mwd/g of U^{235} destroyed	Fuel cost, mills/kw-hr	Mwd/g of U^{235} destroyed	Fuel cost, mills/kw-hr	Mwd/g of U^{235} destroyed	Fuel cost, mills/kw-hr	Mwd/g of U^{235} destroyed	Fuel cost, mills/kw-hr
Low (0.7115–2%)	0	0	0	0	1.07	4.60	2.49	3.57	1.10	4.07	2.63	2.45
↓	0.99	3.61	1.57	3.62	1.24	2.74	2.44	1.48	1.26	2.26	2.34	1.83
to	1.05	2.71	1.51	2.83	1.61	1.51	2.43	1.49	1.51	1.59	2.24	1.62
↓	1.08	2.49	1.45	2.55	1.74	1.38	2.54	1.69	1.70	1.50	2.17	1.71
	1.08	2.49	1.40	2.44	1.88	1.36			1.79	1.57	1.81	2.05
High (3–5%)	1.09	2.50	1.32	2.46	2.13	1.49			1.85	1.63	1.42	2.63

*The material in this table is from the analyses reported in reference 1, but it does not appear explicitly in the reference. The table was furnished by E. A. Eschbach.

nium is not recycled, increasing enrichment, of course, yields higher values of energy production per gram of U^{235} destroyed, for increasing amounts of plutonium are "burned" *in situ*. In these cases, however, the energy production per gram of U^{235} destroyed, although significant in other respects, is not a measure of the basic utilization of fissile isotope, for the fuel cycle is "open" on both ends: U^{235} is fed into the cycle, and plutonium flows out. In such a situation a more appropriate indicator of the utilization might be the energy production per net gram of fissile isotope (U^{235} + Pu^{239} + Pu^{241}) destroyed, but the whole question of utilization is poorly defined unless one specifies an energy-producing role for the plutonium outflow.

Table II-7 illustrates the points discussed above. It shows, for three different reactor cases, the changes in fuel cost, and in energy production per gram of U^{235} destroyed, as enrichment is increased. The enrichment values are not given explicitly because the three different reactor types operate in different ranges, but for each type the enrichment increases from top to bottom of the table. The columns for the first step may be considered to apply either to the first step in a self-contained recycle program or to the typical case in a nonrecycle program. The columns for the fourth step are representative of the equilibrium recycle condition.

References

1. E. A. Eschbach et al., Fuel Cycle Analysis for Successive Plutonium Recycle. I. Results for Five Reactor Concepts, USAEC Report HW-72217, Hanford Atomic Products Operation, February 1962.
2. Stone and Webster Engineering Corp. and Combustion Engineering, Inc., Advanced Pressurized Water Reactor Study (Parts 1–3), USAEC Report TID-8502, April 1959.
3. J. R. Triplett and G. J. Busselman, MELEAGER—A Burnup Code for Fuel Cycle Analysis, USAEC Report HW-68100, Hanford Atomic Products Operation, March 1961.

Section

III

Power Reactor Technology

Reactor Physics

Critical and Exponential Experiments

The results of material buckling measurements at Hanford on uranium-graphite lattices during the past 10 years are summarized in reference 1. Included is a tabulation of more than 300 material buckling measurements and their results. The tabulation is organized on the basis of the following experimental parameters: fuel-slug diameters that varied from 0.925 to 2.5 in.; lattice spacings that varied from $4^{3}/_{16}$ to 15 in.; fuel-element geometries that covered solid rods and two concentric-tube arrangements; fuel enrichments that varied from natural to 1.44% enriched uranium (also given are a few measurements on fully enriched uranium–aluminum alloys); and coolants and coolant fractions that covered air, light water, and monoisopropylbiphenyl as coolants. The exponential piles used ranged, in cross-section size, from a square 4 by 4 ft to a rectangle 8 by 10 ft and, in height, from 7 to 10 ft.

To better define nuclear safety limits in the preparation and processing of reactor fuels, the Physical Constants Testing Reactor (PCTR) at Hanford Atomic Products Operation (HAPO) was used to perform experiments[2] in which the minimum critical U^{235} enrichment in a homogeneous system of H_2O and UO_3 was determined. The experiments consisted of measurements of k_∞ for systems with U^{235} enrichments of 1.006, 1.070, and 1.159 wt.% and hydrogen-to-uranium atomic ratios ranging from 3.5 to 7.5. The experiments were performed by placing the sample mixture, surrounded by an intermediate "buffer" region of the same composition as the sample, in the central cavity of the PCTR. The buffer region was used to provide an equilibrium neutron spectrum (incident on the test sample) which would have the same characteristics as those of the spectrum in an infinite medium of the sample composition. The minimum weight percent enrichment of U^{235} necessary to produce criticality in an infinite UO_2-water mixture was found to be $1.034\ ^{+0.010}_{-0.009}$.

The PCTR was also used to perform experiments[3] in which infinite multiplication factors were determined for hydrogenous systems containing UO_3 and $UO_2(NO_3)_2$ with a uranium enrichment of 3.04 wt.% U^{235}. The UO_3 systems had hydrogen-to-uranium atomic ratios varying between 3.58 and 47.98, whereas the $UO_2(NO_3)_2$ experiments were performed for hydrogen-to-uranium atomic ratios from 6.10 to 31.00. Both water and polyethylene were used as moderators. Solubility considerations limited the possible hydrogen-to-uranium ratios when pure water was used as the moderator, whereas polyethylene could be prepared to make possible any desired ratio. For all systems except those with very high hydrogen-to-uranium ratios, neutron absorber in the form of borated polyethylene was added to the systems to reduce the k_∞ to unity. Calculational methods were then used to determine the unpoisoned values of k_∞.

Reference 4 contains a review of the critical experiments and zero-power tests (conducted at the Martin Critical Experiments Facility) which were performed to provide data in support of, and to confirm the final design of, the Portable Medium-Power Plant No. 1 (PM-1). The experiments were performed on cylindrical, light-water-moderated cores that contained fully enriched tubular fuel elements made of a cermet of uranium dioxide and stainless steel. Also in these cores were various configurations of boron–stainless steel, lumped poison rods. Further reactor control was provided by movable

Y-shaped control rods that contained a cermet of europium oxide and stainless steel.

The PM-1 critical program was composed of the following five sets of experiments:

1. The determination of minimum critical geometry and a limited investigation of the effects of lumped poison rods
2. A detailed investigation of the effects of lumped poison rods in the proposed core design (in this set of experiments, criticality, rod worths, temperature coefficients, and flux and power distributions were investigated as functions of boron concentration in the lumped poison rods)
3. An investigation of "stuck"-control-rod and lifetime conditions
4. A detailed study of a revised core design, wherein measurements similar to those in item 2 were made
5. The investigation of miscellaneous features such as reactivity evaluation of thermal shields, partial-core subcritical measurements, and self-shielding effects in lumped poison rods

A discussion and the results of the analyses performed in conjunction with the experimental program are also included.

Reference 5 contains a progress review of the experimental and theoretical physics programs that constitute the study of heavy-water-moderated, partially enriched uranium metal lattices being conducted at the Massachusetts Institute of Technology (MIT). The experiments were performed on a subcritical assembly wherein the thermal column of the research reactor MITR was used as a plane source of neutrons. The first lattice investigated contained cylindrical rods of natural-uranium metal which were 1.010 ± 0.005 in. in diameter and 60 in. long. The fuel rods were canned in type 1100 aluminum tubes with a 0.028-in. wall thickness and an 0.008-in. radial air gap between the fuel and cladding. The experiments included measurements of the following parameters: δ_{28}, the ratio of fissions in U^{238} to those in U^{235}; δ_{25}, the ratio of epicadmium absorptions in U^{235} to subcadmium absorptions in U^{235}; the U^{238} cadmium ratio; the conversion ratio, i.e., the ratio of U^{238} captures to U^{235} fissions; the effective resonance integral; and the fast flux, i.e., the flux of neutrons with energies greater than the fission threshold of U^{238}.

The exponential assembly at the Savannah River Laboratory (SRL) was used to perform experiments[6] wherein nuclear parameters were determined for a heavy-water-moderated lattice of unclad uranium rods, 3 in. in diameter and enriched to 3.0 wt.% U^{235}. A triangular lattice with an 18-in. pitch, giving a moderator-to-uranium volume ratio of 36.68, was used. Experimental values of k_∞, the infinite multiplication constant, were inferred from the results of measurements that led to determinations of f, η, ϵ, and p—the parameters used to calculate k_∞ by means of the four-factor formula. The same nuclear parameters that had been experimentally determined were calculated by means of the THERMOS IBM-704 code, and a comparison between the analytical and experimental results is included as part of the concluding discussion in the reference.

The experimental studies, performed in the Zero Power Reactor Facility No. 7 (ZPR-VII), which were conducted as a part of the THUD (thorium, uranium, and deuterium) program are reviewed in reference 7. The fuel elements used in these experiments were composed of ceramic ThO_2-$U^{235}O_2$ pellets (nominal diameter, 0.587 cm) clad in aluminum tubes (inside diameter, 0.610 cm; outside diameter, 0.787 cm). The fuel pellets most often used had a thorium-to-U^{235} atomic ratio of 25, although pellets having a ratio of 50 were also available in order to facilitate a variation of the U^{235} content in the cores. Three different lattice arrays, all of which used D_2O as the moderator, were investigated: uniformly distributed rods, patterns of rods compatible with Experimental Boiling-Water Reactor (EBWR) geometry, and clusters of rods wherein the clusters were surrounded by D_2O, H_2O, and air. The most commonly determined nuclear parameters were ϵ, η, p, f, L^2, τ, λ_H, and λ_R. Since a variation of the heavy-water purity occurred during the course of the experiments, the interpretation of the experimental data was somewhat complicated, and no analysis of the results is presented in this report. It is noted, however, that these analyses will be given in a subsequent report.

Previous issues of *Power Reactor Technology* (Vol. 4, No. 4, page 12, and Vol. 5, No. 1, page 5) have called attention to a number of critical and exponential experiments conducted in support of the Spectral Shift Control Reactor (SSCR) basic physics program. These experi-

ments were performed in order to study the nuclear properties of D_2O-H_2O-moderated lattices. The fuel elements used were stainless-steel-clad UO_2 rods of 4 wt.% U^{235} enrichment and aluminum-clad UO_2-ThO_2 rods that had uranium of 93% enrichment (thorium-to-U^{235} atomic ratio of 15). Computational methods that were applicable to SSCR type cores were developed concurrently with the performance of the experiments. The calculated and measured data were to be compared to determine the validity of the analytical model. Progress reports on the theoretical and experimental phases of the program have been issued quarterly.

Reference 8 contains a summary of the results of the critical experiments performed during the course of the SSCR program. Nine different assemblies were studied, and they had moderator mixtures of light and heavy water ranging from 0 to 81.2 mole % D_2O. The majority of the experiments were performed in assemblies containing fuel rods of 4 wt.% U^{235}-enriched UO_2 (fuel diameter, 0.444 in.) which were swaged in stainless steel (outside diameter, 0.4755 in.; wall thickness, 0.0160 in.). The square lattice had a pitch of 0.595 in. and a nonmoderator-to-moderator volume ratio of approximately 1. The critical mass, critical D_2O concentration, buckling, reflector savings, thermal disadvantage factor, cadmium ratios of U^{235} and U^{238}, and epithermal neutron spectrum were measured for a number of different mole concentrations of D_2O in the moderator. In a second set of experiments, boric acid was added to the moderator to determine its effect on the infinite multiplication factor and thus to define better the leakage characteristics of the poisoned as well as the unpoisoned assemblies.

As another phase of the SSCR basic physics program, exponential experiments[9] at elevated moderator temperatures were also performed, using the fuel rods of 4 wt.% U^{235}-enriched UO_2 which were swaged in stainless steel. The lattice spacing and nonmoderator-to-moderator volume ratio were very nearly the same as those for the cold, clean criticals described in reference 8. The exponentials were used to determine the material bucklings for two assemblies: one had no D_2O in the moderator, and the other had 81.5 mole % D_2O in the moderator. The material bucklings were determined, and these are presented in reference 9 as functions of assembly temperature over the range 70 to 400° F.

Reference 10 is an analysis of the experimental data from the SSCR program, the critical and hot exponential parts of which are presented in references 8 and 9, respectively. The computational method, developed to analyze SSCR type assemblies, utilizes the Greuling-Goertzel approximation to describe the neutron slowing-down process in the H_2O-D_2O moderator. The multigroup nuclear parameters for the various compositions were calculated using this slowing-down model as a part of the BPG code. A neutron-balance procedure was then used to generate four-group diffusion-theory input parameters for standard one- or two-dimensional diffusion equation codes. The results of these analyses were correlated and compared to the results determined from the experimental programs. The comparison was good over the range of the parameters measured in the experiments; hence it was concluded that the analytical model was valid for the analysis of cores of the SSCR type.

The Process Development Pile at SRL was used to obtain measurements[11] of the D_2O-coolant void coefficient for fuel elements made up of four concentric natural-uranium metal tubes. These measurements were performed to verify earlier calculations and exponential experiments, which had shown that the nested, or multitube, elements under consideration for a boiling-D_2O-cooled reactor exhibited strong positive void coefficients of reactivity. The fuel assemblies used in the experiments contained four uranium metal tubes with outside diameters ranging from 1.06 to 3.08 in. and wall thicknesses of approximately $\frac{1}{8}$ in. The D_2O-coolant annuli were approximately 0.3 in. thick. Aluminum was used for the cladding around the outside of each uranium metal tube as well as for the insulation and pressure tubes that surrounded each assembly. The triangular lattice pitch between fuel elements was 9.33 in., center to center. These measurements indicated that the removal of all the D_2O coolant from the coolant annuli would result in a 2.8% increase in the infinite multiplication factor of the lattice.

Reference 12 is, in part, a quarterly review of the experiments conducted by the Nuclear Division of the Martin Company in support of the design effort of the PM reactor program and, in particular, the PM type core. The

reference contains data from reactivity measurements and fine flux distributions in central cells and through fuel-tube walls. The cores investigated contained lumped poison in the form of 0.3-, 0.4-, and 0.5-in.-diameter rods with 0, 0.27, 0.52, and 0.84 wt.% natural boron. The PM type lattice is a repeating array of cells, each containing six fuel tubes and one lumped poison rod, on a triangular pitch. The unpoisoned lattices for these experiments were made up of 37 cells, whereas all the poisoned lattices were made up of 61 cells.

Long-Term Reactivity Changes in Thorium

The results of a program for investigating the long-term reactivity changes in irradiated thorium are reported in reference 13. The procedure involved the irradiation of thorium samples in the NRX reactor to various levels of exposure and the measurement of the reactivity effect of the higher isotopes produced by means of oscillator or "train" measurements in the GLEEP reactor. The net effect of the isotope buildup was to reduce the apparent absorption cross sections of the samples in the GLEEP reactor. Analysis of the experiments consisted of an attempt to reproduce theoretically the apparent change in absorption by using basic data on the cross sections and neutron yields of the isotopes involved coupled with a knowledge of the characteristics of the NRX and GLEEP reactors.

The samples were pure natural thorium and were in the form of metal rods, 15.24 cm long by 3.45 cm in diameter, weighing 1635 g. The longest exposure attained was 1.44 neutrons/kilobarn, or 1.44×10^{21} nvt. Very roughly, this would correspond to an exposure of the order 10,000 Mwd/ton if the thorium had contained an admixture of something like 1.5 to 2% of a fissionable uranium isotope.

This reaction chain occurs in the thorium:

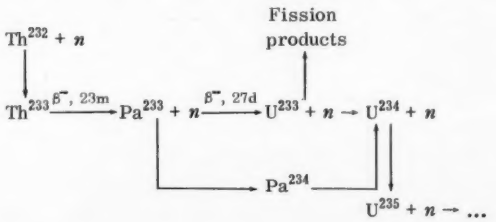

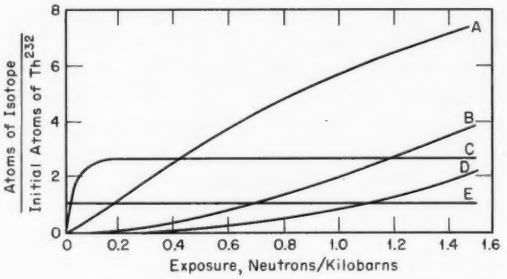

Fig. III-1 Isotopic buildup[13] in a thorium cartridge in the NRX flux of 1.0×10^{13} neutrons/(cm^2)(sec). Curves: *A*, U^{233} ($\times 10^3$); *B*, U^{234} ($\times 10^4$); *C*, Pa^{233} ($\times 10^4$); *D*, U^{235} ($\times 10^5$); and *E*, Th^{232}.

The calculated curves of the isotope concentrations as functions of exposure are shown in Fig. III-1.* These calculations utilized the basic nuclear data tabulated in Table III-1. The neutron spectrum was taken into account by the usual Westcott[14] approach, utilizing experimentally determined epithermal flux fractions. The same data and a similar calculational approach, along with experimental calibration factors and correction factors that have been derived by previous studies on GLEEP, were used to derive the theoretical effect of the exposed sample in the GLEEP reactor.

Both the calculations and the measurements showed an apparent decrease in the absorption cross section of the sample of about 4 barns per initial thorium atom for the longest exposure. It is impractical to reproduce here the resultant curves of apparent cross section as a function of exposure, but it suffices to say that the experimental and calculated results agree to within their estimated uncertainties. These amount to about ±4% in each case and are due to a variety of possible small errors, including errors in (1) experimental technique, (2) evaluation of the flux depression in GLEEP by the sample (and the change in that depression with changes in sample exposure), (3) effective neutron temperature, (4) calibration of GLEEP, and (5) determination of the irradiation exposure. It did appear that a reduction in η of U^{233} to the value 2.26 (a value that would still be within the uncertainty limits,

* Figure III-1 and Table III-1 are reprinted here by permission from the *Journal of Nuclear Energy, Parts A & B*.[13]

Table III-1 HEAVY-ISOTOPE NUCLEAR DATA[13]

	σ_0 (absorption), barns	σ_0 (fission), barns	σ_{RI}, barns	λ, sec^{-1}	η_0
Th^{232}	7.56*		7.6†		
Pa^{233}	80‡		700‡	0.293×10^{-6}§	
Pa^{234}¶				28.7×10^{-6}§	
U^{233}	581*	527*			2.28*
U^{234}	95‡		700‡		
U^{235}	694*	582*			2.07*

* D. J. Hughes and R. B. Schwartz, Neutron Cross Sections, USAEC Report BNL-325 (2nd Ed.), Brookhaven National Laboratory, July 1, 1958.

† The effective resonance integral for these cartridges was calculated from the expression

$$\left(\int \sigma \frac{dE}{E}\right)_{\text{eff}} = A + B\left(\frac{S}{M}\right)^{\frac{1}{2}}$$

where $A = 4.1 \pm 0.3$ and $B = 21.1 \pm 1.2$ (W. G. Pettus, Geometric and Temperature Effects in Thorium Resonance Capture, USAEC Report BAW-TM-203, Babcock and Wilcox Co., Apr. 27, 1959). Allowance was made for the $1/v$ contribution which is included in this expression.

‡ J. Halperin and R. W. Stoughton, Some Cross Sections of Heavy Nuclides Important to Reactor Operation, *Proceedings of the Second United Nations International Conference on the Peaceful Uses of Atomic Energy, Geneva, 1958,* Vol. 16, p. 64, United Nations, New York, 1958.

§ Chart of the Nuclides, 1956.

¶ σ_0 and σ_{RI} for Pa^{234} have been taken as zero.

2.28 ± 0.02, of the Hughes and Schwartz determination) would improve the agreement of the calculated curve with the experimental curve. The net effect of this change in η is to reduce by about 2% the calculated value of the apparent cross-section change produced by the exposure. Work with the samples is continuing, and the intention is to repeat the analysis of the measurements after chemical and mass spectrometric analyses, which will determine the actual isotopic concentrations in some of the samples, have been completed.

Resonance Integrals

Two sets of measurements of resonance integrals for lumped fertile materials have recently been reported. One of these, by Hellstrand and Lundgren,[15] consisted of remeasurements of the integrals for uranium metal and uranium oxide so as to explore the reason for discrepancies between direct measurements of the ratios of epicadmium absorption in metal and oxide and the ratios as predicted by the previously deduced[16] expressions for the resonance integrals. The new measurements indicate that Hellstrand's previous expression for the metal integral should be modified; the new expression is given as

$$RI = 2.95 + 25.8\sqrt{S/M} \qquad (1)$$

where S/M is the surface-to-mass ratio of the lumped absorber. The previous expression for the oxide integral was found to agree with the new measurements to within 0.5%; therefore no change is recommended in the previous expression for oxide:

$$RI = 4.15 + 26.6\sqrt{S/M} \qquad (2)$$

The revised metal expression is said to give better agreement with the metal-to-oxide absorption ratio measurements.

Measurements of the effective resonance integral of thorium metal samples, by the oscillator method, in the Argonne critical assembly ZPR-VII, are reported in reference 17. The resulting expression for the effective integral is

$$RI = (-0.2 \pm 1.3) + (17.2 \pm 2.1)\sqrt{S/M} \qquad (3)$$

The reference also gives other forms of expression for the variation of the integral with S/M.

In all of the above expressions, the $1/v$ component of the integral has been subtracted out.

Reference 18 and, in more detail, reference 19 report the development of a new method of calculating resonance integrals, by a direct numerical integration of the integral equation for the average collision density in the absorber. The problem has been coded in FORTRAN for the IBM-7090 computer.[20] Input consists of the resonance parameters for the individual resonances, the temperature, the composition, and the lattice geometry. As in all theoretical approaches, the unresolved high-energy resonances must be taken into account by theoretical estimates. This limitation is becoming less serious, however, as the resonances in U^{238} and Th^{232} are now resolved up to 1000 ev, and the unresolved part usually contributes less than 10% of the total absorption.[18]

The details of the method are beyond the scope of this review, but the agreement with experimental results is worthy of note. The reference[18] shows computed values of the resonance integrals for uranium rods having radii

of 0.1055 to 1.69 cm and for uranium oxide rods having radii of 0.125 to 2.0 cm; the agreement with the resonance integrals from Hellstrand's formulas (Eqs. 1 and 2) is excellent. A series of computations for thorium metal rods having radii of 0.138 to 2.2 cm gave resonance integrals that can be represented by the following relation:[18]

$$\text{Calculated } RI = I_h + 1.37 + 17.9\sqrt{S/M} \quad (4)$$

where I_h is the contribution of high-energy resonances and $l > 0$ resonances, which should amount to 1 to 2 barns. This gives slightly higher values than the expression of Hellstrand and Weitman[21] for thorium metal:

$$RI = 1.70 + 15.9\sqrt{S/M} \quad (5)$$

However, Nordheim[18] points out that, for comparison with theory, the method of subtracting out the $1/v$ component from the measured integral must be carefully examined. He states that one must invoke negative-energy resonances for thorium to explain the value of σ_{a0}, the capture cross section at 0.0253 ev, and that the cross section will, in fact, fall off faster than $1/v$. He quotes a private communication which estimates the effect, the result of which would be to raise the constant term of Eq. 5 (for comparison with theory) to 3.4 barns. Presumably a similar modification of the expression of Rothman and Ward (Eq. 3) would be indicated. Whether these modifications would be appropriate in making practical applications, in a reactor calculation, of the experimentally determined expressions would depend on just how the details of the neutron balance are handled in the particular calculation.

References

1. D. E. Wood, Material Buckling Measurements on Graphite-Uranium Systems at Hanford: A Summary Tabulation, USAEC Report HW-69525, Hanford Atomic Products Operation, May 1961.
2. V. I. Neeley and H. E. Handler, Measurements of Multiplication Constant for Slightly Enriched Homogeneous UO_3-Water Mixtures and Minimum Enrichment for Criticality, USAEC Report HW-70310, Hanford Atomic Products Operation, Aug. 21, 1961.
3. V. I. Neeley et al., k_∞ of Three Weight Percent U^{235} Enriched UO_3 and $UO_2(NO_3)_2$ Hydrogenous Systems, USAEC Report HW-66882, Hanford Atomic Products Operation, September 1961.
4. Martin Co., Nuclear Div., PM-1 Critical Experiments and Zero Power Testing, USAEC Report MND-M-1858, September 1961.
5. T. J. Thompson et al. (Eds.), Heavy Water Lattice Project Annual Report, USAEC Report NYO-9658, Massachusetts Institute of Technology, Sept. 30, 1961.
6. F. E. Kinard, Nuclear Parameters of Massive Uranium Rods in D_2O, USAEC Report DP-644, Savannah River Laboratory, November 1961.
7. W. C. Redman et al., Critical Experiments with Thoria-Urania Fuel in Heavy Water, USAEC Report ANL-6378, Argonne National Laboratory, December 1961.
8. T. C. Engelder et al., Spectral Shift Control Reactor Basic Physics Program. Critical Experiments on Lattices Moderated by D_2O-H_2O Mixtures, USAEC Report BAW-1231, Babcock and Wilcox Co., December 1961.
9. L. G. Barrett et al., Spectral Shift Control Reactor Basic Physics Program. Exponential Experiments at Elevated Temperatures on Lattices Moderated by D_2O-H_2O Mixtures, USAEC Report BAW-1233, Babcock and Wilcox Co., March 1962.
10. D. B. Wehmeyer et al., Spectral Shift Control Reactor Basic Physics Program, Theoretical Analysis. Part I. Analysis of Experiments, USAEC Report BAW-1230(Pt. I), Babcock and Wilcox Co., March 1962.
11. A. E. Dunklee, PDP Measurements of Coolant Void Reactivity Coefficients, USAEC Report DP-641, Savannah River Laboratory, March 1962.
12. R. L. Baer, PM Research and Development Program, 1st Quarterly Progress Report, April 15, 1961, to June 30, 1961, USAEC Report MND-MD-2560-1, Martin Co., Nuclear Div., March 1962.
13. D. C. C. Gibbs et al., Long-Term Reactivity Changes in Irradiated Thorium, *J. Nucl. Energy, Pts. A & B*, 15(2/3): 130 (October 1961).
14. C. H. Westcott, Effective Cross Section Values for Well-Moderated Thermal Reactor Spectra, Canadian Report CRRP-787 (1958 Revision), Aug. 1, 1958.
15. E. Hellstrand and G. Lundgren, The Resonance Integral for Uranium Metal and Oxide, Letters to the Editors, *Nucl. Sci. Eng.*, 12(3): 435 (March 1962).
16. E. Hellstrand, Measurements of the Effective Resonance Integral in Uranium Metal and Oxide in Different Geometries, *J. Appl. Phys.*, 28(12): 1493 (December 1957).
17. A. B. Rothman and C. E. W. Ward, Effective Resonance Integral of Thorium Metal, *Nucl. Sci. Eng.*, 12(2): 293 (February 1962).
18. L. W. Nordheim, A New Calculation of Resonance Integrals, *Nucl. Sci. Eng.*, 12(4): 457 (April 1962).
19. L. W. Nordheim, A Program of Research and

Calculations of Resonance Absorption, USAEC Report GA-2527, General Atomic Div., General Dynamics Corp., Aug. 28, 1961.

20. G. F. Kuncir, A Program for the Calculation of Resonance Integrals, USAEC Report GA-2525, General Atomic Div., General Dynamics Corp., Aug. 28, 1961.
21. E. Hellstrand and J. Weitman, The Resonance Integral of Thorium Metal Rods, *Nucl. Sci. Eng.*, 9(4): 507 (April 1961).

Section

IV

Power Reactor Technology

Heat Transfer

Conduction

The thermal conductivity of uranium dioxide continues to receive attention. Reference 1, in addition to information on other aspects of UO_2-bearing fuels, contains an account of conductivity measurements made under conditions approximating those in cylindrical UO_2 fuel elements. The basic apparatus used was a radial conduction rig, as illustrated in Fig. IV-1. The heating was accomplished electrically by means of the tungsten wire extending through the center of the column of pellets. Five sight holes were drilled to various depths in some of the pellets, and an optical pyrometer was utilized to measure the UO_2 temperature for subsequent thermal-conductivity calculations. The inside diameter of the cladding tube was varied to provide for five different radial gap sizes between the pellet surface and the tube. One sample of vibratory-compacted UO_2 powder was also investigated. The test section was enclosed in a bell jar, and testing was done in an argon atmosphere to prevent oxidation of the tungsten. Several runs were done with a helium atmosphere, but the data are not reported in the reference.

Results of the experiments are illustrated in Fig. IV-2. The effective thermal conductivity, k_{eff}, is defined as follows:

$$k_{eff} = \frac{Q \ln R_2/R_1}{2\pi L(T_2 - T_1)} \text{ Btu/(hr)(ft)(°F)} \qquad (1)$$

where Q = total heat input, Btu/hr
R_2 = inside radius of cladding, ft
R_1 = radius of tungsten electrode, ft
T_2 = tungsten electrode surface temperature, °F
T_1 = cladding inside surface temperature, °F
L = specimen length, ft

Figure IV-3 is a comparison of the data in reference 1 with those of Kingery, Bates, and Bettis Atomic Power Laboratory (these data have been described previously in *Power Reactor Technology*, Vol. 4, No. 2, page 40, and Vol. 5, No. 1, page 58). The conclusions stated in reference 1 are as follows:

a. There is a significant increase in the effective thermal conductance of a stainless-steel-clad UO_2 fuel element containing a 0.0005-in. radial gap (cold) between the pellets and cladding from that which contains a 0.004-in. radial gap. There is essentially no difference in the effective conductance of stainless-steel-clad UO_2 fuel elements containing radial gaps in the range of from 0.004 to 0.0105 in.

b. At maximum UO_2 temperatures above 1200°C the effective conductance of the fuel element increases with temperature.

c. The effective conductance of a fuel element improves with thermal cycling at high temperatures.

d. The effective conductance of a stainless-steel-clad fuel element containing vibratory-compacted UO_2 powder of 86% of theoretical density is comparable to a fuel element containing UO_2 pellets of 94% of theoretical density and with a radial gap between the pellets and cladding in the range of from 0.004 to 0.0105 in.

e. Appreciable vapor deposition starts at approximately 1800°C.

f. The microstructure of UO_2 obtained by out-of-pile heating is similar to the microstructure of UO_2 irradiated at similar temperature conditions.

The prediction of temperatures within the moderator of a graphite-moderated reactor is treated in reference 2. The basic attack is by integration of the heat-conduction equation with the aid of an analog computer. The problem is complicated, however, by the fact that the thermal conductivities of molded and extruded graphites are anisotropic. Also, the thermal conductivity depends on the integrated fast-neutron dose and on the temperature during

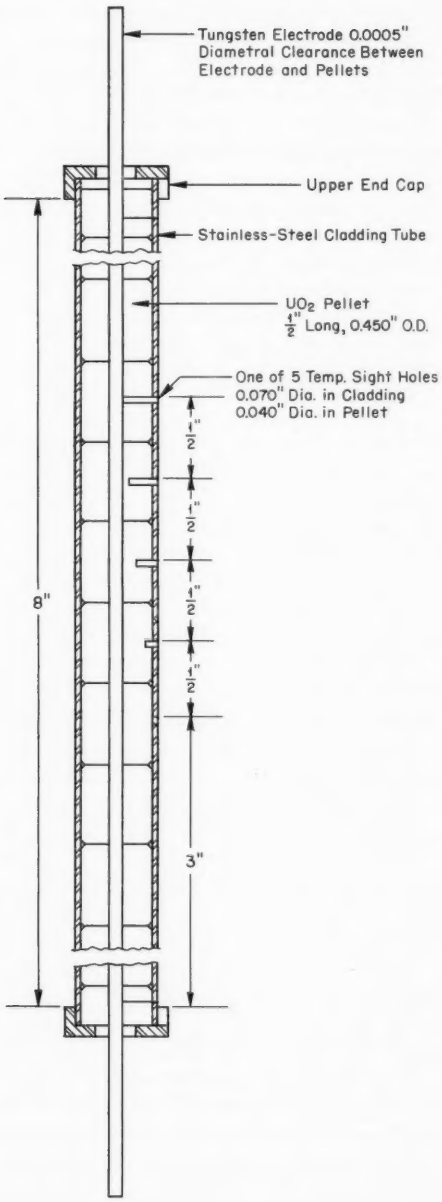

Fig. IV-1 Cross section of the UO_2 fuel-element specimen assembly.[1]

irradiation. A semiempirical method is used to correlate the effect of these variables on the thermal conductivity, and the temperature calculations are illustrated by applications to the Sodium Reactor Experiment (SRE) and the Hallam Nuclear Power Facility (HNPF).

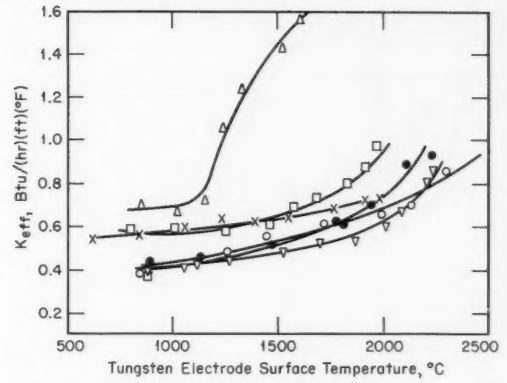

Fig. IV-2 Effect of radial gaps between pellets and cladding on thermal conductance.[1] All tests were performed with argon. Δ, 0.0005-in. radial gap, pellets. □, 0.0025-in. radial gap, pellets. ●, 0.004-in. radial gap, pellets. ∇, 0.009-in. radial gap, pellets. ○, 0.0105-in. radial gap, pellets. ×, compact powder having 86% of the theoretical density.

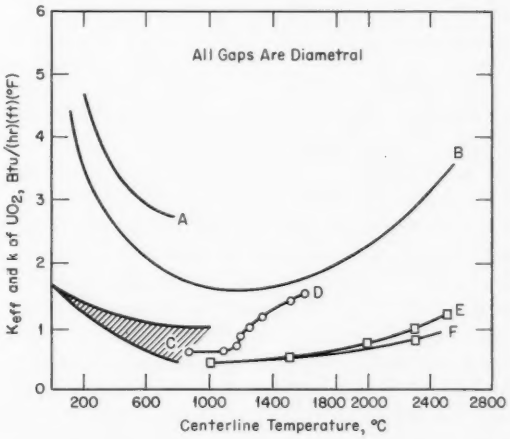

Fig. IV-3 Comparison of thermal-conductivity data.[1] *A*, Kingery (*k* of UO_2). *B*, Bates, *Nucleonics*, June 1961 (*k* of UO_2). *C*, Bettis Atomic Power Laboratory (K_{eff} of 3.5; 8- to 13-mil gaps; helium or xenon plus krypton). *D*, Combustion Engineering (K_{eff}; 1-mil gap; argon). *E*, Combustion Engineering (K_{eff}; 8-mil gap; argon). *F*, Combustion Engineering (K_{eff}; 21-mil gap; argon).

References 3 and 4 illustrate various analytical and numerical techniques for the solution of conduction problems, and reference 5 discusses a transient technique for the measurement of thermal diffusivity.

Pressurized Water

Heat-transfer considerations for the Materials Testing Reactor (MTR) and the Engineering Test Reactor (ETR) are discussed in reference 6. Although these are low-temperature reactors, some of the conclusions are applicable to the thermal design of power reactors. Figure IV-4

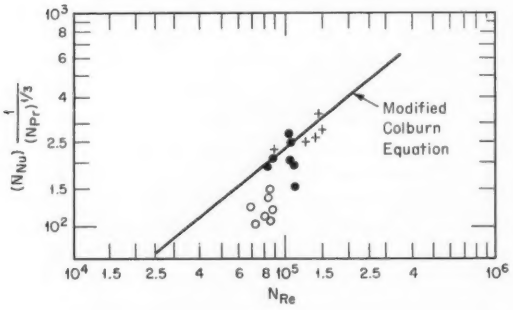

Fig. IV-4 Forced-convection heat-transfer data in a simulated ETR flow channel.[6] Approximate heat flux: ○, 1×10^5 Btu/(hr)(sq ft); ●, 3.5×10^5 Btu/(hr)(sq ft); +, 7×10^5 Btu/(hr)(sq ft).

illustrates data taken in a simulated ETR flow channel (0.110 by 2.624 by 36 in.) at three different heat fluxes. The modified Colburn equation is also plotted on the figure, and the reference concludes that "... for rectangular flow channels the use of the modified Colburn equation below heat fluxes of 10^5 Btu/hr-ft^2 is questionable." The reference also discusses the applicability of artificially roughened heat-transfer surfaces and suggests that the power of the ETR and MTR could be substantially increased by roughening the fuel plates.

Reference 7 reports briefly the results of pressure-drop measurements taken in a seven-rod fuel-element bundle. The bundle is stated to be square, with pitch-to-rod diameter ratios of 1.0 and 1.13. The authors conclude that the use of the hydraulic diameter (4 × flow area/wetted perimeter) does not correlate the effect of variations in the pitch of the rods in a bundle; the use of experimental data is recommended. Unfortunately, the test section contained, in addition to the seven rods, some spacers that served to equalize velocities in the bundle, and no details are given of the spacer arrangement.

References 8 and 9 contain transport and thermodynamic data for water near the critical pressure. These publications present, in addition, a bibliography of over 100 reports applicable to the subject. Reference 10 reports on an analytical and experimental study of free convection to supercritical water. The authors conclude that the heat transfer to a supercritical fluid in free convection can be adequately described by the boundary-layer equations when property variations, which are large in the cases of specific heat and the coefficient of expansion, are included.

Boiling Water

Reference 11 is a discussion of the prediction of void fractions in boiling channels. The author proceeds by integrating bubble diffusion equations, assuming negligible slip velocity and utilizing an empirical bubble growth and collapse relation. The boundary conditions correspond to the case of axial symmetry, with no vapor phase entering the channel; it is presumed that the bubbles enter the liquid by diffusion from the wall and that the heat not used for vapor production enters the liquid phase directly. The resulting equation, which is implicit in void fraction and distance along the channel, was solved by appropriate approximations and numerical techniques. Experimental data were then utilized to compute values for constants representing the rate of bubble production and bubble growth rate. An interesting result was reached by a comparison of the bubble production constant and the heat flux, which are related, of course, by a conservation-of-energy equation. It was shown that, as heat flux is increased, an increasing amount of heat enters the liquid phase as sensible heat and that the liquid phase may have as much as 10°F of superheat. This nonequilibrium situation causes the author to question the widely used Martinelli-Nelson void-fraction correlation (reference 12) since the assumption of thermodynamic equilibrium was made in reference 12 for forced-circulation boiling. The following equation is presented as an approximation for regions that lie at large distances from the channel inlet and in which the average void fraction is greater than 0.4:

$$\frac{1}{1-C_m} \approx \left(\frac{\alpha_q Q_0}{h\, \rho_L\, c_p}\right)^{1/2} \frac{x}{u_m} \qquad (2)$$

where C_m = mean total fraction voids across channel cross section, dimensionless
α_q = bubble growth or collapse rate constant, °F/hr
Q_0 = constant uniform heat flux, Btu/(hr)(sq ft)
h = half the channel spacing, ft
c_p = heat capacity at constant pressure, Btu/(lb)(°F)
x = distance along channel, ft
u_m = mean superficial liquid velocity in channel, ft/hr
ρ_L = liquid density, lb/cu ft

coefficients and pressure gradients were determined experimentally over the range of variables shown in Table IV-1.* The forced-convection-boiling heat-transfer correlation is illustrated in Fig. IV-5.* The data points are not given, but a scatter of about ±35% is reported. This is assigned to the difficulty in measuring the temperature drops through the tube wall. In Fig. IV-5, B_0, the boiling number, is defined as the quotient of the heat flux and the product of the mass flow and the vaporization enthalpy, h_{fg}. The parameter X_{tt} is the conventional Lockhart-Martinelli parameter. The authors note that at low values of B_0 the Nusselt (Nu)

Table IV-1 DATA CLASSIFICATION AND RANGE[14]

Bulk boiling series	Test section		Range of variables			
	Length, in.	Internal diam., in.	Heat flux (q/A), Btu/(hr)(sq ft) × 10^5	Mass velocity (G), lb/(sec)(sq ft)	Pressure (P_{in}/P_{out}), psia	Exit quality, %
B*	15, 20	0.1162	1.13 to 7.8	204 to 665	57/49 to 384/352	10 to 51
D*	30, 40	0.1162	1.75 to 8.16	192 to 700	130/100 to 505/422	14 to 53
E	15, 30, 40	0.1181	1.43 to 1.45	197 to 911	116/64 to 381/313	8 to 56
F	15, 30	0.2370	1.23 to 7.59	81 to 230	101/99 to 306/302	8 to 57
G†	30	0.4317	0.653 to 2.46	49 to 69	106/105 to 314/313	10 to 43

*Pressure-drop data only.
†Heat-transfer data only.

Note that in this equation the void fraction is a function of the heat flux, the liquid velocity, and the channel spacing; this is not the case for the Martinelli-Nelson correlation.

Another void-fraction correlation is presented in reference 13. The technique used was to modify the Bankoff correlation by means of a statistical fit to experimentally determined void-fraction data. The Bankoff correlation is

$$\text{Slip ratio} = \frac{1 - \text{void fraction}}{K - \text{void fraction}} \qquad (3)$$

The correlation presented in the reference relates the parameter K and a parameter Z, which is a function of Reynolds number, the Froude number, and the liquid volume fraction that would apply if there were no slip. The relation is presented graphically and apparently is valid for both upward and horizontal cocurrent flow of steam-water and air-liquid mixtures at pressures from atmospheric to several thousand pounds per square inch.

Forced-convection boiling in tubes is treated in reference 14. Specifically, local heat-transfer value is primarily a function of X_{tt}; at large values of B_0, the heat transfer becomes independent of X_{tt}. This behavior was explained by assuming the flow pattern to be annular, with liquid flowing on the wall and vapor in the core. If the liquid layer can support the temperature difference necessary to transmit heat without nucleation occurring, then there is evaporation at the interface but no nucleation. As heat flux is increased, the higher wall superheat results in nucleation. Without nucleate boiling the thermal resistance is determined by the presence of the liquid layer, and the correlation in terms of X_{tt} implies a heat-momentum analogy. For large ratios of heat flux to mass flow, nucleation predominates and the heat transfer is independent of the flow characteristics of the system; the boiling number then correlates the data. A qualitative discussion of annular or climbing film flow can be found in a recent British publication.[15]

*Table IV-1 and Fig. IV-5 are reprinted here by permission from *Nuclear Science and Engineering*.[14]

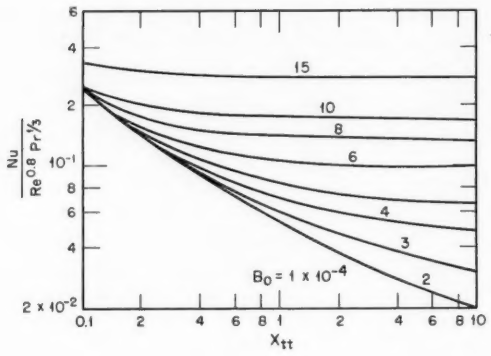

Fig. IV-5 Forced-convection-boiling heat-transfer correlation.[14]

Stability of Boiling Channels

Two reports on the stability of a boiling channel have been issued.[16,17] Both reports proceed by integration of the equations expressing conservation of mass, momentum, and energy, although the many assumptions and techniques used are quite different, and the references should be consulted for this information. Reference 16 contains an interesting section in which the physical mechanisms of instability are examined. Although the assumptions and simplifications make generalizations subject to unknown errors, it is shown that a sufficient condition for instability results from a system wherein a steady-state increase in the mass flow rate produces a reduction in the two-phase pressure drop. The effect of channel orientation is considered, and it is concluded that a vertical channel would be less stable than a horizontal channel for the same static flow rate and power. Momentum changes are important and, in general, result in a destabilizing effect for an increase in acceleration pressure drop. The reference closes with a comparison of the analytical results with some experimental data with "excellent" agreement reported.

Reference 17 is addressed particularly to an examination of the SRE, although the analysis is stated to be applicable to any sodium graphite reactor. Although many of the assumptions are peculiar to the SRE, the analog studies are of general interest; in addition, the model allows for a number of parallel channels, and runs for three and seven parallel channels are discussed. The report approaches the stability problem from a safety standpoint since the SRE does not normally boil sodium. In particular the report attempts to calculate how fast "boiling disease," or vapor blocking of coolant channels, is propagated radially across the core in the event of the addition of reactivity as a slow ramp.

Gaseous Coolants

Reference 18 contains the results of a series of experiments that were designed to determine the local heat-transfer coefficients and local and average friction factors for nitrogen flowing through tubes of circular cross section. The range of variables studied is given in Table IV-2. After a discussion of existing correlations, the experimental data and new correlations are presented. The design of an apparatus for achieving gas temperatures up to 4000°F is described.

Table IV-2 RANGE OF VARIABLES FOR GAS-COOLING TESTS WITH NITROGEN[18]

Flow rate, lb/hr	1.24 to 32.6
Inlet gas temperature, °F	~70
Maximum gas temperature, °F	784
Maximum surface temperature, °F	1455
Maximum T_w/T_b	2.08
Bulk Reynolds number	1830 to 90,000
Heat flux, Btu/(hr)(sq ft)	733 to 138,000
Axial location parameter (x/D)	2 to 127

Short Notes

Reference 19 is a report concerned with the ability of a steam-cooled fuel element of a particular design to dissipate shutdown heat. This problem was reviewed in the June 1961 issue of *Power Reactor Technology*, Vol. 4, No. 3, page 13, and this latest report is an addition to the literature on the subject. Reference 20 is a publication of the Defense Metals Information Center on the emittance of various ceramics and graphites. References 21 through 27 report on fundamental analytical and experimental studies on pool boiling of various liquids. The remaining two references[28,29] are translations of Russian heat-transfer articles.

References

1. B. E. Murtha and W. P. Chernock, The Development and Testing of the UO_2 Fuel Element System, USAEC Report CEND-141, Combustion Engineering, Inc., June 1961.
2. R. L. Carter, An Empirical Prediction of Temperature Gradients in Moderator Graphite Within Operating Nuclear Reactors, USAEC Report NAA-SR-6616, Atomics International, Feb. 15, 1962.
3. G. W. Lehman, Temperature Distribution in a Hollow Cylindrical Cup with a Stem, USAEC Report NAA-SR-6550, Atomics International, Feb. 15, 1962.
4. D. Bagwell, TØSS, An IBM-7090 Code for Computing Transient or Steady-State Temperature Distributions, USAEC Report K-1494, Union Carbide Nuclear Co., Oak Ridge Gaseous Diffusion Plant, Dec. 1, 1961.
5. M. Cutler and G. T. Cheney, Heat-Wave Techniques for the Measurement of Thermal Diffusivity, USAEC Report GA-2706, General Dynamics Corp., General Atomic Div., Dec. 1, 1961.
6. G. W. Gibson and O. K. Shupe, Annual Progress Report on Fuel Element Development for FY 1961, USAEC Report IDO-16727, Phillips Petroleum Co., Mar. 9, 1962.
7. Letters to the Editors: The Hydraulic Resistance for Longitudinal Flow of Liquid over a Bundle of Rods, *J. Nucl. Energy, Pts. A & B*, 16: (1962).
8. E. S. Nowak and R. J. Grosh, An Investigation of Enthalpy Data for Water and Water Vapor in the Critical Region, USAEC Report ANL-6505, Argonne National Laboratory, September 1961.
9. E. S. Nowak and R. J. Grosh, On the Equation of State for Water and Water Vapor in the Critical Region, USAEC Report ANL-6508, Argonne National Laboratory, November 1961.
10. C. A. Fritsch and R. J. Grosh, Free Convection Heat Transfer to a Supercritical Fluid: An Analytical and Experimental Study, USAEC Report ANL-6486, Argonne National Laboratory, November 1961.
11. G. Houghton, An Analysis of Vapor Void Profiles in Heated Channels, *Nucl. Sci. Eng.*, 12(3): 390–397 (March 1962).
12. R. C. Martinelli and D. B. Nelson, *Trans. ASME*, 70: 695 (1948).
13. G. A. Hughmark, Holdup in Gas-Liquid Flow, *Chem. Eng. Progr.*, 58(4): 62 (April 1962).
14. V. E. Schrock and L. M. Grossman, Forced Convection Boiling in Tubes, *Nucl. Sci. Eng.*, 12(4): 474–481 (1962).
15. P. M. C. Lacey et al., Climbing Film Flow, British Report AERE-R-3962, January 1962.
16. A. B. Jones, Hydrodynamic Stability of a Boiling Channel, USAEC Report KAPL-2170, Knolls Atomic Power Laboratory, Oct. 2, 1961.
17. H. H. Cappeï, Multichannel Boiling Stability for Sodium Graphite Reactors, USAEC Report NAA-SR-6527, Atomics International, Mar. 1, 1962.
18. M. E. Davenport et al., Heat Transfer and Pressure Drop for a Gas at High Temperature, USAEC Report TID-13485, Stanford University, Nuclear Technology Laboratory, May 1961.
19. W. E. Littleton and W. Ross, Shutdown Cooling Test, USAEC Report ACNP-6124, Allis-Chalmers Manufacturing Co., Dec. 15, 1961.
20. W. D. Wood et al., The Emittance of Ceramics and Graphites, Report DMIC-Memo-148, Battelle Memorial Institute, Defense Metals Information Center, Mar. 28, 1962.
21. D. A. Huber and J. C. Hoehne, Pool Boiling Investigation of Benzene, Diphenyl, and Benzene-Diphenyl Mixtures Under Pressure, USAEC Report NAA-SR-6681, Atomics International, Dec. 1, 1961.
22. J. A. Clark et al., Low Heat-Flux Boiling, First Quarterly Progress Report for the Period July 1, 1961, to October 1, 1961, USAEC Report TID-14556, University of Michigan, College of Engineering, January 1962.
23. H. J. Ivey, Preliminary Results on the Effect of Acceleration on Critical Heat Flux in Pool Boiling, British Report AEEW-R-99, September 1961.
24. G. B. Wallis, Two-Phase Flow Aspects of Pool Boiling from a Horizontal Surface, British Report AEEW-R-103, September 1961.
25. H. A. Johnson et al., Temperature Variation, Heat Transfer, and Void Volume Development in the Transient Atmospheric Boiling of Water, USAEC Report SAN-1001, University of California, Berkeley, Institute of Engineering Research, January 1961.
26. R. C. Noyes, An Experimental Study of Sodium Pool Boiling Heat Transfer, USAEC Report NAA-SR-6769, Atomics International, Mar. 30, 1962.
27. Yan-Po Chang, Final Report: Section 1, An Analysis of the Critical Conditions and Burnout in Boiling Heat Transfer; Section 2, A Correlation of Boiling Heat Transfer from the Nucleation Theory — Including Effects of System Acceleration and Forced Convection, USAEC Report TID-14004, University of Notre Dame, August 1961.
28. Heat Power Engineering, Part 1, USAEC Translation AEC-tr-4496, translated from a publication of the Publishing House of the Academy of Sciences, U.S.S.R., Moscow, 1959, United States Atomic Energy Commission, December 1961.
29. M. A. Mikheev (Ed.), Problems of Heat Transfer, USAEC Translation AEC-tr-4511, translated from a publication of the Publishing House of the Academy of Sciences, U.S.S.R., Moscow, 1959, United States Atomic Energy Commission, January 1962.

Section

V

Power Reactor Technology

Shielding

Computer Program for Shield Design

A shield-design program for the 32K Philco-2000 computer,* called SPAN-3, is described in a report from the Bettis Atomic Power Laboratory.[1] The report gives a brief description of the problems that can be solved with SPAN-3, the methods of solution, and the instructions for using the program. The appendixes show sample input forms, results from sample problems, and references.

The program calculates the spatial distribution of the fast-neutron dose rate, the uncollided gamma flux, the gamma dose rate, and the gamma energy absorption rate. The program is also capable of calculating the thermal-neutron-flux distribution in a cold (60 to 180°F) or hot (450 to 650°F) water region. The geometry of shield and source is basically cylindrical, although the program is capable of including the effects of slab shielding regions which may occur beyond the cylindrical region. The source region must be a right circular cylinder or a section of a right circular cylinder coaxial with and included within the annular shields. The source distribution is represented by point sources in a mesh within the source region. The source strength can be given for each source point and in the case of gamma sources can be represented by up to 20 energy groups. The attenuation between the point sources and the detector is computed using exponential kernels. The gamma energy absorption rate and dose rate buildup factors are represented by the sum of two exponentials. The total dose rate, energy absorption rate, or flux at the detector is found by performing a numerical integration over the source region using the Gauss quadrature method.

*_Power Reactor Technology_ does not attempt to cover the computer-program literature comprehensibly. This particular program appears to be general enough in scope to be called to the attention of the reactor designer.

Abstracts of Shielding Literature

The unclassified literature on radiation shields and shielding which was published in reports and journals from July 1956 to January 1961 is abstracted in a report[2] that was compiled by the AEC's Division of Technical Information. The references are indexed under author, report number, and subject. The abstracts are grouped under the country of origin and are also listed under the issuing agency.

References

1. W. H. Guilinger et al., SPAN-3, A Shield Design Program for the Philco-2000 Computer, USAEC Report WAPD-TM-235, Westinghouse Electric Corp., Bettis Atomic Power Laboratory, February 1962.
2. H. D. Raleigh (Comp.), Radiation Shields and Shielding, USAEC Report TID-3303(Suppl. 1), April 1961.

Section

VI

Power Reactor Technology

Containment: Iodine Removal

In real or hypothesized reactor accidents that result in the release of fission products, the one fission product that usually is estimated to present the largest inhalation hazard in the surrounding areas is radioactive iodine. Usually the iodine release is controlling in setting the allowable leakage rate of the containment building for both the low-population zone and the population center, or, conversely, if the leakage rate is set, the iodine hazard usually determines the isolation requirements. The practices that are currently in use in the United States for estimating the iodine escape are rather conservative: often the release of 50% to the reactor building is assumed, and 50% of this fraction is in turn assumed to be available for leakage from the building.[1] Since the provision of high degrees of leaktightness and the provision of large isolation areas are both expensive, it is highly desirable to arrive at realistic methods of estimating the iodine release and, if possible, to find means of reducing the fraction available for leakage from the building. Several reports that treat some aspects of these subjects have been issued.[2–5]

Reference 2 indicates that the pressure-suppression system for reactor containment, which has its most widely known application on the Humboldt Bay reactor, results in a reduction of the free iodine fraction as well as a reduction of the maximum pressure in the containment building. Briefly, the system involves enclosing the reactor pressure vessel within a container called a dry well, which is itself located within the containment building proper and which is vented to the building through a pool of water. If the reactor vessel is breached, steam and water will enter the dry well, and, as the pressure increases, the steam will be forced into the pool of water through the vents and will be condensed. The tests that have been run on the system are reported in reference 2. As part of these tests, elemental iodine crystals were released with the water and steam to determine how much of the iodine would be entrained in the pool of water. The tests showed that, shortly after the release of 1 lb of elemental iodine, less than $5.8 \times 10^{-5}\%$ was released to the containment building; and 5 hr later $7.2 \times 10^{-4}\%$ had been released. The measured separation factor is thus between 10^{-5} and 10^{-6}. The results can, of course, be affected by scale, geometry, and chemical processes, but in any case it appears that a substantial reduction in the iodine released to the containment building can be effected. Also of interest in the tests are the data on some of the other elements released, along with their resulting entrainments, as shown in Table VI-1.*

The United Kingdom Atomic Energy Authority (UKAEA) has run some interesting experiments on the behavior of iodine in containment vessels, as reported in reference 3. It was the contention of the authors that the concentrations of iodine expected in the containment building following an accident would be so low as to make it difficult to study their behavior in laboratory apparatus. Therefore they conducted the experiments in the DIDO and PLUTO reactor containment shells. Crystalline stable I^{127}, with radioactive I^{132} as a tracer, was vaporized into a stream of filtered nitrogen that was released to the building atmosphere. The duration of the release process was not more than 15 min, and the building air circulators were operated for a period of 30 min after each release, an operating period that previous tests had indicated was ample to give practically complete mixing of the building air.

*Table VI-1 is reprinted here by permission from the American Society of Mechanical Engineers.[2]

Table VI-1 RESULTS OF TESTS ON ENTRAINMENT OF SIMULATED FISSION PRODUCTS IN WATER[2]

Element	Initial amount in pressure vessel	% released to containment volume	Conc. in containment volume, mole %
Krypton	250 std. cm³	$25^{-50\%}_{+100\%}$	$0.003^{-50\%}_{+100\%}$
Xenon	250 std. cm³	< 45	< 0.005
Iodine	1 lb	5.8×10^{-5}	1.83×10^{-8}
		7.2×10^{-4}*	2.3×10^{-7}*
Sodium iodide	110 g	1.7×10^{-4}	1.4×10^{-6}
Zinc sulfide	110 g	2.1×10^{-6}	2.7×10^{-10}

Containment volume (after firing)	78.5 cu ft (air)
Pool volume	129 cu ft
Pressure vessel volume	3.12 cu ft

*At 5 hr.

The quantities of iodine released in the several tests were sufficient to give average concentrations in the containment building ranging from 0.013 to 14.1 $\mu g/m^3$ of air. Most of the tests were run at 1 $\mu g/m^3$. The total iodine concentration in the air, as measured by air samples, is shown in Fig. VI-1* as a function of time after release. Five hours after release the iodine concentration in the air appeared to reach a nearly constant value, showing that equilibrium between the building surfaces and the air had been attained. For run *A*, which was a low-concentration run, the rate of decrease of the air concentration was small, probably because most of the iodine was deposited on airborne particulate matter and, except for gravitational settlement of the particles, was retained in the air, where it remained as an inhalation hazard. When initial iodine concentrations of about 1 $\mu g/m^3$ were used, the iodine concentrations fell by about a factor of 50 in about 4 hr; whereas, when initial concentrations of 10 $\mu g/m^3$ were used, they fell by about a factor of 10.

The reported data[3] suggest that surface areas may have become nearly saturated at an airborne concentration of 1 $\mu g/m^3$, but a later report tells of an experiment on iodine-removal systems which was being conducted at the same time and which could have affected the results.[4] During the 1-μg releases, the building air was circulated through experimental iodine-removal systems. The volume of air passing through the various experimental iodine-removal systems was equivalent to the building volume every 79 to 130 min, depending on the system being tested. This must have affected the iodine concentration, making the factor of 50 suspect. It is obvious that many factors affect the results; some of these factors are the building volume-to-surface-area ratio, types of surfaces, amount of water vapor present, and amount of foreign contaminants and particulate matter in the air.

Another interesting observation was the result of introducing further stable I^{127} into the

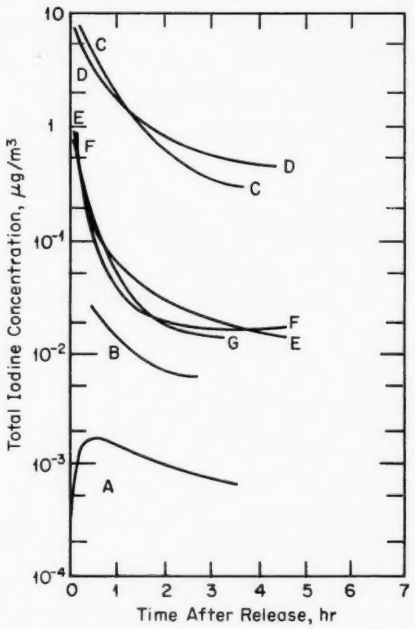

Fig. VI-1 Variation of the total iodine concentration with time in the PLUTO containment building.[3]

Run	Source strength I^{127}, mg	Source strength I^{132}, mc	Calculated added concentration, $\mu g/m^3$	Calculated added concentration, Dis/(min)(m³)	Maximum measured concentration, dis/(min)(m³)
A	0.09	28.2	0.013	8.9×10^6	1.45×10^6
B	0.95	22.9	0.14	7.2×10^6	1.75×10^6
C	99	30.6	14.1	9.7×10^6	5.4×10^6
D	99	20.1	14.1	6.4×10^6	3.0×10^6
E	7	2.7	1.0	8.5×10^5	9.3×10^5
F	9.9	48.9	1.4	1.5×10^7	1.0×10^7
G	10	39	1.4	1.2×10^7	5.5×10^6

*Figures VI-1 to VI-3 and Table VI-2 are reprinted here by permission from the United Kingdom Atomic Energy Authority (to be published in *Journal of Nuclear Energy*, Pergamon Press).

Table VI-2 DETAILS OF THE COPPER AND CARBON BEDS[4]

	Copper bed	Carbon bed
Type of packing	Wire mesh	6–10 mesh granules
Bulk density, lb/cu ft	10	30
Specific surface, sq ft/cu ft	100	500
Bed depth, in.	72	10
Bed diameter, in.	36	66
Total contact surface, sq ft	4000	10,000
Total packing weight, lb	400	600

air after the concentration of the initial release had apparently reached equilibrium. The result was an increase in the I^{132} activity in the air, showing that some of the stable iodine had exchanged with some of the I^{132} on the building surfaces. This is suggested as a method of decontaminating containment-building surfaces after an accident.[3]

Another method of reducing the fission-product concentration, particularly that of iodine, is to circulate the containment-building air through a filter and adsorption unit. This type of system was run experimentally in the PLUTO containment building during the 1 $\mu g/m^3$ runs *E*, *F*, and *G*, shown in Fig. VI-1. The PLUTO containment building was already equipped with a scrubber unit. This unit is 15 ft high by $3\frac{1}{2}$ ft in diameter and contains three horizontal contacting trays. The scrub liquor is 5% aqueous sodium carbonate circulated in a closed cycle. For the tests, four 1000-cfm glass-paper frames with a nominal filtration efficiency of 99.95% for particles of mean size 0.5 μ were added on the upstream side. Also tested were a copper bed unit and a carbon bed unit. The details of these units are shown in Table VI-2.

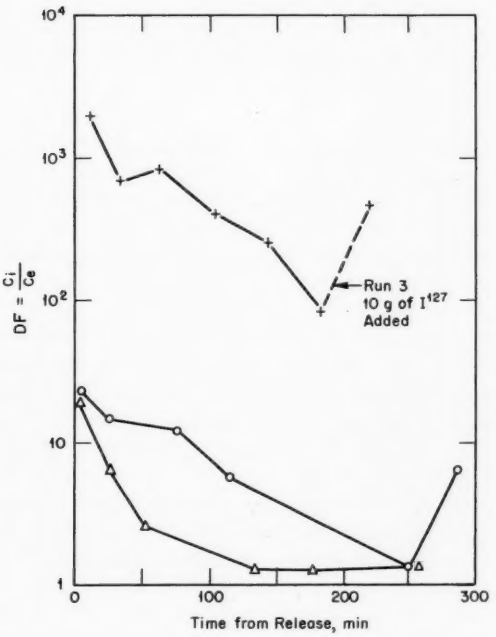

Fig. VI-2 Overall decontamination factors of each system as a function of time from the iodine release.[4] O, run 1, filter plus scrubber. Δ, run 2, filter plus copper bed. +, run 3, filter plus carbon bed. C_i is the concentration at the inlet to the filter, and C_e is the concentration leaving the absorption unit.

The overall decontamination factors as functions of time after the iodine release for the three systems are shown in Fig. VI-2. The decontamination factors of the filters are shown in Fig. VI-3. As can be seen in Fig. VI-2, the filter plus the carbon bed is by far the best system. The scrubber and the copper bed are ineffective for the chemical form of the iodine passing through the system. This suggests that it is no longer elemental iodine but is of a form that is readily adsorbed by carbon. In any case it can be seen in Fig. VI-3 that the bulk of the iodine in the first few minutes after release is stopped by the glass particulate filters. Some of the iodine stopped by the filters was probably attached to airborne particles, but some, no doubt, was elemental iodine, which is known to adsorb on glass surfaces. With the addition of a relatively large amount (10 g) of I^{127} in run 3, the decontamination factor of the filter fell below 1, showing that the iodine on the filter readily underwent isotopic exchange and that the filter had reached its capacity to remove elemental iodine.

Another approach to iodine removal is the so-called "dousing method" that is designed for use in the Canadian NPD-II reactor.[4,5] The NPD-II is designed without a containment shell as such, but, if an accident should occur, the nonvolatile fission products would be contained within the room housing the reactor and steam-generating equipment and the volatile fission products would be released in a controlled manner.[5] An important part of this control is the dousing, which is the introduction of a large volume of water into the room as fog and spray. To determine the effectiveness of the

dousing water in removing the iodine from the air, some small-scale laboratory experiments have been performed.[5]

Drums of two sizes were used in the experiments: 26 and 45 gal. Fog was produced at approximately 25 ml/min in each drum, and spray was introduced into the 26-gal drum at 10 liters/min and into the 45-gal drum at 14.2 liters/min. The iodine was introduced as I_2 in steam. The results of 64 separate experiments are summarized in Fig. VI-4,* which shows the distribution of iodine between air and water a few minutes after dousing. The solid line represents a constant ratio of 10^{-4} between the air and water concentrations. Several parameters were varied, such as the number of grams of I_2 introduced, the *p*H of the dousing water, and the volume of water in the spray. The total weight of iodine introduced varied between 5.8×10^{-8} to 4.7×10^{-2} g. Over most of this range, as can be seen in Fig. VI-4, the air-to-water concentration ratio departed very little from the 10^{-4} value, but a definite increase in the ratio at the highest concentrations does occur, making extrapolation of the data to higher concentrations doubtful. The *p*H was varied between 4.6 and 7.3, and, although the effect was small, the lower *p*H resulted in the higher concentration ratio, the effect being more pronounced as the concentration increased. The volumes of dousing water used were 5, 25, and 45 liters; the air concentration increased as the amount of water was decreased, but an approximately constant air-to-water concentration ratio was maintained. In some experiments the airborne activity was swept out of the drum; in a few hours the air concentration of iodine again reached its previous level. This is not unreasonable since most of the iodine is contained in the water.

In summary it appears that pressure suppression, dousing, and the filter plus carbon bed systems can reduce significantly the airborne iodine. It seems probable also that deposition on internal building surfaces will reduce the airborne iodine significantly even when these schemes are not used. Further investigation seems to be warranted in all cases.

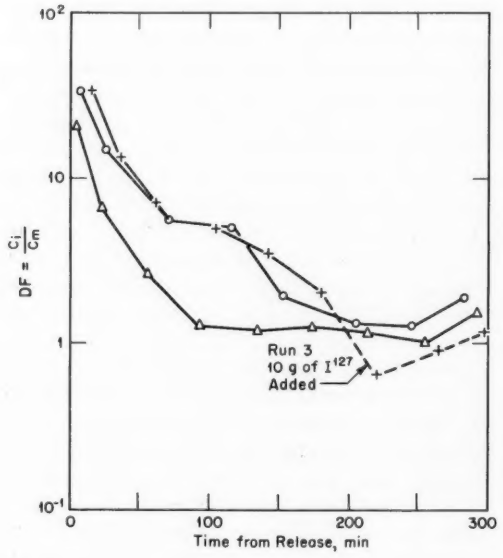

Fig. VI-3 Decontamination factors of the filters as a function of time from the iodine release.[4] ○, run 1. △, run 2. +, run 3. C_i is the concentration at the inlet to the filter, and C_m is the concentration leaving the filter and entering the absorption unit.

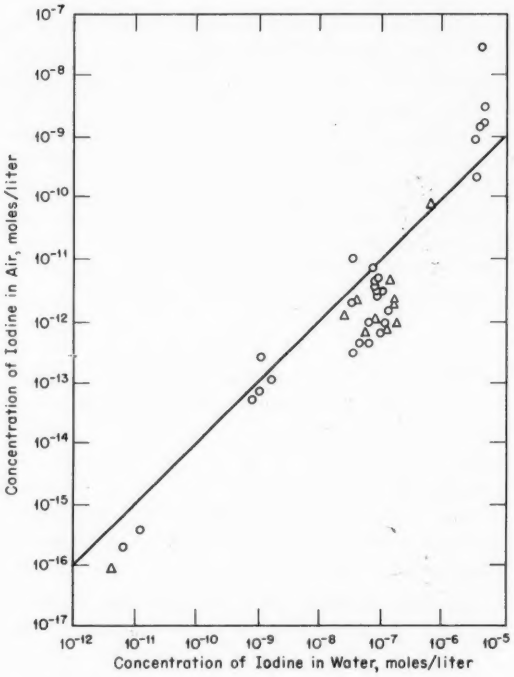

Fig. VI-4 Distribution of iodine between air and water immediately after dousing.[5] ○, 26-gal drum. △, 45-gal drum.

*Figure VI-4 is reprinted here by permission from Atomic Energy of Canada, Ltd.[5]

References

1. J. J. DiNunno et al., Calculation of Distance Factors for Power and Test Reactor Sites, USAEC Report TID-14844, Mar. 23, 1962.
2. C. C. Whelchel and C. H. Robbins, Pressure Suppression Containment for Nuclear Power Plants, ASME Paper No. 59-A-215, Sept. 15, 1959.
3. W. J. Megaw and F. G. May, The Behaviour of Iodine Released in Reactor Containers, British Report AERE-R-3781, July 1961.
4. J. B. Morris et al., The Removal of Low Concentrations of Iodine from Air on a Plant Scale, British Report AERE-R-3917, December 1961.
5. L. C. Watson et al., Iodine Containment by Dousing in NPD-II, Canadian Report CRCE-979(AECL-1130), Oct. 27, 1960.

Section

VII

Power Reactor Technology

Materials

Radiation Embrittlement of Steels

The effects of radiation on steels, the most important of which is the elevation of the nil ductility temperature (NDT) of ferritic steels, were reviewed at some length in the September 1960 issue of *Power Reactor Technology*, Vol. 3, No. 4, pages 38 to 57. The intent of this review is to call attention to work published since that review was written. A report[1] of an AEC-sponsored conference on the effects of radiation on structural materials was published shortly thereafter; it contains a considerable body of experimental data as well as articles in closely related fields. In addition to papers that add to the store of available data, two papers have appeared which make contributions to the basic techniques of investigating the embrittlement problem. The first of these[2] shows that the radiation-induced increase in NDT is the same when determined by drop-weight specimens (2 by 5 by $\frac{5}{8}$ in.) as when determined by standard Charpy V-notch impact specimens. The second[3] is an analytical study, which, on the basis of an assumed mechanism of radiation damage, investigates the effect of the neutron-energy spectrum under which the irradiation is carried out.

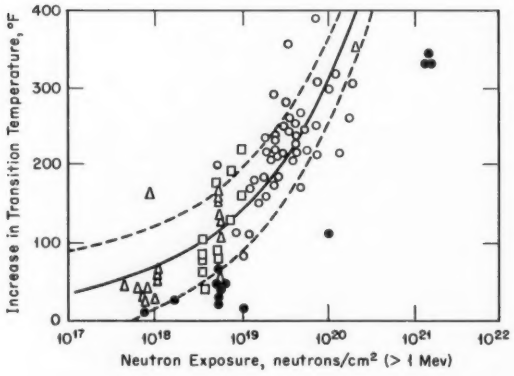

Fig. VII-1 Effect[4] of neutron radiation on the notch toughness of carbon and low-alloy steels irradiated below 500°F. The solid points were not used in the statistical analysis. ○, subsize cantilever type impact specimens. △, Charpy V-notch impact specimens. □, Charpy V-notch slow-bend specimens. —, mean. ---, 75% tolerance limits at 95% confidence.

Reference 4 is a rather extensive review of radiation effects on steel. It also presents the results of a statistical analysis which fits a curve to observed data relating the increase in NDT to the neutron exposure. The increase in NDT was assumed to vary as the cube root of the exposure, after a suggestion by Cottrell.* The result of the analysis is shown† in Fig. VII-1; the equation of the line, which resulted from a linear regression analysis, is $\Delta T_F = 31.084\ (\mathrm{nvt}/10^{17})^{1/3} + 2.087$, where ΔT_F is the increase in transition temperature in degrees Fahrenheit. Some points that were far from the curve were omitted from the regression analysis.

A summary of data[5] covers the effects of radiation on structural metals up to about the middle of 1961, and an appendix in reference 5 is a rather extensive annotated bibliography. References 6 and 7 are shorter reviews, and

*Porter[4] cites the following paper by A. H. Cottrell: Theory of Brittle Fracture in Steel and Its Application to Radiation Embrittlement, in *Conference on Brittle Fracture*, p. 1, Culcheth Laboratories, England, Nov. 1, 1957. Other correlations are mentioned in *Power Reactor Technology*, Vol. 3, No. 4.

†Figure VII-1 is reprinted here by permission from the American Society for Testing Materials.[4]

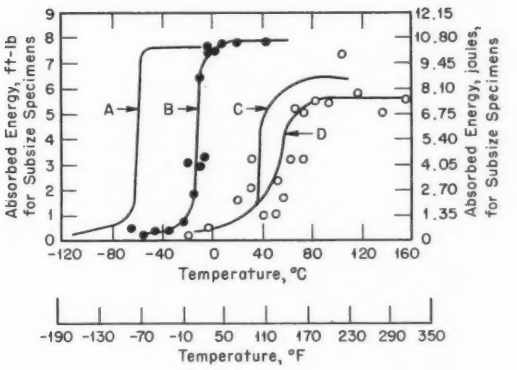

Fig. VII-2 Effect of annealing after neutron irradiation on the notch impact properties of ASTM A-201 mild steel.[11] *A*, unirradiated. *B*, ●, annealed 6 hr at 335°C (635°F) and irradiated to 6.2×19^{19} nvt; air cooled. *C*, irradiated to 6.5×10^{19} nvt. *D*, ○, annealed 6 hr at 260°C (500°F) and irradiated to 6.2×10^{19} nvt; air cooled.

references 8 and 9 are recently published Russian articles that consider some of the more basic aspects of radiation damage in metals. Reference 10 is a review stressing those aspects of the subject which are of importance in the practical application of the results to reactor pressure-vessel design and operation.

Inasmuch as some serious attention is being given to the possibility of annealing existing pressure vessels after they have accumulated some level of irradiation in service, to remove part or all of the deleterious irradiation effects, particular interest centers on the questions of how effective such annealing would be and what the temperature level and duration of the annealing process would have to be. The effects of temperature on radiation damage and on the recovery from radiation damage are complex. Although irradiation of carbon steels at rather high temperatures (above about 600°F) produces significantly less damage than irradiation at lower temperatures, temperatures in the intermediate range (between perhaps 230 and 540°F) appear to give greater damage than irradiation at lower temperatures. Similarly, when samples irradiated at low temperature were "annealed" at 500°F, the embrittlement apparently was actually increased somewhat, although annealing at the higher temperature of 635°F gave a significant recovery of ductility. The measurements of this effect are shown in Fig. VII-2, which is taken from reference 11. A further complication occurs because the temperature of irradiation apparently affects the response to annealing at a higher temperature. In general, an increase in the temperature of irradiation appears to require an increase in annealing temperature to achieve a given degree of recovery. A summary of the current status of practical knowledge concerning annealing effects is given in the following excerpt.*[10]

> Certain observations on the effects of postirradiation heat-treatment on the notch ductility of reactor pressure-vessel steels may be enumerated on the basis of the preliminary data:
>
> 1. For steels irradiated at low temperatures (200 to 300°F), essentially complete recovery is possible with a short-term heat-treatment at temperatures as low as 600°F.
>
> 2. After irradiation at higher temperatures, these same steels exhibit less recovery under comparable annealing conditions.
>
> 3. A re-embrittlement phenomenon following initial recovery of notch ductility appears after about 24 hr of annealing treatment.
>
> 4. The degree of re-embrittlement is apparently a function of the irradiation temperature, the total neutron exposure, and the time and temperature of postirradiation heat-treatment.
>
> 5. Annealing temperatures of 750°F or more are required to eliminate the re-embrittlement effect.

Austenitic stainless steels do not have a ductile-brittle transition either before or after irradiation. Irradiation does increase the hardness, yield strength, and ultimate strength and decreases the elongation, but there is no unacceptable deterioration even after quite large exposures. Table VII-1† shows the results of irradiation of type 347 stainless steel over a period of six years in a high-flux research reactor. The effects of postirradiation annealing of stainless steels have been studied, and it has been determined that irradiation effects can be practically completely removed by annealing, as illustrated in Fig. VII-3.‡ These samples were irradiated to 1.8×10^{20} nvt at 40 to 70°C and then annealed at a series of temperatures

*Reprinted here by permission from *Mechanical Engineering*.[10]

†Table VII-1 is reprinted here by permission from the *Journal of the British Nuclear Energy Conference*.[6]

‡Figures VII-3 and VII-4 are reprinted here by permission from the *Journal of Nuclear Energy, Parts A & B*.[8]

Table VII-1 EFFECTS OF HIGH NEUTRON DOSES ON ROOM-TEMPERATURE TENSILE PROPERTIES OF TYPE 347 AUSTENITIC STAINLESS STEEL[6]

Dose, neutrons/cm^2 (>100 ev)	Yield strength (0.2% offset), psi	Ultimate tensile strength, psi	Elongation, %	Reduction in area, %
0	61,600	95,800	63.2	78.0
2.4×10^{21}	98,000	109,000	51.6	78.5
7.2×10^{21}	97,300	109,700	50.6	77.8
2.6×10^{22}	100,800	107,250	44.0	65.0
3.76×10^{22}	106,930	115,310	32.0	74.0

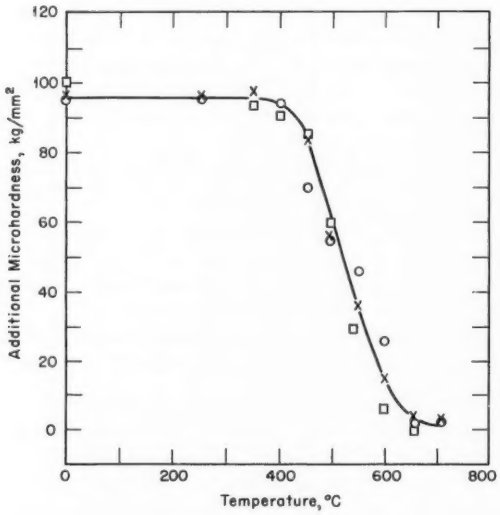

Fig. VII-3 Change in the increase in microhardness of irradiated steels as a function of annealing temperature.[8] ○, 18% chrome–9% nickel steel. □, 18% chrome–12% nickel steel. ×, 18% chrome–12% nickel–2% molybdenum-titanium stabilized steel.

for 30 min. After each anneal the microhardness was determined. It should be noted that unstabilized stainless steels, such as type 304, could be annealed for only a very short time in the 440 to 650°C temperature range owing to the occurrence of carbide precipitation.

Some attention has been given by Ibragimov et al.[8] to the mechanism of irradiation embrittlement. The theoretical analyses proceed from measurements of the rate of annealing of microhardness at different temperatures; a typical set of curves is shown in Fig. VII-4. The main features of the analysis may be summarized as follows:

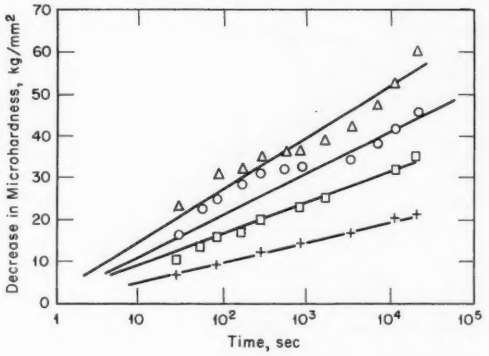

Fig. VII-4 Decrease in the microhardness of irradiated iron as a function of the time of holding at various temperatures.[8] △, 383°C. ○, 363°C. □, 347°C. +, 323°C.

1. The hardness increase results from radiation-induced lattice defects.

2. The flat section in the 363 and 383°C curves (Fig. VII-4) would indicate that, at the beginning of annealing of irradiated specimens, two types of radiation-induced defects are present with different degrees of thermal stability.

3. It was assumed that the decrease in hardness could be represented by the equation

$$\Delta H(t,T) = A_1 C_1^0 \left(1 - e^{t/g_1(T)}\right) + A_2 C_2^0 \left(1 - e^{t/g_2(T)}\right)$$

where $\Delta H(t,T)$ = the decrease in hardness
A_1 and A_2 = constants
C_1^0 and C_2^0 = the initial concentrations of type 1 and type 2 defects
t = annealing time
$g_1(T)$ and $g_2(T)$ = the mean times for removal of type 1 and type 2 defects at temperature T

4. By applying the analysis to the experimental data, it was established that the activation energy for the removal of type 1 and type 2 defects was 16,500 and 28,700 cal/mole, respectively. The reference discusses the possible natures of the two types of defects.

Materials for Nuclear Superheaters

Integral nuclear superheat reactors require materials for fuel jackets and other structural

applications which are capable of operation at high temperature in an atmosphere of direct-cycle steam. It is evident that low-cross-section materials for this application are not now available, and current designs rely on stainless steels or other alloy steels with high nickel content in the superheater sections. The adequacy of these alloys has not, however, been demonstrated in practice, and failures of experimental superheater elements in the Superheat Advance Demonstration Experiment (SADE) test loop in the VBWR have emphasized the possibility of corrosion difficulties.

In-pile testing in SADE has been in progress since the middle of 1959. Six fuel-element assemblies have been tested, the longest exposure having been 990 hr of operation to failure.[12–14] Two of these six tests were removed for scheduled examination after relatively brief in-pile exposures, but the other four elements failed at from 492 to 990 hr at temperatures corresponding to steam exit temperatures of 750°F or above. All these failures were caused by corrosive attack. A completely documented case[13] is that of fuel element SH-4B. This element was of the tubular type and was similar in configuration to the other elements tested; it had a fueled length of 3 ft, an outside diameter of $1\frac{1}{4}$ in., and an inside diameter of $\frac{3}{4}$ in. The steam coolant flowed downward on the outside and then up the inside of the tube. The fuel, UO_2 in hollow pellet form, was 4.55% enriched. The inner and outer cladding, which was weld-drawn tubing of type 304 stainless steel, had a wall thickness of 0.028 in. and was designed to collapse on the cladding. The intended operating conditions called for a maximum cladding temperature of 1200°F, producing 925°F (maximum) steam at 1000 psi. Actual irradiation of the element in the SADE loop was interrupted for three months, but, at the end of the initial 15-day period, a cladding temperature of 910°F had been attained for a period of 72 hr. During the second period of irradiation, the cladding temperature was increased again in steps until after 80 hr at 1150°F (steam exit temperature 850 to 900°F) failure occurred, after a total of 492 hr of irradiation.

Although the usual in-pile loop experimental difficulties had evidently been encountered, trouble was also experienced with exposure of the element to reactor water of comparatively high chloride (3 ppm) content from inleakage through a flange and from carryover with the steam during high-power operation or transient periods. The normal reactor water was in the 0.1-ppm chloride range. Samples of crud taken from a region near the defect on the element showed as much as 10,000 ppm chloride per 1,000,000 ppm iron in this deposit. Postirradiation examination also showed residual stresses as high as 36,000 psi in the jacket tubing.

The major defect found was a $\frac{1}{2}$-in. split near the middle spacer on the element outside diameter. Three pinholes were also found on the outside diameter, but the inside diameter was free of defects. Metallographic examination of the failed tube showed considerable carbide precipitation and grain-boundary attack, as might be expected in an unstabilized stainless steel operating in the sensitization range. Pictures of the major defect showed intense intergranular attack, with some grains completely pulled out in sectioning. Intergranular attack was also clearly evident in the pictures of the pinhole leaks; one example of a true transgranular crack near a weld area was observed. Similar modes of failure were evidently encountered in the other three failed elements, but the conditions detailed above, i.e., the presence of ample amounts of chlorides, high stresses, and operation in the sensitization range, for the SH-4B element, give the clearest indication of a situation in which intergranular stress-corrosion failure might be expected in an unstabilized stainless steel.

These early in-pile failures, however, are in contrast to the behavior of elements in out-of-pile tests under nominally similar conditions. Tests carried out by General Electric in the CL-1 superheated-steam out-of-pile loop[15] indicated good performance for type 304 stainless steel at metal temperatures up to 1100°F for test times up to 2500 hr. Both conventional coupons and specimens of the alloy as tubes with internal electrical heating were tested. These tubular heat-transfer specimens were arranged to provide heat fluxes of 175,000 Btu/(hr)(sq ft)—a realistic value for the expected fuel-element application. Steam was heated from 564°F (saturated) at the inlet to 1050°F at the outlet. Unlike most steam loop tests, these tests maintained 16 ppm of O_2 and 2 ppm of H_2 in the steam by the electrolytic decomposition of water. Such oxygen level should approximately duplicate the reactor oxygen content. The boiler water was held to a chloride content of 0.03 ppm, but this was

equivalent to 75 mg of chloride fed to the test section in 1000 hr of operation. Iron, chromium, copper, and nickel chlorides were identified in the scale. In this series of tests in CL-1, no failures were found from chloride stress corrosion, but the specimens were, of course, unstressed. Some intergranular attack occurred in areas of scale fluxing, but the general behavior was quite promising.

Since these rather optimistic results did not explain the subsequent in-pile failures discussed above, the CL-1 loop was later modified in an attempt to duplicate the SADE loop performance.[16] The chloride content of the feedwater was increased to 1.5 ppm, but the major alteration was the installation of a device that placed the test sheaths under a stress equivalent to a 0.1% elongation in 1000 hr. However, even with these modifications the early failures typical of the in-pile tests did not occur until the loop was operated in a manner that would expose the heated test surfaces to wet steam for an appreciable time. It was concluded that the presence of moisture in the steam was essential to the type of failure under investigation. Although transgranular cracks were occasionally found in these tests, gross grain-boundary attack on the highly sensitized metal was found in the specimens operated above 1000°F. The preponderance of intergranular attack might give rise to some speculation as to what the behavior of a stabilized stainless steel would have been under these conditions.

These in-pile and out-of-pile tests raise important questions as to the adequacy of the steels currently under consideration for nuclear superheat reactors. The susceptibility of the austenitic stainless steels to chloride stress corrosion is well known; however, tremendous quantities of these steels have been used in conventional steam-plant superheaters. Failures in these stainless-steel superheaters are certainly not unknown, but they obviously do not occur with a frequency that makes their use impractical. This seemingly better performance may be partially attributed to the very low oxygen content (< 0.1 ppm) in the steam and to the use of much thicker stainless-steel tubes. Thus the major question is whether the same stainless steels can be used in nuclear superheaters, where the sections must necessarily be thin and where the oxygen content of the steam is high (typically some 30 ppm). The work discussed above would indicate that the radiolytic oxygen content in reactor steam is not so important as the presence of moisture in the steam. However, other data[17] indicate that a relation may exist between the oxygen-chloride content and the susceptibility to stress corrosion of austenitic stainless steels exposed to the steam phase with intermittent wetting.

At present there are insufficient data to produce a meaningful correlation between in-pile and out-of-pile data or with conventional superheater operational data.

A literature search[18] has been made which sought information on the behavior of materials in conventional steam service and which compiled the available information on nickel-base and other high-temperature alloys. The objective of the search was to select the most promising nuclear superheat materials. Although the report is not all inclusive in an extremely complex field, it cites some 146 references. Some of the more important conclusions can be briefly summarized:

—No present application exactly duplicates nuclear superheat conditions. In industrial applications, when the austenitic stainless steels have been subject to failure, preventive measures, short of the substitution of an alternate material, have in general been unsuccessful. Inconel has shown generally better resistance to stress-corrosion cracking than the austenitics. At the present state of knowledge, it is not possible to predict the resistance of a given alloy to stress corrosion in a new environment.

—None of the numerous theories of stress corrosion appear to explain all the phenomena. The aluminum-containing ferritic steel (406) shows promising corrosion behavior. Nickel contents above 35% increase resistance to stress corrosion. The ferritic lattice appears inherently more resistant to stress corrosion than the austenitic lattice.

—The survey of the available information resulted in the selection of Inconel, Incoloy, Hastelloy X, RA-330, Hastelloy N, Nionel, AISI-406, IN-102, and 17-4 CuMo as the most promising of candidate materials. The selection was based on the predicted corrosion performances of the alloys and on their strength and mechanical properties, availability, cost, formability, and fabricability. With the exception of AISI-406, the alloys have comparatively high cross sections.

It was apparent from the literature survey that, although several apparently attractive materials may be available (at the cost of high neutron absorption), the information regarding them is too limited to define the best choice without considerable experimental work.

Graphite

The problem of the extent of dimensional changes in moderator graphite after long exposures at high temperature is important to the design of such power reactors as the Experimental Gas-Cooled Reactor (EGCR). An experiment carried out by Hanford[19] personnel at the General Electric Testing Reactor (GETR) measured contractions and changes in interplanar spacings of graphites of different fabrication histories. The irradiation was carried out in a special capsule in which heat was supplied from gamma energy only. The thermocouples failed during irradiations; however, during the time the thermocouples remained in operation, their readings were in agreement with the estimated temperatures. The exposure time was 75.6 days at full power, and the calculated maximum flux was 3.2×10^{21} nvt (>0.18 Mev), a flux equivalent to 24,000 Mwd/adjacent ton* for a conventional graphite-moderated reactor. Although nickel (n,p) flux monitors were included in the capsule, difficulties were encountered with the experimental measurements, and reliance was placed on the calculated values for integrated flux. Those difficulties in direct measurement were attributed to the uncertainty in the effective thermal-neutron cross section of the Co^{58} product of the nickel (n,p) reaction, which consists partly of short-lived metastable Co^{58m}. The metastable isomer is believed to have an absorption cross section greater than 150,000 barns.[19] For temperatures in the 800 to 1200°C range, it appeared that the needle-coke graphites showed the lowest contraction and that high graphitization temperatures (>3100°C) plus the use of "flour" (small particle size) filler produced a superior product.

Another test[20] by the Hanford group exposed EGCR graphite in the GETR to 38,000 Mwd/adjacent ton [5.7×10^{21} nvt (>0.18 Mev)], the highest graphite exposure so far reported. Two capsules were employed sequentially. The irradiation of most of the specimens was carried through from the first to the second capsule. Specimen temperatures were between 475 and 850°C. In this test eight of the nine thermocouples used in each capsule remained in operation through the irradiation. The difficulties with direct flux measurements discussed above were also encountered so that reliance was placed on calculation for the integrated flux values. The EGCR graphite showed a contraction rate of −0.15% per 10^{21} nvt at 575°C. Contraction was greater in the transverse direction than in the parallel direction. No important differences were found in the behavior of specimens from various locations in the extruded bar, and no indication was found that the rate of contraction lessens with continued exposure.

In addition to the problem of dimensional changes in graphite, the matter of the effect of irradiation on thermal conductivity is important to all graphite-moderated-reactor designs. For reactors employing canned graphite, the question of gas release by irradiation and temperature effects is also quite important. The Sodium Reactor Experiment (SRE), for example, is concerned with gas release to a much greater extent than with mechanical properties since the graphite in the design has no load-bearing requirements. Work reported by Atomics International[21] showed no gas-pressure buildup in stainless steel or zirconium cans containing TSP graphite at temperatures between 300 and 400°C at irradiation levels up to 1.8×10^{21}. The fact that the pressure changes within the cans were completely accounted for by the gas laws, on the assumption of no increase in number of moles of gas, was attributed to "gettering" of the desorbed gas by the stainless-steel or zirconium cans. Measurement of 33 of the specimens showed all dimensional changes to be less than 0.1%.

Thermal-conductivity changes were measured on TSP, CS-GBF, CS-AGOT, TS-AGOT, and TS-GBF graphite that had been exposed to temperatures between 300 and 440°C and to integrated fast-neutron fluxes (>1 Mev) in the 1.0 to 2.5×10^{20} nvt range. A radial heat flow apparatus was used, calibrated against Armco iron specimens. For the 20 specimens tested, the k_0/k (thermal-resistivity ratio) values varied from 1.55 to 3.30 at 30°C. For TSP graphite, k_0/k

*Megawatt-days per ton of uranium fuel adjacent to the graphite.

values of 1.58, 1.51, and 1.44 were measured at 400, 500, and 600°C, but 1 hr at 1000°C removed 30 to 45% of the radiation damage. For the exposures employed the amount of radiation damage was independent of temperature between 300 and 400°C.

The Harwell workers have investigated the effects of irradiation on the thermal conductivity, thermal expansion, Young's modulus, and crystal lattice spacings of graphite.[22] Experiments were carried out in DIDO and PLUTO. The capsules were provided with electrical heating in addition to the gamma heating so that temperature control was sufficiently precise to maintain the specimen temperatures within a range of −0 to +10°C of nominal values. Because of the difficulties with nickel flux monitors, as discussed above, cobalt monitors provided the basis for flux measurements. In the range studied (150 to 360°C), considerable increases in thermal resistivity were found which, of course, decreased with increasing temperature. At 350°C, k_0/k rose to 4.25 for a dose of 5.9×10^{20} nvt. Annealing was fastest (i.e., the recovery of conductivity per degree of temperature increase was largest) at 1100°C. At an annealing temperature of 1500°C, little damage remained, and this remainder was removed at 1850°C.

The thermal-expansion data showed considerable differences in behavior between specimens cut perpendicular and parallel to the extrusion direction when they were irradiated at 150 and 200°C. At 250°C the behavior of the two sets of specimens was similar, but at 350°C the perpendicular specimens showed much higher total changes in expansion. Irradiation effects on Young's modulus were also complex, and the direction of cut and the irradiation temperature had a marked effect on specimen behavior.

Zirconium

Considerable interest has recently been shown in zirconium alloys for possible use in steam at temperatures from 300 to 600°C. Harwell[23] has reported in-pile work at the British Experimental Pile O (BEPO) on Zircaloy-2 in steam. The comparatively low flux (not given) available in this reactor more than doubled the rate of oxide film growth on Zircaloy-2 in steam at high temperatures. The action was most marked at 450 and 500°C and decreased at 600°C. At 350°C no effect was found. The marked decrease in corrosion resistance was attributed to the fast-neutron component, since experiments in pure gamma flux showed no effect and since the shielding out of most of the thermal neutrons by the use of pyrex ampoules caused no change. Such a serious deterioration in corrosion resistance as a result of reactor radiation has apparently not been reported previously for Zircaloy-2. If confirmed, these results would throw doubt on the use of zirconium at temperatures much above present levels. Out-of-pile work is also reported in the same paper on alloys such as zirconium−2½% niobium, zirconium−½% copper−½% tungsten, as well as on the Zircaloys, in steam at 400 and 500°C. From the standpoint of hydrogen absorption, the zirconium−½% copper−½% tungsten alloy was found to be superior.

In contrast to this rather discouraging in-pile work, other British workers[24] have reported a new technique for improving the corrosion characteristics of zirconium in high-pressure steam. The technique was discovered when it was observed that pure zirconium, when exposed to 1000-psi steam at 500°C in pyrex capsules, showed anomalously low rates of weight gain. It was then found that pure zirconium, which would ordinarily gain 5400 mg/dm² in 500°C 1000-psi steam in the first 24 hr of exposure in a stainless-steel autoclave, would, when 30 g of powdered pyrex glass was added to the autoclave, gain only 30 mg/dm². This marked inhibitory effect was found also when pure boron was added to the autoclave and, to a somewhat lesser extent, in alloys containing from 0.3 to 1.0 wt.% boron. However, the inhibitory effect appeared to make little difference in the hydrogen absorption by the specimens. Preliminary short tests of aluminum and beryllium in boron-steam also showed substantial decreases in corrosive attack. With regard to the mechanism by which boron produces its beneficial effect, it appears that the protective oxide films in inhibited steam show less cracking than in normal steam, and the authors suggest that the boron may modify the mechanical properties of ZrO_2 in the vicinity of crack tips to inhibit crack propagation.

Uranium Metal

Uranium as metal would be the preferred fuel for some reactor types if it were not for the

temperature limitations of the metal. One of the major limitations on temperature is, of course, the swelling of the metal due to fission-gas release and pore formation. Experimental studies of gas release and swelling are beset with all the difficulties to be expected in attempting to make precise measurements of burnup, fluxes, and in-pile specimen temperatures.

Work at Hanford[25] has, however, provided data pertinent to one of the basic questions concerning swelling in irradiated uranium, i.e., whether the volume changes found in uranium irradiated at high temperature are, or should be, the same as those found in cool-irradiated uranium annealed out of pile.

Two sets of experiments were carried out. In the first, three NaK capsules, each containing an unalloyed uranium rod that was coextrusion clad with Zircaloy-2, were irradiated in the Materials Testing Reactor (one capsule) and the Engineering Test Reactor (two capsules) to burnups of 0.19 to 0.26 at.%. These burnup figures were derived from heat-generation data, but in the case of one capsule the calculated value was found to be within 15% of the figure obtained from chemical analysis for burnup. The significant specimen temperature was assumed to be the maximum volume-average temperature during the last 10% of the exposure. In view of the complex relations between time, temperature, burnup, and swelling, and the variations to be expected in in-pile operation, this temperature is probably as meaningful as any which could be selected. The values of this temperature were 385, 482, and 605°C for the three capsules.

For the annealing experiments, beta heat-treated, unclad uranium rods were inserted in stainless-steel cans and irradiated in a water loop. The volume-average temperature of the metal was estimated as 550°C at the start, dropping to 350°C at the end. Burnups were determined by chemical analysis. Annealing for both 1- and 100-hr periods was carried out at six temperatures between 400 and 880°C. Densities were determined by buoyancy techniques in tetrabromoethane, and the total porosity was calculated from microscopic pore measurements. Plotting of the swelling as R (the change in volume divided by burnup) versus the temperature — either that of the irradiation or that of the ex-reactor annealing — gave surprisingly good agreement, and the authors state that post-irradiation annealing experiments may provide reasonably accurate predictions of swelling behavior.

Savannah River[26] has also reported on uranium irradiation. This irradiation was carried out in an engineering investigation of the behavior of a prototype fuel element for a heavy-water reactor. Although an exposure of only 955 Mwd/ton was attained, the heat fluxes [275,000 pcu/(hr)(sq ft)] and surface temperatures (250°C maximum) used were realistic relative to the expected use of the element. The experimental fuel element was fabricated by Nuclear Metals by a coextrusion process, which produced the tubular element with core, cladding (Zircaloy-2), and end seals in one extrusion operation. The element was 11 ft in overall length and had a 9-ft fueled length; the outside diameter was 2.07 in., and the inside diameter was 1.46 in. The element was irradiated in the high-pressure water-cooled E-20 loop at Chalk River. It had been originally intended to expose the element for a longer period, but mechanical difficulties prevented its reinsertion in the loop. The total exposure of 995 Mwd/ton is relatively low, but the observations that the general appearance of the exposed element was good, that no measurable bowing was found, that diametral changes were minor, and that the volume change in the uranium was only $1\frac{1}{2}$% would indicate generally promising behavior for the element.

Argonne[27] is continuing to report data on the first core of the Experimental Breeder Reactor No. 1 (EBR-I). Although these irradiations were finished in 1954, the information on the behavior of the uranium–2 wt.% zirconium alloy is still of importance. The alloy rods tested had had six different heat-treatments, and the different positions of the specimens in the core had resulted in burnups for slugs of from 0.08 to 0.189 at.% with calculated metal temperatures of 307 to 383°C. Volume increases were from 2.1 to 15.5%, with length changes of the slugs ranging from +2.96 to −0.39%. The combination of the six metallurgical histories with the various irradiation exposures and temperatures made interpretation difficult, but it was apparent that the as-cast alloy specimens exhibited more dimensional stability than the wrought slugs. Water quenching of the wrought specimens from 800°C produced a more stable material than did slow cooling.

References

1. USAEC Conference on the Status of Radiation Effects Research on Structural Materials and the Implications to Reactor Design, Chicago, Illinois, October 15–16, 1959, USAEC Report TID-7588, October 1960.
2. J. R. Hawthorne and L. E. Steele, The Effect of Neutron Irradiation on the Charpy V and Drop-Weight Test Transition Temperatures of Various Steels and Weld Metals, in USAEC Conference on the Status of Radiation Effects Research on Structural Materials and the Implications to Reactor Design, Chicago, Illinois, October 15–16, 1959, USAEC Report TID-7588, p. 140, October 1960.
3. A. D. Rossin, Radiation Damage in Steel: Considerations Involving the Effect of Neutron Spectra, *Nucl. Sci. Eng.*, 9(2): 137 (February 1961).
4. L. F. Porter, Radiation Effects in Steel, presented at the Symposium on Materials in Nuclear Application, *Am. Soc. Testing Mater., Spec. Tech. Publ. No. 276*, 1959.
5. F. R. Shober, The Effect of Nuclear Radiation on Structural Metals, REIC Report 20, Radiation Effects Information Center, Battelle Memorial Institute, Sept. 15, 1961.
6. H. M. Finniston, Some Metallurgical Features of Nuclear Reactors, *J. Brit. Nucl. Energy Conf.*, 5(1): 37 (January 1960).
7. D. R. Harries, The Effects of Neutron Irradiation on the Properties of Iron and Steels, *J. Brit. Nucl. Energy Conf.*, 5(3): 133 (July 1960).
8. S. S. Ibragimov et al., An Investigation of the Structure and Properties of Several Steels and Other Metals After Irradiation with Fast Neutrons, *J. Nucl. Energy, Pts. A & B*, 16: 45 (January 1962).
9. I. M. Boronin et al., Mechanical Properties and Microstructures of Certain Structural Materials After Neutron Irradiation, *J. Nucl. Energy, Pts. A & B*, 16: 93 (February 1962).
10. J. R. Hawthorne et al., How Neutron Exposure Alters Reactor Steels, *Mech. Eng.*, 84(5): 64 (May 1962).
11. P. P. Trudeau, Effects of Neutron Irradiation on Mechanical Properties of Ferritic Steels and Irons, *Proceedings of the Second United Nations International Conference on the Peaceful Uses of Atomic Energy, Geneva, 1958*, Vol. 5, p. 475, United Nations, New York, 1958.
12. R. T. Pennington, Nuclear Superheat Project Tenth Quarterly Progress Report, October–December 1961, USAEC Report GEAP-4024, General Electric Co., Atomic Power Equipment Dept.
13. C. N. Spalaris et al., Design, Fabrication, and Irradiation of Superheat Fuel Element SH-4B in VBWR, USAEC Report GEAP-3796, General Electric Co., Atomic Power Equipment Dept., Sept. 1, 1961.
14. R. T. Pennington, Nuclear Superheat Project Ninth Quarterly Progress Report, July–September 1961, USAEC Report GEAP-3877, General Electric Co., Atomic Power Equipment Dept.
15. G. G. Gaul and W. L. Pearl, Corrosion of Type 304 Stainless Steel in Simulated Superheat Reactor Environments, USAEC Report GEAP-3779, General Electric Co., Atomic Power Equipment Dept., Oct. 16, 1961.
16. G. G. Gaul et al., Stress Corrosion of Type 304 Stainless Steel in Simulated Superheat Reactor Environments, USAEC Report GEAP-4025, General Electric Co., Atomic Power Equipment Dept., Feb. 26, 1962.
17. D. J. DePaul (Ed.), *Corrosion and Wear Handbook for Water Cooled Reactors*, pp. 201–204, McGraw-Hill Book Company, Inc., 1957.
18. C. N. Spalaris et al., Materials for Nuclear Superheat Applications—A Literature Survey, USAEC Report GEAP-3875, General Electric Co., Atomic Power Equipment Dept., Jan. 5, 1962.
19. J. M. Davidson and J. W. Helm, The H-1 High Temperature Graphite Irradiation Experiment, USAEC Report HW-64286, Hanford Atomic Products Operation, April 1961.
20. J. M. Davidson and J. W. Helm, The H-3 Irradiation Experiment: Irradiation of EGCR Graphite, Interim Report No. 1, USAEC Report HW-71500A, Hanford Atomic Products Operation, Oct. 16, 1961.
21. J. J. Gill and R. E. Taylor, Radiation Effects on Moderator Graphite in the SRE, USAEC Report NAA-SR-6404, Atomics International, Jan. 15, 1962.
22. W. N. Reynolds and J. N. W. Simmons, The Effect of High Flux Neutron Irradiation on the Physical Properties of Graphite, British Report AERE-R-3871, November 1961.
23. B. Cox, Some Studies of the Compatibility of Zirconium Alloys with Steam, British Report GCM/UK/35, February 1962.
24. C. F. Britton and J. N. Wanklyn, Inhibition by Boric Acid of the Oxidation of Zirconium in High Pressure Steam, *J. Nucl. Mater.*, 5(3): 326 (April 1962).
25. T. K. Bierlein et al., Swelling in Uranium: A Comparison of the Effects of Irradiation and Postirradiation Annealing, USAEC Report HW-69393, Hanford Atomic Products Operation, April 1961.
26. R. C. Pugh, Irradiation of a Uranium Metal Fuel Tube at Chalk River, USAEC Report DP-667, E. I. du Pont de Nemours & Co., November 1961.
27. W. F. Murphy et al., Examination of Uranium–2 Wt.% Zirconium Experimental Fuel Slugs Irradiated in EBR-I, USAEC Report ANL-6114, Argonne National Laboratory, February 1962.

Section

VIII

Power Reactor Technology

Radioactivity Problems

Deposition and Decontamination

It is well known that the coolant systems of pressurized-water reactors gradually accumulate deposits of radioactive materials as operation proceeds. Although these deposits are far less troublesome than the early developers of the pressurized-water systems had feared they might be, they nevertheless do represent a real inconvenience, and it is important to understand how their formation may be minimized, and how they may best be removed from time to time as may be necessary to facilitate maintenance and to keep radiation levels within reasonable bounds. A Hanford report[1] describes experiments on the deposition of radioactivity in pressurized-water loops, and other reports[2–5] cover decontamination.

Four Hanford K recirculation test loops were used in the study of deposition. These loops, whose normal function is the in-pile testing of fuel elements, simulate rather well the conditions in the primary coolant system of a pressurized-water reactor. The loops were, however, employed for their normal function during the deposition tests, and consequently the test program did not have complete freedom in the selection of test variables. A diagram of a typical loop is shown in Fig. VIII-1. The in-reactor portion (the process tube) was Zircaloy-2. In three of the loops the outside portion was AISI type 304 stainless steel, and in the fourth loop it was carbon steel. The outlet temperature from the process tube ranged from 185 to 270°C, and the loop was pressurized to about 1650 psi. Heat was generated in the process tube by test fuel pieces installed therein.

In addition to observations of deposition in the loop proper, measurements were made of deposition on coupons of various alloys which were installed in a section of Zircaloy tube piping (the mockup tube, Fig. VIII-1) connected in parallel with the main loop piping. This tube was located 150 to 175 ft from the reactor, its inside diameter was 2.09 in., and the flow in the tube was regulated to approximately 18 gal/

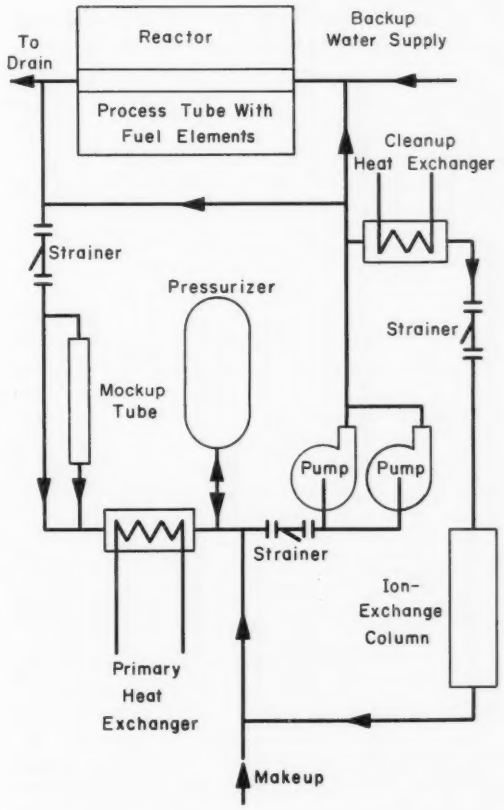

Fig. VIII-1 Schematic diagram of typical Hanford K loop.[1]

min. The alloys tested were AISI types 304 and 316 stainless steels, A-245 carbon steel, X-8001 aluminum alloy, Inconel X, Monel, Zircaloy-2, and Stellites 6 and 12. Samples tested were polished coupons, coupons on which an oxide film had been previously formed, and coupons that had been previously subjected to decontamination procedures. The water used was a high-purity demineralized water. Preliminary observations were made with high, low, and neutral *p*H, but the main body of information was taken with high-*p*H water, consistent with anticipated conditions in the New Production Reactor (NPR); the *p*H was maintained at about 10 by LiOH solutions and lithium-based ion-exchange resins.

Many pages of tabular data, which cannot be summarized here, are included in the report.[1] In general, it was found that most of the corrosion and wear products originate in the out-of-reactor portions of the circuits, although small fractions come from the Zircaloy in-reactor portion. In the coolant circuit this material passes through the reactor section and becomes activated; it may recirculate for several cycles, acquiring further activation, before it is deposited somewhere in the coolant loop or removed by the coolant cleanup system. The summary of results and conclusions is quoted below:

1. Significant quantities of Na^{22}, Cr^{51}, Mn^{56}, Fe^{59}, Co^{58}, Co^{60}, Cu^{64}, As^{76}, Se^{75}, Zr^{95}-Nb^{95}, Ag^{110m}, Sb^{124}, and Np^{239} were adsorbed on A245 carbon steel, AISI 304 and AISI 316 stainless steels, Stellites 6 and 12, and Zircaloy-2 test coupons, all of which were exposed to a high-temperature high-*p*H coolant in a carbon steel loop system. With the exception of Np^{239}, the same species also were the prime activity contributors on A245 carbon steel, AISI 304 stainless steel, and Zircaloy-2 in a stainless steel loop operating with a high *p*H coolant. Comparable systems would have the same radioactive species and comparable activity levels if the operating conditions were the same.[*]

2. Generally, the adsorption data for Na^{22}, Cr^{51}, Fe^{59}, and Se^{75} in the carbon steel system and Cr^{51}, Fe^{59}, Co^{58}, and Co^{60} in the stainless steel system increased in regular, systematic fashions. This permitted plots of radioactivity levels with respect to time. Adsorption trends can be predicted from these data.

3. Autoradiographs of contaminated specimens from stainless and carbon steels with high *p*H coolants showed that the radioactivity was associated with two different materials on the metal oxide surfaces: particulate and adsorbed materials. The autoradiography results also suggested that a significant portion of the transported radioactive material in these systems was associated with small particulate matter—a heavier concentration of adsorbed radioactive material appeared on the bottom half of the horizontal pipe.

4. Radiation readings and autoradiography showed that deposition and adsorption of radioactive materials in the K loops depended on temperature. This was discovered during the examination of a two-pass heat exchanger. Most of the radioactivity was concentrated in the first pass (the region with the highest temperature drop).

5. In almost all cases, prefilming of carbon and stainless steel specimens in noncontaminated, high temperature systems reduced the amount of activity adsorbed by these test pieces when they were exposed in radioactive systems. Prefilming of both carbon and stainless steel systems with a high temperature oxide film before in-reactor operation would reduce the adsorbed activity levels.

6. Inconclusive results were obtained in the study to determine the effect of coupon orientation to coolant flow on radionuclide adsorption.

7. Generally, decontamination pretreatments of test specimens increased the amount of adsorption. This increase also was noted for Zircaloy-2. However, it had no operational significance for Zircaloy-2, since it was discovered that none of the decontaminating processes used as pretreatments can remove the high temperature oxide film from this material after it has formed.

8. Film stripping with cellulose acetate demonstrated that less than 26 per cent of the activity found on test specimens of carbon steel and stainless steel was particulate or loosely adhering matter.[*]

9. The major constituent in the oxide films in the high temperature carbon steel loop was identified as Fe_3O_4 by X-ray powder photography. Some traces of γFe_2O_3 also were found in these films. In the high temperature stainless steel loop operated with a high *p*H coolant, the films were αFe_2O_3 and γFe_2O_3.

10. The (n,γ) reactions provided most of the activity associated with coolant systems operating at high, neutral, and low *p*H. However, the (n,p) reaction in the high *p*H stainless steel system provided an important portion of the total adsorbed activity.

11. The adsorbed activity levels were somewhat higher on test specimens exposed in the high *p*H coolant in the stainless steel loop system than they were in a carbon steel system in a given exposure time.

*Quotation corrected by letter from HAPO. — *The Editor*

12. Inconel X and Monel, when exposed to neutral and low *p*H coolants, adsorbed very large amounts of Ag^{110m}. The behavior of these two alloys would preclude their use with low *p*H coolants unless this troublesome isotope can be removed from the system.

13. The Ag^{110m} isotope was one of the major radioactive species adsorbed on all metals in neutral and low *p*H coolants. One of the major activity problems associated with the operation of low *p*H coolants would be solved if the source of this material could be eliminated.

14. Only a small portion of the adsorbed activity in the K loops resulted from the activated corrosion products of the in-reactor tube itself. In the pressure-tube type of reactors at Hanford, the primary source of activated corrosion products is the out-of-reactor portion of the loop.

15. Further work is needed to define fully the activity adsorption mechanisms in the pressurized water reactor coolant systems at Hanford.

The most recent report on decontamination of water-cooled reactor systems is a progress report[2] on the decontamination study that is being carried out at Hanford. References 3 and 4 are previous progress reports on this project. A brief general review of the subject of decontamination, with an extensive bibliography, is given in reference 5.

The basic problem in decontamination of reactor systems is to find a solvent or reagent that will dissolve or remove the radioactive deposits without attacking the base metal to a serious degree. The problem is particularly difficult because the contaminants may not be in the form of a simple mechanical deposit. In particular, the oxide film on the metal often is the haven for the deposition and adsorption of the activated metal, and removal of the contamination may involve the removal of the oxide film. In such a case the film must be removed with as little corrosion of the metal as possible, and some sort of protective film should be redeposited.

The Hanford decontamination study is attacking both the decontamination problems associated with activated corrosion products and those associated with deposits from failed fuel elements. The program encompasses a wide range of experimental approaches, including laboratory evaluations, pilot-plant tests, and in-reactor demonstrations. At the present stage of the project, the procedures recommended for Hanford reactor types—which may not be optimum but have been shown to be effective—are summarized in the following quotation:[2]

1. To decontaminate a stainless steel reactor, containing no carbon steel in the primary system, the APACE procedure is the most satisfactory. The APACE procedure consists of recirculation of alkaline permanganate followed by a water flush, and a recirculation of inhibited ammonium citrate followed by a water flush. If rupture debris and fission products are present, as after failure of a fuel element, the APACE procedure should be preceded by recirculation with 10 volume per cent (vol.%) nitric acid. In case only rupture debris is present, the nitric acid treatment may suffice and the APACE will not be required.

2. To decontaminate a reactor in which at least part of the primary system is of carbon steel, the recommended procedure consists of: (a) recirculation with alkaline permanganate followed by a water flush and (b) recirculation with a bisulfate compound, followed by a water flush. If fission products and rupture debris are present, this process should be preceded by recirculation with a solution containing sodium carbonate, sodium bicarbonate, and hydrogen peroxide to dissolve the uranium oxides.

3. To decontaminate only the carbon steel portion of the reactor, the alkaline permanganate may be omitted. This procedure is simpler but, in some cases, has not been too effective. Phosphoric acid mixtures may be substituted for the bisulfate mixtures.

4. For the present Hanford low-temperature reactors cooled by once-through treated river water, a proprietary compound based on sulfamic acid has given the best results. Results from preliminary testing with a sulfuric-oxalic acid mixture appear promising.

The report[2] also discusses the criteria for satisfactory decontaminants, laboratory tests of new inhibitors and reagents, and procedures for dissolving UO_2 from a loop system after a fuel-element rupture.

Studies conducted at the Savannah River Laboratory on the decontamination of type 304 stainless-steel heat exchangers are reported in reference 6. Static and dynamic decontamination experiments were done in the laboratory with approximately nine different decontaminating solutions, using sections of tubing removed from the contaminated heat exchangers. The recommended decontaminating agent was a 10 wt.% oxalic acid solution, with 0.01*M* ferric sulfate added as an inhibitor, and was used on the full-size units. The report gives detailed procedures on the design of the decontamina-

Table VIII-1 DECONTAMINATION RESULTS[6]

Heat exchanger	1	2	3	4	5
Time in service, months	57	64	84	60	74
No. of acid flushes	3	2	1	2	1
Total activity removed:					
Nonvolatile beta, curies	1.7	6.3	3.4	1.5	3.5
Alpha, microcuries	2550	2380	0	641	2300
Radiation level of hot end tube sheet:					
Before (mr/hr at 3 in.)	150	300	*	*	*
After (mr/hr at 3 in.)	50†	20	300	40	150
Decontamination factor	3†	15	*	*	*

*The heads were not removed before decontamination flushing; therefore "before" readings were not obtained, and decontamination factors were not calculated.

†Later the radiation level was reduced and the decontamination factor was increased by cleaning activity from the blind staybolt holes in the tube sheet.

tion facility used and the steps in the decontamination procedure. Table VIII-1 shows some of the results.

Radioactive Maintenance on VBWR

Reference 7 is an account of modifications to the Vallecitos Boiling-Water Reactor (VBWR) which involved radioactive portions of the plant; it is useful as a description of the practical solutions that were found to problems of major maintenance operations on an activated boiling-water reactor system.

The major modifications to the reactor consisted of the replacement of the single original recirculation pump by two pumps of larger capacity, the necessary rearrangement of piping, and the installation of a new reactor-vessel core structure to reduce core bypass leakage.

The removal of the old pump and piping and the replacement of the core structure were carried out by General Electric personnel; the new pump and piping installations were made by contractor personnel without previous experience on radioactive systems. Special emphasis was given to careful planning of the work and to rehearsals of procedures and practice on mock-ups.

Many operations were to be carried on in the reactor enclosure building, where special care was required to minimize the dispersal of airborne radioactivity that might interfere with work scheduled to be run concurrently. Special portable exhaust hoods were designed for welding and cutting operations, which were effective enough that only the workmen actually doing the welding, grinding, and cutting had to wear fresh-air masks. The exhaust was filtered and conducted into the stack where the regular monitoring system kept watch on the exhaust to the atmosphere.

There were several operations to be performed in connection with the modification:

1. Cut and prepare old piping for the welding in of new sections
2. Locally decontaminate the open ends of the pipe
3. Weld in new piping
4. Remove old core structure
5. Perform annual boiler inspection required by law
6. Remove and reinstall control rods
7. Install new core structure

A power hacksaw of an unusual, but commercially available, type was used to make the cuts in the existing piping, since this reduced the amount of grinding necessary to prepare the cut ends for rewelding and also produced much less airborne radioactivity than the arc-air cutting rig originally contemplated. The significant feature of the hacksaw was that it clamped onto, and supported itself by, the pipe being cut. After cutting, the open ends of the pipe were brushed and scrubbed to reduce the radioactivity coming from these sources. This procedure proved effective and accomplished the purpose at low cost. To reinstall the new piping, a root pass was made first, using the exhaust hoods and fresh-air masks. After this was done, the contamination was contained in the piping and the rest of the welding was done in a near-normal manner without hoods or fresh-air masks.

The removal of the old core structure, which was quite hot, required some special temporary construction. A special dock, runway, and track with dolly were built through the removable patch in the containment vessel so that heavy loads could be handled. The core structure was lifted out and dropped into the adjacent fuel-storage pool, where it was cut up and loaded into drums for disposal in the plant waste-disposal area.

With careful planning and careful monitoring, an internal inspection of nozzle welds was made in the vessel by the state-licensed inspector without exceeding the allowable limits of radiation exposure.

Initial plans were to remove the control rods by encasing them in a shielding cask. Experience proved, however, that they could be transferred to the pool rapidly enough without the cask to avoid exceeding permissible personnel exposure limits, even though the estimated radiation level at the tip of the hottest rod was 5000 r/hr.

When the reactor vessel was open and stripped, the vessel liner was found to be slightly bulged and cracked where it was welded to the vessel walls near the vessel flange. The liner was removed and replaced during the shutdown. This was mostly a straightforward job, but special attention had to be given to the control of airborne radioactivity.

As a result of the experience gained in this work, it was concluded[7] that the maintenance problems in a nuclear plant need not be appreciably more difficult than in a fossil-fueled plant if proper attention is given to developing sound plans and techniques for carrying out the work.

Effect of Gamma Radiation on Ion-Exchange Resins

The most effective way of minimizing contamination in a water-cooled reactor system is to maintain a high degree of water purity by an effective cleanup system. In such a system most of the radioactive material will be collected in the filters and ion exchangers, whence it can be disposed of with relative ease. In such an application the ion-exchange resins will obviously be exposed to large doses of gamma radiation from the collected radioactive ions, and it is essential to determine that this gamma exposure will not seriously impair the effectiveness of the resin. Reference 8 is a report on the effects of gamma doses (in the range of 10^8 to 10^9 rads) on the physical and chemical properties and the specific capacities of four different ion-exchange resins.

Table VIII-2 shows the results obtained from the capacity measurements after irradiation of the cation resins; Table VIII-3 shows the same information with respect to the anion resins. The general results are quoted as follows:[8]

> These investigations showed that the main source of radiation damage to mono-functional cation exchange resins of the sulfonated polystyrene type is in breaking of the cross-linkages, while quaternary amine anion resins suffer more extensive damage through degradation of functional groups. The extent of damage to the anion resins is dependent on the nature of the functional group and the attached ion.

Detection of Fuel-Element Failures

Reference 9 describes an instrument for the detection (but not the location) of fuel-element failures in the Savannah River reactors. In these reactors the D_2O moderator-coolant is blanketed by a helium cover gas. Fuel-element failures release fission-product krypton and helium, which find their way into the cover gas. The instrument takes samples of the cover gas periodically (every 10 min) on an automatic cycle, separates the fission gases from background radioactive gases (such as Ar^{41}) by gas chromatography, and makes a quantitative analysis of the fission-gas content by means of a beta scintillation counter.

The cycle of the instrument starts with an automatic sampling of the cover gas, which is passed through a chromatograph column. This column is a tube filled with a molecular-sieve material. Different gases have different retention or passage times, and an automatic timer vents off the unwanted gases and passes the fission gases to a counting cell where a count rate meter determines the amounts present, down to trace quantities. This intelligence is recorded on a chart, and, if the fission-product content exceeds certain preset values, an alarm is actuated.

The material in the chromatograph column is easily poisoned by water vapor and CO_2 or other acid gases; therefore a pretreatment of the sample gases is necessary to remove these substances. The pretreatment apparatus is a trap containing another molecular-sieve material of different arrangement which retains

Table VIII-2 EFFECT OF GAMMA RADIATION ON CATION-EXCHANGE RESINS[8]

Resin	Irradiation conditions	Dose, rads	Total capacity, meq/g of dry resin	Salt-splitting capacity, meq/g of dry resin
Dowex 50W-X12, 50–100 mesh	H form	None	5.17	5.17
Dowex 50W-X12, 50–100 mesh	H form, immersed in H_2O	0.88×10^8	5.09	5.04
Dowex 50W-X12, 50–100 mesh	H form, dry	0.76×10^8	5.00	4.98
Dowex 50W-X12, 50–100 mesh	H form, dry	1.10×10^8	5.19	5.00
Dowex 50W-X12, 50–100 mesh	H form, dry	2.67×10^8	5.19	4.78
Duolite C-10, 16–40 mesh		None	6.80	3.68
Duolite C-10, 16–40 mesh	H form, dry	1.5×10^8	6.24	3.06

Table VIII-3 EFFECT OF GAMMA RADIATION ON ANION-EXCHANGE RESINS[8]

Resin	Irradiation conditions	Dose, rads	Total capacity, meq/g of dry resin	Salt-splitting capacity, meq/g of dry resin
Dowex 1-X8, 50–100 mesh	OH form	None	3.80	3.80
Dowex 1-X8, 50–100 mesh	OH form, moist	1.06×10^8	2.47	1.88
Dowex 1-X8, 50–100 mesh	OH form, moist	1.69×10^8	2.15	1.64
Dowex 1-X8, 50–100 mesh	OH form, moist	2.67×10^8	1.58	0.57
Dowex 1-X8, 50–100 mesh	Cl form	None	3.81	3.81
Dowex 1-X8, 50–100 mesh	Cl form, air dried	0.76×10^8	2.96	2.77
Dowex 1-X8, 50–100 mesh	Cl form, immersed in H_2O	0.87×10^8	2.76	2.55
Dowex 1-X4, 20–50 mesh	NO_3 form	None	4.81	4.78
Dowex 1-X4, 20–50 mesh	NO_3 form, moist	1.10×10^8	4.15	3.69
Permutit SK, 20–50 mesh	OH form	None	4.47	2.87
Permutit SK, 20–50 mesh	OH form, moist	1.69×10^8	4.25	1.80
Permutit SK, 20–50 mesh	OH form, moist	2.67×10^8	4.12	1.29
Permutit SK, 20–50 mesh	Cl form	None	4.47	2.87
Permutit SK, 20–50 mesh	Cl form, dry	1.06×10^8	4.28	1.95
Permutit SK, 20–50 mesh	Cl form, moist	1.08×10^8	4.13	2.25

the water vapor and acid gases without significantly delaying or separating the fission-gas isotopes. A fresh supply of helium is required as an elutriant. This purifies and neutralizes the system between samplings and carries the sample into the various processes when required. The helium is one of the gases vented to the radioactive gas-disposal system.

This instrument has been subjected to laboratory tests, as well as in-service tests on the Savannah River reactors, and has performed satisfactorily.[9]

Waste Disposal

The January 1962 issue of *Chemical Engineering Progress* contains a series of three articles,[10–12] each of which describes the radioactive waste-disposal system of a particular reactor plant.

The first article in the series[10] is an evaluation of the waste-disposal system of the Shippingport Pressurized-Water Reactor. The article contains a description of the system and a report of the operating experience with the process through initial power operation, refueling, and return to power operation. The operating experience has shown that the amount of radioactivity discharged from the plant is only about 20% of the design value. During power operation of the plant, the volumes of contaminated waste that are handled by the disposal system are considerably lower than the design volumes, and therefore the system operates at fractional capacity. However, the volumes of radioactive waste that were generated during the refueling operations were considerably greater than expected, and a sizable buildup of wastes was experienced.

The accumulation of waste can be attributed to two factors: (1) large amounts of "nonactive" waste solutions became contaminated to the degree that normal discharge to the effluent channel was not possible, and (2) the failure of the waste-system evaporator to function properly hampered treatment of chemical wastes.

The nonactive waste apparently became contaminated by the introduction of laundry waste water containing Co^{60} washed off the outer garments of personnel who had worked in the vicinity of the reactor head. After the source of contamination was determined, outer garments were laundered separately, and the waste solution was discharged to special waste tanks. Other laundry water and the water from showers were discharged to the nonactive waste tanks. This procedure prevented further difficulties with the contamination of normally nonactive wastes, but the volume accumulated before instituting the procedure still remained to be processed. Meanwhile, difficulties with the evaporator resulted in a buildup of chemical wastes, some of which had to be deployed to storage tanks. The accumulation of large volumes of solutions that required treatment before discharge placed a high load on ion exchangers, and the fact that the laundry and chemical wastes were included resulted in early saturation of the resins and rapid decreases in the effectiveness of the exchangers. The flexibility and capacity of the Shippingport systems are such, however, that the refueling operations were not delayed by waste-disposal problems. By instituting rigid control procedures, operating personnel were able to process the accumulated wastes and have the system ready to perform its normal functions by the time power operation was resumed after the refueling. The operating experience at Shippingport is said[10] to emphasize the importance of a large, flexible system capable of handling large volumes of low-activity wastes as well as small volumes of high-activity wastes.

Operating experience at the Dresden Nuclear Power Station provides designers with performance data for the liquid radioactive waste system of a large boiling-water reactor.[11] Early operating experience dictated some changes in the waste system that was originally provided for the plant, and the incorporation of these changes has resulted in satisfactory performance of the system through power-operation and shutdown periods. The major changes involved increasing substantially the filter capacity of the waste system and changing from a disposable cartridge filter to precoat type filters that can be backwashed and recharged.

The third article[12] describes the radioactive waste-handling system that would be provided for a proposed 360-Mw(e) sodium graphite reactor. The requirements of the system are based on operating experience with the SRE; additional experience is expected from the operation of the 76-Mw Hallam Nuclear Power Facility. The author[12] states that the capital costs of radioactive waste-disposal facilities

in U. S. commercial nuclear-power stations amount to between 1% and 7% of total plant costs and that the system specified for the proposed 360-Mw(e) sodium graphite plant could be built for the lower figure. The capacities of the systems that are described in the article appear small relative to those which have been used in the water-cooled plants. For example, a comparison of the estimated amount of waste from the laundry and the personnel showers in the proposed sodium graphite reactor with the actual amounts of waste from like facilities at Dresden shows such a difference. At the 184-Mw(e) Dresden plant, laundry wastes for a one-year period amounted to about 84,000 gal, whereas the estimated yearly volume from laundry and shower facilities at the sodium graphite plant is 20,000 gal, a difference of about a factor of 8 in volume per megawatt of plant power rating. During periods of power operation at Shippingport, the waste-volume/megawatt ratio is about 150 times as great as that for the sodium graphite plant, but the experimental nature of the Shippingport plant makes its inclusion in the comparison questionable. Indeed, there is no reason why waste volumes from one type of plant should approximate those from another, but, where significant differences do exist, it is important to recognize them and their causes.

References

1. L. D. Perrigo, A Study of Radionuclide Adsorption in the K Recirculation Loops, USAEC Report HW-69612, Hanford Atomic Products Operation, May 1961.
2. J. A. Ayres et al., Decontamination Studies for HAPO Water-Cooled Reactor Systems, Progress Report, September 1, 1960–September 1, 1961, USAEC Report HW-71259, Hanford Atomic Products Operation, Feb. 16, 1962. Additional data are presented in USAEC Report HW-71260.
3. T. F. Demmitt et al., Decontamination Studies for HAPO High Temperature Reactor Recirculation Systems, Progress Report, June 1959 to January 1960, USAEC Report HW-62806, Hanford Atomic Products Operation, Mar. 28, 1960.
4. J. A. Ayres et al., Decontamination Studies for HAPO Water-Cooled Reactor Systems, Progress Report, January 1, 1960–September 1, 1960, USAEC Report HW-67937, Hanford Atomic Products Operation, Dec. 27, 1960. Additional data are presented in USAEC Report HW-71260.
5. A. B. Meservey, Procedures and Practices for the Decontamination of Plant and Equipment, *J. Nucl. Energy, Pt. B*, 3: 189–210 (February 1962).
6. C. A. Meyer, Decontamination of Reactor Heat Exchangers—Savannah River Plant, USAEC Report DP-703, E. I. du Pont de Nemours & Co., Inc., May 1962.
7. J. B. Violette, Radioactive Maintenance Experiences at Vallecitos Boiling Water Reactor, Report 402-TP-2, General Electric Co., Vallecitos Atomic Laboratory, September 1961.
8. L. L. Smith and H. J. Groh, The Effect of Gamma Radiation on Ion Exchange Resins, USAEC Report DP-549, Savannah River Laboratory, February 1961.
9. W. R. Kritz, An Automatic Gas Chromatograph for Monitoring of Reactor Fuel Failures. Part IV. Model 2 Design, USAEC Report DP-668, Savannah River Laboratory, January 1962.
10. C. S. Abrams et al., Performance of the Radioactive Waste Disposal System at the Shippingport Station, *Chem. Eng. Progr.*, 58(1): 70–78 (January 1962).
11. W. Kiedaisch, Liquid Radioactive Waste Handling, *Chem. Eng. Progr.*, 58(1): 79–81 (January 1962).
12. R. L. Cummings, Radioactive Waste Systems for a Sodium-Cooled Reactor, *Chem. Eng. Progr.*, 58(1): 82–84 (January 1962).

Section

IX

Power Reactor Technology

Design Practice

Piqua Nuclear Power Facility

The Piqua Nuclear Power Facility (PNPF) is a small plant [11.4 Mw(e)], but it is of interest as the first organic-moderated nuclear power station. The organic-moderated reactor generates steam in an external steam generator, and the steam is then supplied to existing turbogenerator equipment in the municipal power station in the City of Piqua, Ohio.

The reactor uses partially enriched uranium, as a uranium-molybdenum-aluminum alloy, in nested double-annular fuel assemblies that are clad with aluminum. The coolant-moderator is an isomeric mixture of ortho-, meta-, and paraterphenyls. The reactor is controlled by 13 absorber control rods that move inside the central regions of selected fuel assemblies; these rods are driven by magnetic jacks. The reactor core is contained in a carbon steel pressure vessel. The main heat-transfer system comprises the reactor, one steam generator, one superheater, two coolant pumps, and associated auxiliaries. The reactor, the entire primary coolant loop, and the fuel-storage and -handling facilities are located in the containment building, and the coolant purification equipment, the control room, and plant auxiliaries are located in an adjacent building. The main characteristics of the plant are as follows:

Reactor power, Mw(t)	45.5
Reactor coolant flow rate, lb/hr	5.5×10^6
Reactor coolant flow rate, gal/min	12,000
Reactor coolant temperature at reactor inlet, °F	519
Reactor coolant temperature at reactor outlet, °F	575
Steam flow, lb/hr	150,000
Outlet steam temperature, °F	550
Outlet steam pressure, psia	441
Feedwater temperature, °F	268
Boiler heat duty, Btu/hr	145.3×10^6
Superheater heat duty, Btu/hr	10.3×10^6
Number of steam generators	1
Number of superheaters	1
Electrical output, net Mw	11.4

Fuel Assemblies

Each fuel assembly comprises a set of annular fuel elements in a thin-walled, annular stainless-steel coolant duct of full core length. In cross section (Fig. IX-1) the assembly consists of two finned annular elements within the coolant-flow duct. The clearances between the annular elements and between the elements and the duct walls are essentially only those necessary for assembly. The fins on the elements are in the form of long-pitch spirals, with the sense of rotation of the spirals opposite on the opposing surfaces of the inner and outer elements. Thus there are many possible points of contact between the tips of the fins of the inner and outer elements. Contact at some of these points is expected during initial operation, and all points of fin intersection may contact later in life because of slight swelling of the fuel. The uranium-molybdenum-aluminum fuel alloy is bonded to the finned aluminum fuel-element cladding through an intermediate, nickel layer which is 1 mil thick and which prevents diffusion of the aluminum into the fuel alloy. Longitudinally each assembly contains four sets of the coaxial tubular elements, and these are stacked to attain the full core length. The stainless-steel can (coolant duct) is provided with end fittings: the lower one locates the assembly in the bottom grid plate of the reactor (Fig. IX-2), and the upper one supports the assembly from the upper grid plate and makes a seal with that grid plate to prevent bypassing of the downward-flowing organic coolant.

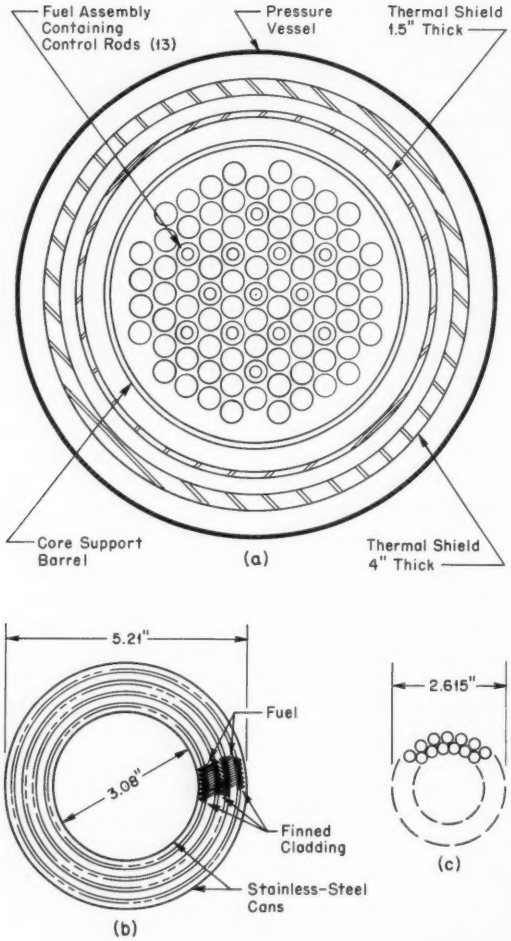

Fig. IX-1 Horizontal cross section through PNPF core and core components.[1] *(a)*, core. *(b)*, fuel assembly. *(c)*, control rod.

Each fuel assembly contains a stainless-steel wire screen at the entrance to the coolant-flow annulus to prevent the entrance of large particulates. Each assembly is also provided with a flow orifice at its upper (inlet) end. For assemblies containing control rods, this orifice consists of a movable plug within an orifice plate. It can be adjusted over the flow range of 75 to 200 gal/min when the reactor is shut down and the vessel head is removed.

The development of the fuel elements and the method of fabricating them were reviewed in the December 1960 issue of *Power Reactor Technology*, Vol. 4, No. 1, pages 60 to 62.

Inner-fuel-annulus mean diameter, in.	3.60
Outer-fuel-annulus mean diameter, in.	4.63
Inner-fuel-annulus thickness, in.	0.208
Outer-fuel-annulus thickness, in.	0.208
Inner-steel-can inside diameter, in.	3.08
Inner-steel-can wall thickness, in.	0.010
Outer-steel-can outside diameter, in.	5.21
Outer-steel-can wall thickness, in.	0.010
Active fuel length (each segment), in.	13.5
Total active fuel length, in.	54
Fuel alloy composition, wt.%:	
Uranium	96.4
Molybdenum	3.5
Aluminum	0.1
Fuel enrichment, wt.% U^{235}	1.94 ± 0.03

Control-Rod Assemblies

The control-rod assembly is a unitized package containing the absorbing element, its magnetic-jack drive, and associated mechanisms, all in one long steel tube that is immersed in the organic liquid. The lower end of the tube fits over the top end fitting of a fuel element and allows the absorbing element to project axially down into the tube formed by the inner can wall of the fuel element. The control assembly is positioned at the bottom by its engagement with the upper end fitting of the fuel element, and it is also positioned near the top of the pressure vessel by the top guide plate (Fig. IX-2). The fuel assemblies that accommodate the control rods are identical to the normal assemblies except for the upper end fitting. The coolant-flow system for a control rod and the associated fuel assembly is shown in Fig. IX-3. Thirteen control assemblies are used, in the positions indicated in Fig. IX-1.

The control element proper is made up of small stainless-steel tubes filled with boron carbide and brazed together to form a double ring (Fig. IX-1). The tubes are plugged at the ends and welded into drilled end rings.

The magnetic-jack control-rod drive has four coils — for hold, grip, lift, and pulldown — which, when energized in proper sequence, move the rod in discrete steps of 0.05 in. Upon loss of power the rod falls freely into the core and scrams the reactor. Rod-position indication is electromagnetically produced through the use of small coils located along the path of the rod extension shaft. Position is determined by measurement of the inductance, which varies as the shaft moves through. Belleville springs stop the rod at the

lower limit of its travel when it is dropped on scram. Prototype tests showed that, for a 48-in. drop, the total scram time is 725 msec and that a single bounce of 2 to 3 in. occurs when the rod bottoms. The actuating and positioning coils are hermetically sealed in stainless steel; the movable parts of the mechanism operate in the organic liquid.

Absorber material	B_4C
Absorber cladding	304 stainless steel
Absorber-tube diameter, in.	$\frac{1}{4}$
Absorber-tube wall thickness, in.	0.035
Absorber length, in.	48
Absorber tubes per element	48
Outside diameter of composite absorbing element, in.	2.6
Total absorber travel, in.	48
Drive-position-indicator diameter, in.	6
Drive-position-indicator length	16 ft $1\frac{11}{16}$ in.
Total element and drive assembly length	21 ft $3\frac{3}{8}$ in.
Maximum control-element surface temperature, °F	546
Maximum withdrawal rate, % Δk/sec	0.008

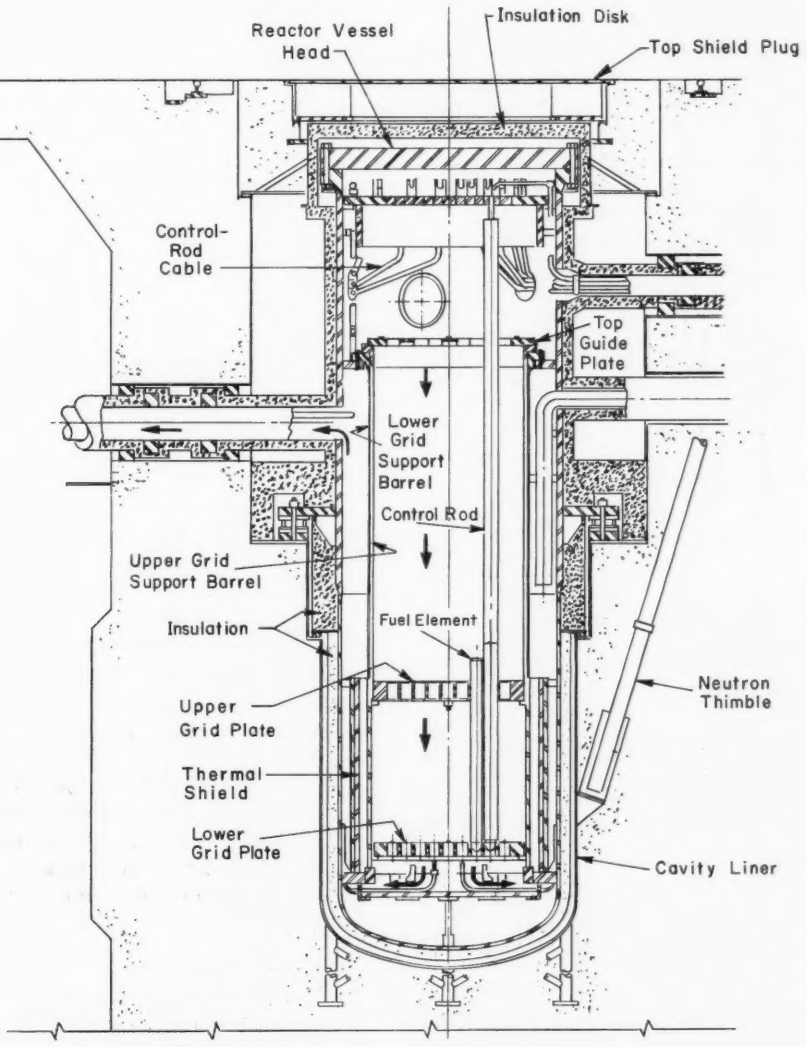

Fig. IX-2 Vertical cross section through PNPF reactor.[1]

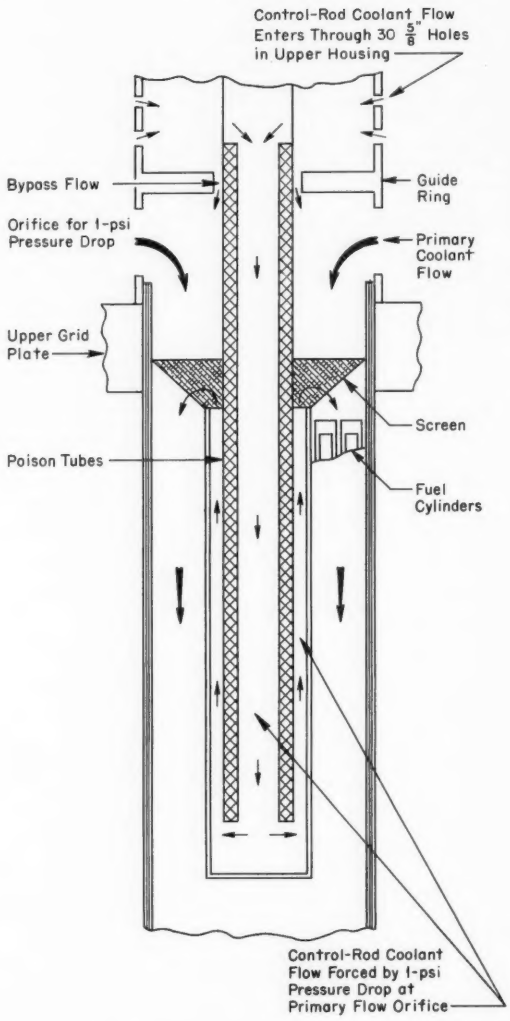

Fig. IX-3 PNPF control-rod coolant flow.[1]

Reactor Core and Core Structure

The reactor core contains 85 fuel assemblies (including the 13 that contain control rods) in a 6-in. triangular lattice, arranged to form a right cylinder of hexagonal cross section (Figs. IX-1 and IX-2). It is located near the bottom of the pressure vessel and is immersed in the organic (hydrocarbon) that acts as a coolant, moderator, and reflector. The permanent core structure consists simply of an upper and a lower grid plate, each of which is hung by a support barrel from an internal flange near the top of the vessel. The fuel assemblies hang from the upper grid plate and are positioned at their lower ends by the lower grid plate. The lower grid support barrel serves also as a flow barrier that defines the flow pattern of the organic coolant-moderator by directing it downward through the fuel assemblies and into a plenum at the bottom of the vessel. From the plenum the organic coolant-moderator returns upward in the annulus outside the lower grid support barrel and leaves the vessel from nozzles near the upper end.

Initially the normal core loading will be decreased by about 15 fuel assemblies, and these will be replaced by dummies to reduce the excess reactivity.

Lattice	Equilateral, triangular shape
Pitch, in.	6.0
Number of regular fuel assemblies	72
Number of control fuel assemblies	13
Total uranium in equilibrium core, kg	6910
Total U^{235} in equilibrium core, kg	134
Core size, ft:	
Equivalent diameter	5.0
Active height	4.5
Core composition, vol.%:	
Coolant-moderator	69.9
Uranium-molybdenum-aluminum fuel alloy	17.2
Aluminum	12.1
Stainless steel	0.8

Fuel Program, Reactivity Changes, and Power Distribution

The initial fuel has a relatively high excess enrichment. To limit the excess reactivity, some fuel-assembly locations will initially be filled with dummy assemblies, which will be replaced by fuel assemblies as burnup proceeds. In the equilibrium cycle approximately one-fourth of the fuel assemblies will be replaced by fresh assemblies at each reloading. The average core exposure between reloadings will be approximately 1000 Mwd/ton. Reloading of the reactor requires shutdown and removal of the pressure-vessel head.

Reloading scheme	1/4-core batches
Average burnup between reloads, Mwd/ton	1000
Operating time between reloads, months	4–6

Average exposure at discharge, Mwd/ton	2700–4000
Reactivity effects, % k_{eff}:	
Temperature defect, 360 to 550°F	1.06
Xenon plus samarium (equilibrium)	3.2
Fuel depletion	1.8
Flux flattening and control margin	1.8
System reactivity at 360°F	7.86
Total control-rod worth	12.2
Shutdown margin at 360°F	4.34
Reactivity coefficients:	
Coolant temperature, Δk_{eff}/°F	-1.0×10^{-5}
Fuel temperature, Δk_{eff}/°F	-1.1×10^{-5}
Moderator temperature, Δk_{eff}/°F	-5.3×10^{-5}
Total temperature, Δk_{eff}/°F	-7.5×10^{-5}
Coolant void, Δk_{eff}/% coolant void	-40.0×10^{-5}
Reactivity effect of water added to coolant	Negative
Maximum-to-average ratios:*	
Radial peak-to-average flux ratio	1.47 max.
Axial peak-to-average flux ratio	1.47 max.
(Max. thermal-neutron flux in fuel)/(av. thermal-neutron flux in fuel)	3.93
(Max. heat flux in core)/(av. heat flux in core)	2.59

Heat Removal

Coolant enters the core from the top, flows vertically downward through the core, and then turns and flows upward in the annulus between the grid support barrel and the pressure vessel to the outlet nozzle. The coolant-flow distribution to the various fuel assemblies is adjustable, upon reactor shutdown and removal of the pressure vessel head, by the orifices in the fuel-assembly inlets.

Organic-coolant data on heat-transfer and fluid-flow properties and on design limits were reviewed in the September 1961 issue of *Power Reactor Technology*, Vol. 4, No. 4, pages 76 to 83.

Coolant	Terphenyl
Flow rate, lb/hr	5.5×10^6
Reactor inlet temperature, °F	519
Reactor outlet temperature, °F	575
Maximum allowable fuel-element surface temperature, °F	750
Maximum operating fuel-element surface temperature, °F	713
Coolant boiling point at operating pressure, °F	913
Nominal operating pressure, psia	120
Maximum coolant velocity, ft/sec	12.7
Burnout heat flux at core hot spot, Btu/(hr)(sq ft)	450,000
Maximum operating heat flux, Btu/(hr)(sq ft)	89,500
Average core heat flux, Btu/(hr)(sq ft)	34,600
Core pressure drop, psi	27

Pressure Vessel (Fig. IX-2)

Type	Cylindrical with torispherical bottom head
Material	Mild steel, SA212
Wall thickness, in.	$1\frac{1}{8}$–$2\frac{1}{4}$
Bottom head thickness, in.	$1\frac{1}{8}$
Top head thickness, in.	9
Inside diameter, in.	92
Inside height, ft-in.	$27-3\frac{1}{2}$
Operating pressure, psig	105
Design pressure, psig	300
Operating temperature, °F	575
Design temperature, °F	750
Major nozzles:	
Main coolant inlet	1–20 in.
Main coolant outlet	2–14 in.
Degasification-pressurization inlet	1–6 in.
Degasification-pressurization outlet	1–6 in.

Main Heat-Transfer System

This is a single coolant loop, and it consists of the two main coolant pumps, the superheater, and the steam generator. The entire loop is of carbon steel construction except for some of the pump parts which are stainless steel.

Main coolant pumps:	
Type	Horizontal, centrifugal
Capacity (each pump), gal/min	6000
Total developed head, psi	90
Seal	Mechanical, with labyrinth backup
Driving motors	400-hp, water-cooled, explosionproof

*The relations among these ratios are not evident from reference 1.

Superheater:	
Type and materials	Shell-and-tube, carbon steel
Shell-side fluid	Reactor coolant
Tube-side fluid	Steam
Shell-side inlet temperature, °F	575
Shell-side outlet temperature, °F	571
Tube-side inlet temperature, °F	456
Tube-side outlet temperature, °F	550
Heat transfer, Btu/hr	10.3×10^6
Steam generator:	
Type and materials	Vertical shell-and-tube, carbon steel
Shell-side fluid	Boiling water
Tube-side fluid	Reactor coolant
Shell-side inlet temperature, °F	268
Shell-side outlet temperature, °F	456
Tube-side inlet temperature, °F	571
Tube-side outlet temperature, °F	519
Heat transfer, Btu/hr	1.45×10^8
Design pressure (tube side), psig	300
Operating pressure (tube side), psia	120
Design pressure (shell side), psig	500
Operating pressure (shell side), psig	435

Nuclear Instrumentation

Source range, 4.5×10^{-6} to 4.5 watts: two identical channels using BF_3 detectors provide log count rate and period indication and alarms.

Intermediate range, 0.45 watt to 4.5 Mw: two channels using compensated ion chambers provide log N and period indication, alarm, and initiate reactor protective action.

Power range, 0.45 to 45.5 Mw: three channels using uncompensated ion-chamber detectors provide log N, linear N, and period indication and alarm. In addition, these channels initiate reactor protective action.

Plant Control Systems

The plant control systems automatically regulate the reactor power and the outlet steam pressure under load variations from 20 to 100% of full load.

The reactor outlet temperature controller automatically operates control rods to maintain constant reactor outlet temperature. The total reactivity available to the automatic controls is less than 0.5% k_{eff}. The maximum reactivity addition rate is 0.008% k_{eff}/sec.

The steam pressure controller regulates steam pressure to ± 5 psi by operating a three-way butterfly valve. The valve bypasses part of the organic flow around the boiler to the reactor inlet.

The setback system, which is for use when an off-normal condition occurs, inserts three reactor control rods at normal speed as long as the off-normal condition exists. It responds to signals from period, from high core outlet temperature, and from high reactor power-to-flow ratio.

Failed-Fuel-Element Location

Fuel-element failure is detected by continuously monitoring the bulk outlet coolant stream. The location is then determined by monitoring the coolant from each fuel channel.

A system of 85 tubes, each of which is $\frac{5}{8}$ in. in diameter, is used to sample coolant at the core outlet. One tube inlet is located under each bottom-grid coolant outlet hole. The tubes pass through a special nozzle to the outside of the pressure vessel and then to a selector valve. Coolant from each fuel channel is sampled for delayed-neutron activity by a BF_3 counter to determine which of the 85 fuel assemblies has failed.

Reactor Auxiliaries

The PNPF has auxiliary systems for coolant degasification, purification, and pressurization; for shutdown cooling; and for disposal of gaseous, aqueous, and organic wastes. Designs and tests of the prototype systems for coolant purification, coolant degasification, organic-waste disposal, and gaseous-waste disposal were reviewed in the March 1961 issue of *Power Reactor Technology*, Vol. 4, No. 2.

Figure IX-4 shows the flow diagram of the coolant degasification, pressurization, and purification systems and the shutdown cooling system. The coolant degasification system removes (1) the hydrogen and light hydrocarbons that are

produced by radiolytic decomposition and (2) the water that may enter the coolant from steam-generator leakage. The coolant is sprayed into T-15, the degasifier tank, which is maintained under vacuum. Water, hydrogen, and light hydrocarbons are removed as gas at the top, and the reactor coolant is taken out the bottom. The reactor pressure is controlled by valve CV, which controls the rate at which coolant is sprayed into the tank. Any coolant vaporized in the tank is condensed in the degasifier condenser or in the degasifier aftercondenser and is returned to the degasifier tank. Coolant is returned to the reactor by the pressurizing pump P-3. When the reactor is shut down, decay heat is removed by X-2, the decay heat exchanger, and the coolant bypasses the degasification tank.

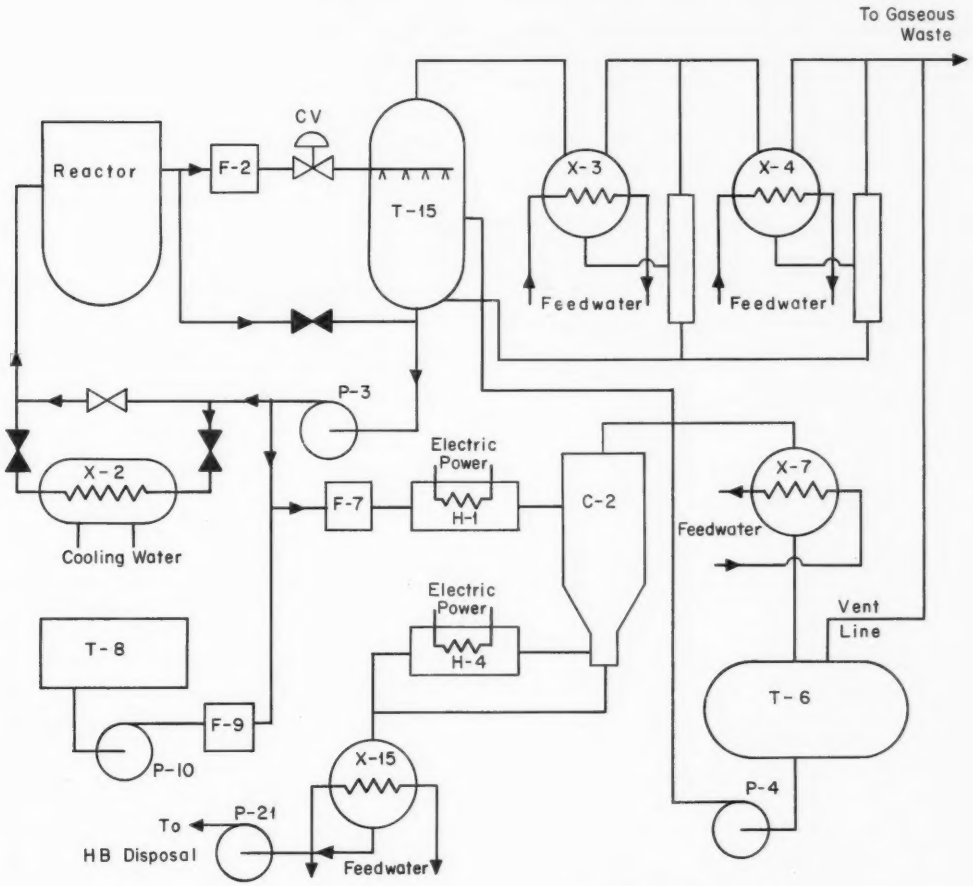

CV	Reactor Pressure-Control Valve	P-21	Bottoms-Transfer Pumps
C-2	Purification Column	T-6	Product-Receiver Tank
F-2	Degasifier-System Filters	T-8	New-Coolant Storage Tanks
F-7	Column Feed Filters	T-15	Degasifier Tank
F-9	New-Coolant Filters	X-2	Decay Heat Exchanger
H-1	Column Feed Heater	X-3	Degasifier Condenser
H-4	Bottoms Heater	X-4	Degasifier Aftercondenser
P-3	Pressurizing Pumps	X-7	Column Condenser
P-4	Coolant-Makeup Pumps	X-15	Bottoms Cooler
P-10	New-Coolant Pump		

Fig. IX-4 PNPF coolant degasification and purification systems.[1]

In addition to the light hydrocarbons, some high-boiler (HB) compounds that have higher molecular weights and higher boiling points are formed. To remove these, a portion of the discharge from the pressurization pump P-3 is diverted through the vacuum distillation column C-2. The purified coolant vapor from the top is condensed and returned to the degasifier, and the HB liquid is removed from the bottom of the column, cooled, and pumped to the organic-waste-disposal system. New coolant makeup is added from storage tank T-8 to the stream entering the vacuum still. The expected coolant makeup rate is 60 lb/hr.

Design characteristics of the major reactor auxiliary components are given below.

Degasifier tank, 5 ft in diameter by 10 ft:	
Design pressure, psig	150
Design temperature, °F	750
Operating pressure, psia	5 (vacuum)
Main coolant-stream inlet temperature, °F	575
Total impurity removal, lb/hr	8.5
Total inlet flow, lb/hr	91,900
Purification column, 1.5 ft in diameter (top section) by 8 in. in diameter (bottom section) by 12 ft:	
Height of packing, ft	4
Packing material	½-in. Raschig rings
Design pressure, psig	150
Design temperature, °F	800
Operating pressure, psia	1.0 (vacuum)
Inlet temperature, °F	700
Total HB removed, lb/hr	58
Total inlet flow, lb/hr	262
Pressurizing pumps:	
Number	2
Type	Horizontal, centrifugal
Motors	50-hp variable speed d-c
Seal type	Mechanical
Backup seal	Labyrinth
Total developed head at flow rate, psi at gal/min	133/200
Total developed head at flow rate, psi at gal/min	28/500
Heat-transfer duties:	
Column feed heater, H-1, kw(e)	65
Bottoms heater, H-4, kw(e)	10
Column condenser, X-7, Btu/hr	150,000
Bottoms cooler, X-15, Btu/hr	40,000
Degasifier condenser, Btu/hr	250,000
Degasifier aftercondenser, Btu/hr	25,000
Decay heat exchanger, Btu/hr	1,300,000

Aqueous Wastes

Aqueous wastes are collected in a sump in each building and are then pumped to a settling basin. Light and heavy organics are separated for burning, and water is passed through a filter and a diatomaceous-earth organic absorber to the holdup tank. From there the water is pumped

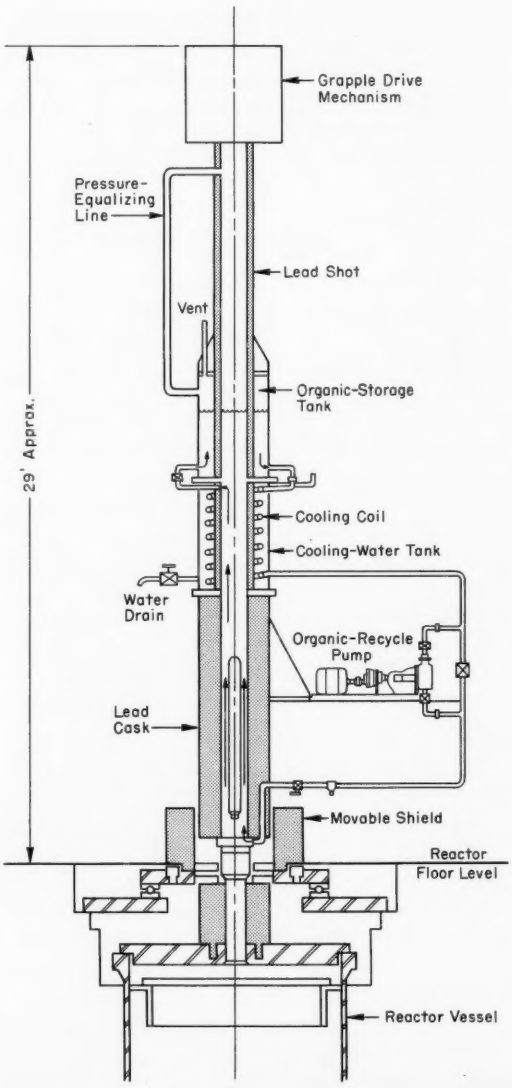

Fig. IX-5 PNPF fuel-handling machine.[1]

through demineralizers to other holdup-tank compartments or is discharged to the sewer.

Gaseous-Waste Disposal

Gaseous wastes are collected under vacuum in the organic trap. The gases then flow through a steam ejector and are discharged through the stack after passing through adsorbers and holdup tanks.

Organic-Waste Disposal

Organic wastes are almost entirely HB compounds that have been separated from the coolant. This waste is stored in a compartmented tank and is then burned. The combustion products are filtered before being discharged to the atmosphere. The compartmented tank is sized to store a six-month accumulation of wastes.

Refueling

For refueling, the reactor is shut down, and the head is removed and replaced with a rotating shield. Spent fuel is transferred from the reactor to the fuel pool in the fuel-handling cask, and new fuel is transferred from the new-fuel storage racks to the reactor on the return trip. The fuel-handling cask is a vertical lead-shielded cylinder, is approximately 25 ft high, and has grappling and hoisting mechanisms mounted at the top. It also has an emergency cooling system in case of failure during transfer of fuel between the reactor and the pool. The cooling system floods the cask with organic, which is then cooled by water. The cask moves laterally on a traveling bridge that moves between the reactor and the fuel pool. Total height of the machine above floor level is approximately 29 ft. The refueling machine is shown in Fig. IX-5.

Buildings

The steel containment building is designed for an internal pressure of 5 psig. A maximum pressure of 4.9 psig will occur if the boiler ruptures completely and if all building ventilation

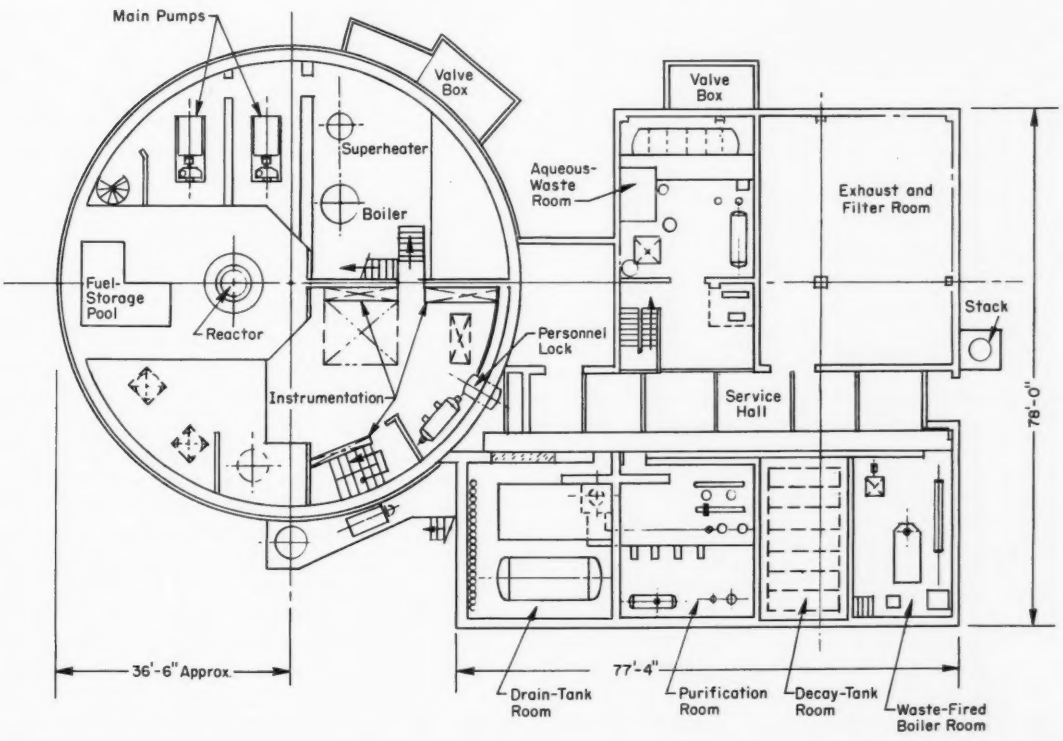

Fig. IX-6 PNPF plant and equipment layout.[1]

valves are closed. Other accidents result in lower pressure. The containment building houses the reactor, all components of the main coolant loop, the degasifier, the decay heat exchanger, the pressurizing pumps, the spent-fuel storage pool, the new-fuel storage room, the fuel-handling cask, and a 30-ton polar crane. The building has an 18-in. concrete lining around the inside above grade. It has three air locks: an equipment access air lock and a personnel access air lock at the reactor room floor level, and a personnel escape air lock at the lower process room level.

Design pressure, psig	5, ASME Code
Test pressure, psig	6.25
Leak rate	0.2% per day per psi; 1.0% per day at 5 psig
Geometry	Vertical cylinder, with hemispherical top head
Diameter (scaled), ft	73
Height (estimated), ft	85, straight side of shell

The conventional insulated steel panel auxiliary building houses the control room, all waste-disposal equipment, and other auxiliaries. The layout of plant and equipment is shown in Fig. IX-6.

Reference

1. Atomics International, Final Safeguards Summary Report for the Piqua Nuclear Power Facility, USAEC Report NAA-SR-5608, Aug. 1, 1961.

Section

X

Power Reactor Technology

Operating Experience: Shippingport

The Shippingport Atomic Power Station has now been in operation for more than four years. A large amount of information on the project has been published in the form of progress, topical, and special reports. Reference 1 lists more than 1500 of these reports. However, a recent paper prepared for the U. S.–Japan Atomic Industrial Forum[2] is a convenient summary, covering experience during the first four years of operation and plans for future operation.

Shippingport, currently rated at 60 Mw(e) [turbine capability is 100 Mw(e)], is located on the south bank of the Ohio River, approximately 40 miles west of Pittsburgh. The nuclear portion of the plant is owned by the Atomic Energy Commission. The Duquesne Light Company owns the turbine-generator facilities, operates the plant, purchases the steam produced by the operation of the reactor, and feeds the electrical output to its lines. The reactor portion of the plant was designed and developed by the Bettis Atomic Power Laboratory under the direction of, and in technical cooperation with, the Naval Reactors Branch of the AEC's Division of Reactor Development. Descriptions of the plant are given in references 3 and 4. Some of the more general data on the plant are summarized in Table X-1, and the operating history of the station is shown diagrammatically in Fig. X-1.

The general performance of the plant has been good. It has shown itself capable of responding promptly and safely to load changes and has operated successfully at rated power for long periods of time. On Mar. 12, 1962, for example, the reactor completed a 3000-hr run at an average station load factor of 100%.

Nominally the plant has been operated as an integrated unit of the utility network; however, the day-to-day operations have been determined principally by the specific requirements of the AEC's Shippingport test program carried out to advance reactor technology. The reactor core consists of a seed and blanket arrangement of fully enriched and natural-uranium fuel elements. The enriched portion of the reactor is referred to as the seed, and the natural-uranium portion is referred to as the blanket. The reactor is still operating with its first blanket, but the seed has been depleted and replaced twice. Operation with core 1 will continue for approximately another year, after which the higher-powered and advanced core 2 will be installed, and modifications will be made to allow operation of the plant at the higher power level. The characteristics of core 1 and core 2 are compared in Table X-2. The continuing operation with core 1 has three main objectives:[2]

1. Continuing the large-scale irradiation of natural UO_2 fuel elements with Zircaloy-2 cladding to determine the maximum MWD/T burnup that these fuel elements can withstand.
2. Obtaining information on the physics characteristics and thermal performance of seed and blanket cores as a function of fuel depletion, and demonstrating the continued generation of a high fraction of the power from natural uranium in such cores.
3. Obtaining data on the long-term behavior of major plant components, and thus acquire a realistic basis for judging the adequacy of component design specifications. Further, this operational experience should pilot the long-term performance to be expected from similar components in plants now under construction or in early stages of operation.

Reactor Operating Experience

The reactor core comprises an annular seed region and an inner and an outer blanket region

Table X-1 SHIPPINGPORT HIGHLIGHTS[2]

	Seed 1	Seed 2	Seed 3
Project history:			
Project was authorized in July 1953			
Ground was broken in September 1954			
Construction was started in March 1955			
Operation with core 1:			
Date of initial criticality	12-2-57	4-12-60	10-7-61
Date plant reached full power (60,000 kw net)	12-23-57	5-7-60	10-24-61
Lifetime, effective full-power hours (EFPH)	5806	7900	7000 (est.)
Total electricity generated, kw-hr gross	388,500,000	514,300,000	
Average load factor, %	37	70	
Average load factor excluding testing, %	75	97	
Date refueling started	11-2-59	8-16-61	
Date refueling was completed	4-11-60	10-6-61	
Loading data for core 1 (blanket is 12.6 metric tons of natural uranium):			
Uranium in seed, kg of U^{235}	75	90	90
Boron in seed, g of natural B	0	170	170
Loading data for core 2 (blanket is 17.1 metric tons of natural uranium):			
Uranium in seed, kg of U^{235}	336		
Boron in seed, g of B^{10}	456		
Total electricity generated and fuel-burnup data:			
Total electricity generated on core 1, kw-hr (gross output as of May 1, 1962)	1,194,000,000*		
Approximate amount of electricity delivered to Duquesne Light Co. system, kw-hr (net output as of May 1, 1962)	1,090,000,000*		
Total operating time on core 1, EFPH	17,440*		
Peak burnup in core 1 blanket fuel (natural UO_2), Mwd/ton of UO_2	25,000*		
Average burnup in core 1 blanket fuel, Mwd/ton of UO_2	5750*		

*As of May 1, 1962.

(Fig. X-2). The fuel assemblies for both regions are square in cross section. The seed clusters contain plates of U^{235} alloyed with Zircaloy-2 and clad with Zircaloy-2 (Fig. X-3); the blanket assemblies are made up of rod type UO_2 elements that are jacketed in Zircaloy-2 (Fig. X-4). The plates are 0.069 in. thick, and the rod type elements have an outside diameter of 0.411 in. The cruciform hafnium control rods are installed only in seed bundles.

The power split between the seed and the blanket is shown, for operation with seeds 1 and 2, in Figs. X-5*a* and X-5*b*. There is substantial increase in the blanket power fraction during the life of a seed. The increase is greatest for the first seed and less for subsequent seeds. There are two reasons for this increase: (1) The blanket region gains reactivity with exposure, since its local conversion ratio is greater than unity, and this reactivity gain leads to a gradual increase in the blanket power fraction; however, the reactivity gain is a relatively slow one. (2) At the start of seed life, there is a large current of thermal neutrons from the blanket to the seed which reduces the effective blanket reactivity and hence its power fraction; as the seed depletes, its absorption per unit volume becomes more

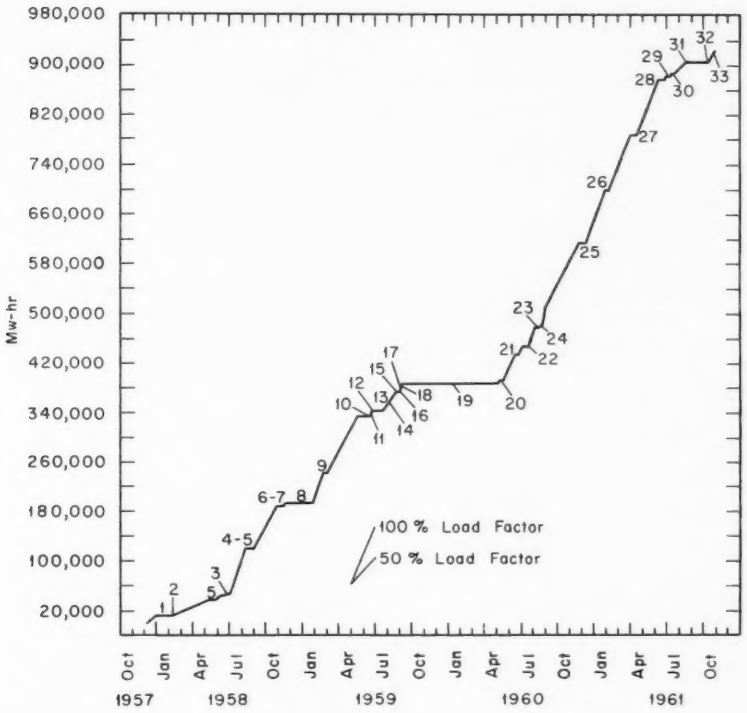

1. Reactor Shut Down for Test and Training
2. Leak Discovered in Steam Generator
3. Coolant Loop Pump Failed
4. First 1000-Hr Reactivity Lifetime Test
5. Shut Down for Maintenance and Testing
6. Second 1000-Hr Reactivity Lifetime Test
7. Shut Down for Maintenance and Testing
8. Moisture-Separator Failure Discovered; Plant Remained Shut Down Through January 1959
9. Repair of Turbine Governor
10. Periodic Operation for Training Purposes
11. Shut Down for Maintenance and Testing
12. Periodic Operation for Testing Plant Dynamic Response
13. Shut Down for Capacity Reduction and Hot Subpower Tests
14. Final Reactivity Lifetime Test; Final Run at Full Power for Core 1, Seed 1
15. Low-Power Physics Testing
16. 50-Mw Operation for End of Core Life Tests
17. Shut Down Because of Xenon Buildup
18. Final Power Run at 20 Mw
19. Shut Down To Replace Core Seed 1; Full Power Resumed
20. Low-Power Physics Testing
21. Maintenance — Replacement of E-12 Control-Rod-Drive Mechanism
22. Low-Power Physics Testing
23. Testing and Student Training
24. Return of 1-B Loop to Service
25. Low-Power Physics Testing
26. Low-Power Physics Testing and Maintenance
27. Low-Power Physics Testing — 240-Hr Samarium Transient Test; Start of Final Full-Power Run
28. End of Seed 2 Ability To Override Equilibrium Xenon at 100% Power — Physics Testing
29. Testing, Maintenance, and Operator Training
30. Core Physics Testing — End of Seed 2 Life Tests
31. Start of Refueling and Replacing Seed 2
32. Initial Approach to Criticality, Seed 3
33. Full-Power Operation with Seed 3

Fig. X-1 Operating history of Shippingport station.[2]

Table X-2 GENERAL CHARACTERISTICS OF FIRST AND SECOND SHIPPINGPORT CORES[2]

	Core 1	Core 2
Rating	231 Mw(t); 67 Mw(e) with 3 coolant loops	505 Mw(t); 150 Mw(e) with 4 coolant loops
Power density:		
Seed	75 kw/liter	157 kw/liter
Blanket	25 kw/liter	35 kw/liter
Design core lifetime:		
Seed	3000 EFPH	10,000 EFPH
Blanket	8000 EFPH	20,000 EFPH
Fuel elements:		
Seed	Zircaloy-2-clad enriched-metal-alloy plates of uranium–Zircaloy-2	Zircaloy-4-clad enriched UO_2–ZrO_2 compartmented plates
Blanket	Zircaloy-2-clad UO_2 rods	Zircaloy-4-clad UO_2 compartmented plates
Core pass:		
Seed	1	1
Blanket	1	2
Core height	6 ft	8 ft
Nuclear control	32 rods and distributed burnable poison in the seed (seed 2)	20 rods and lumped burnable poison in the seed
Orifices	Fixed	Adjustable
Ports in reactor vessel head (for refueling)	10	1

comparable to that of the blanket, and hence the magnitude of this thermal current decreases and the blanket power fraction tends to increase.

Seed 2 lasted approximately 20% longer than anticipated. This is interpreted as an indication that the reactivity of the blanket is being maintained better than anticipated.

The reactor core is extensively instrumented. Thermocouples are buried in the seed fuel to measure the central temperature. Other thermocouples measure the water temperature at many core locations. Flow measurements with Venturis are made on some individual seed and blanket clusters. The failed-fuel-element detection and location (FEDAL) system samples water from each blanket cluster and pipes the water to a delayed-neutron monitor located outside the reactor vessel. Nuclear instrumentation monitors the neutron leakage (which is proportional to reactor power) at four corners outside the core.

The Shippingport reactor is the first reactor to use uranium oxide fuel, and most of the basic technology of oxide fuels has been developed as part of the research and development program for the reactor. Because UO_2 elements have become the accepted type for large water-cooled power reactors and because with the seed-blanket arrangement it is feasible to irradiate the blanket fuel elements to their metallurgical limit, the performance of these elements in Shippingport is of particular interest. During the life of the blanket, two blanket clusters with slightly defective elements have been located by the FEDAL detection system. These defective clusters were replaced during the second refueling of Shippingport. No defects have been detected in the other 111 blanket clusters. Examinations of samples of blanket fuel that were removed at the time of replacement of seed 1 yielded the following results:[2]

1. No significant dimensional changes occurred in three bundles, selected respectively from the most highly depleted region, an intermediate flux region, and a low-power, low-flow region.
2. The structure of the UO_2 fuel was virtually unaltered by irradiation.
3. Fission gas release measurements, made on fifteen fuel rods from the region of maximum depletion, compared reasonably well with the rates computed on the basis of solid state diffusion theory. These data are also in agreement with release rates obtained experimentally in in-pile loop tests under comparable conditions.

4. The Zircaloy-2 cladding had an average hydrogen content of 60 ppm based on measurements of five samples of Zircaloy-2 from each of three fuel rods. Individual values ranged from 50 to 100 ppm. These hydrogen values represent the sum of the hydrogen originally present in the Zircaloy-2 material (40 ppm) plus the amount absorbed from the reaction with water during corrosion testing of the fuel elements at the time of manufacture (10 ppm) and the amount absorbed during core operation (10 ppm). The levels are well below the 200–250 ppm level above which hydrogen embrittlement could be of concern.

5. The techniques currently being employed for predicting the irradiation-induced isotopic changes in blanket fuel appear to be adequate. Of particular interest is the rate of plutonium buildup in the blanket. Reasonably good agreement was obtained between the measured and calculated values at the end of seed 1 lifetime [see Fig. X-6].

6. The maximum local deposit of crud was approximately 160 mg/dm^2 (about 0.5 mil thick), which would cause a negligible rise in the surface temperature of the cladding.

A review of the fuel-element examination was given in the December 1961 issue of *Power Reactor Technology*, Vol. 5, No. 1, page 66.

The postirradiation examination of blanket fuel that was removed when seed 2 was removed[5] disclosed that the integrity of the fuel

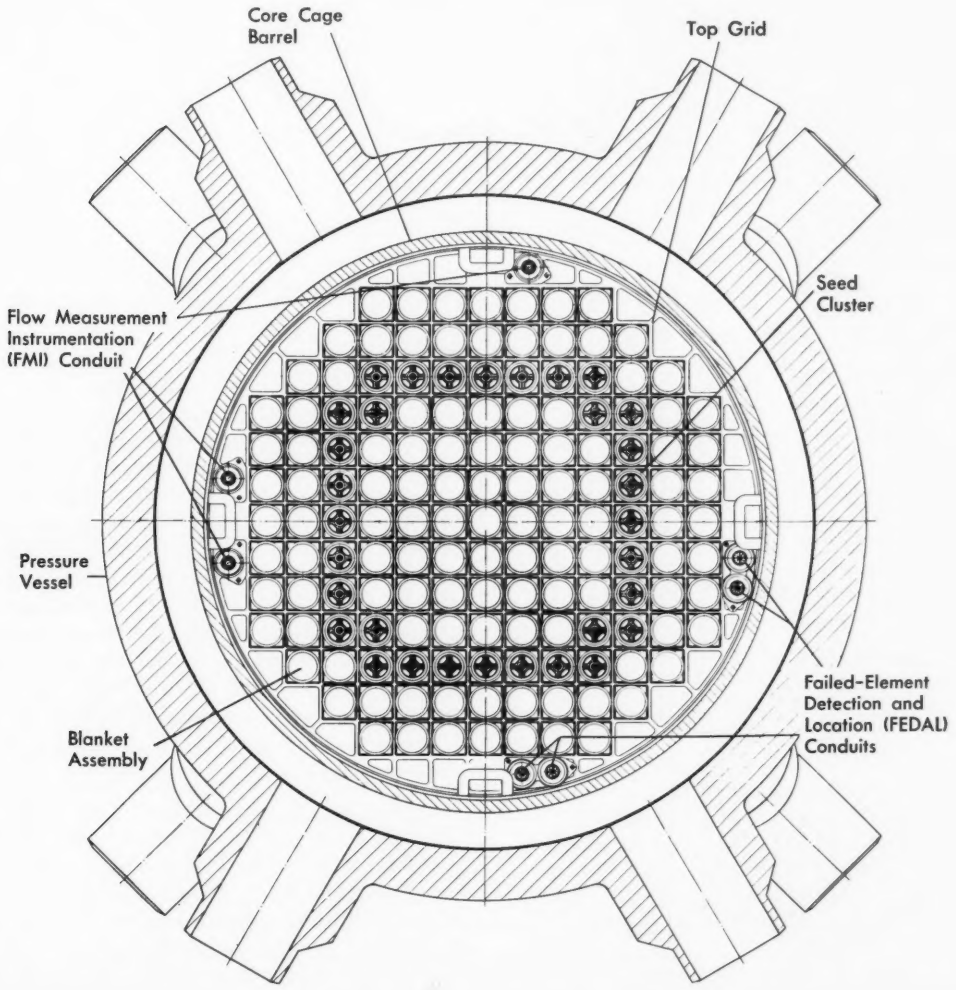

Fig. X-2 Cross section through outlet nozzle,[3] Shippingport PWR.

was still sufficiently good for one and probably two more seed lives. The blanket was designed to have a lifetime of 8000 effective full-power hours (EFPH); on May 1, 1962, after 3737 EFPH of operation with seed 3, the accumulated blanket lifetime was 17,440 EFPH. The average exposure of blanket fuel at that time was 5750 Mwd/ton of UO_2, and the estimated maximum was 25,000 Mwd/ton. The most highly exposed fuel rod examined (13,000 Mwd/ton), which was

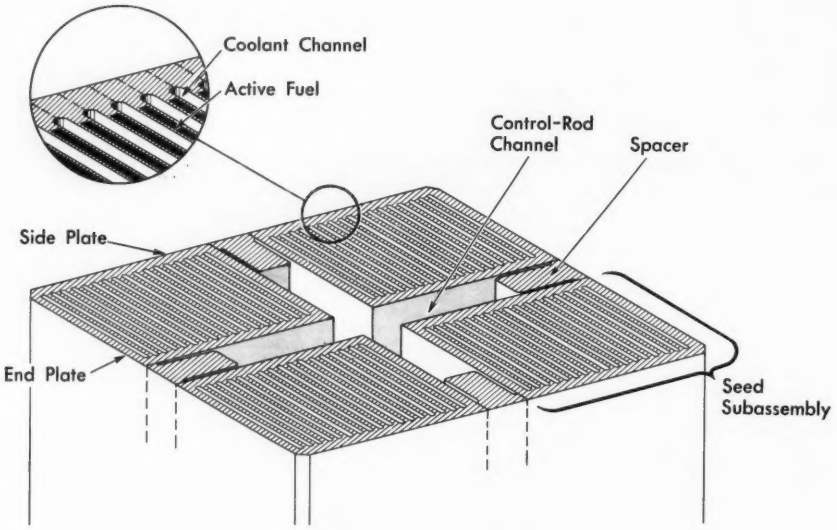

Fig. X-3 Seed fuel cluster,[3] Shippingport PWR.

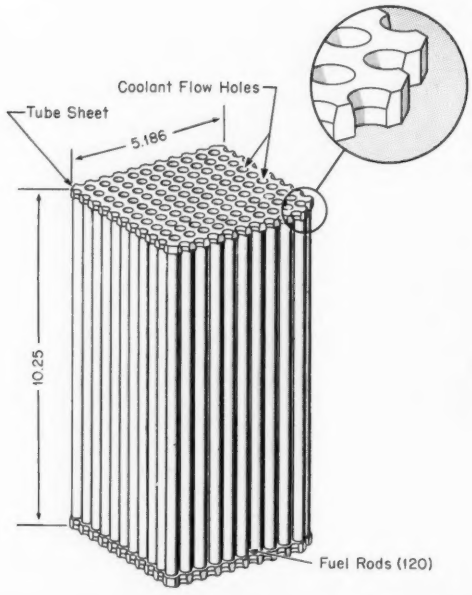

Fig. X-4 Shippingport PWR blanket bundle[3] (seven bundles are stacked in each blanket assembly).

examined after seed 2 operation, showed no distortion or change in dimensions. An analysis of the free fission gas released by the UO_2 showed that 0.3% of the Kr^{85} produced had been released. Metallographic examination of the fuel showed no abnormal cracking or grain growth, and the 4-mil radial expansion annulus between fuel and cladding was still intact. Similar examination of the Zircaloy-2 cladding showed no unusual hydride formation, and the external rod-surface corrosion film was similar to that observed on blanket rods after one seed life. Hydrogen analysis on the Zircaloy-2 showed that the average hydrogen content of the cladding was less than 80 ppm.

In assessing the significance of the Shippingport fuel performance, it is necessary to take into account the operating temperatures of the fuel elements, which appear to be substantially lower than those anticipated in current designs of slightly enriched water-moderated reactors. Since no grain growth is observable in the fuel that has been examined, one can conclude that the centerline temperature was less than the

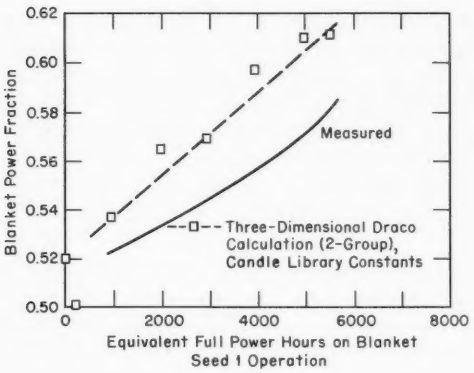

Fig. X-5*a* Shippingport PWR core 1 blanket power fraction,[2] seed 1.

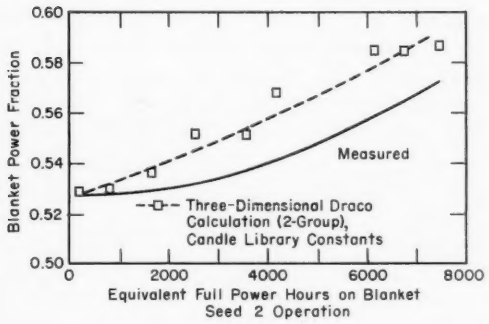

Fig. X-5*b* Shippingport PWR core 1 blanket power fraction,[2] seed 2.

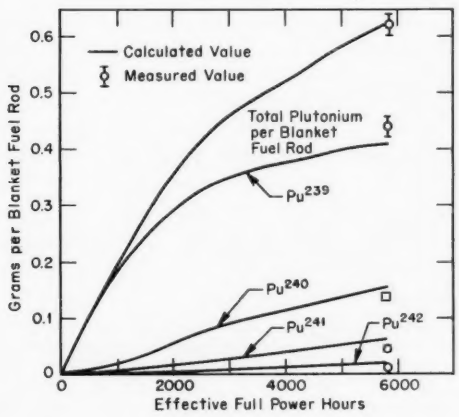

Fig. X-6 Plutonium buildup in core 1 blanket rod,[2] Shippingport PWR.

grain-growth threshold of about 2900°F. This assumption is compatible with the low value of observed fission-gas release. Operation at these temperatures allows the irradiated fuel to be depleted to higher burnups, resulting in extraction of large amounts of energy from the natural uranium as well as minimizing the effects of cladding defects on fuel-element performance.

Figure X-6 shows the calculated buildup of plutonium isotopes in the blanket during the first seed lifetime and includes measured values at the end points.

Spatial power oscillations due to xenon transients were observed in the core during the operation with seed 1. The spatial power asymmetry was first observed by nuclear detectors during a rapid xenon depletion test. The power tilt oscillated on a period of approximately 24 hr, and the amplitude increased with time. A trace of the oscillation is shown in Fig. X-7. The measured coolant temperature also indicated the same power tilt. This power oscillation was eliminated by repositioning the control rods by less than 1 in. The tendency to develop spatial oscillations was also observed in the course of a long full-power run. The oscillations were observed to converge at a core lifetime of about 2900 EFPH and practically disappeared when the controlling group of control rods (group 2) was fully withdrawn a few effective full-power hours later. During seed 2 operation, no spontaneous oscillations were observed. A deliberate attempt to create an oscillation resulted in a convergent amplitude oscillation. This was interpreted[2] as an indication that with seed 2, with the control rods more withdrawn and a more highly irradiated blanket, the core quadrants behaved in a more closely coupled fashion than with seed 1.

Replacement of the first seed with a longer-lived second seed was accomplished about two years after the plant was started up. A detailed description of the refueling is given in reference 6. A review of the first refueling was published in the March 1961 issue of *Power Reactor Technology*, Vol. 4, No. 2, page 52. The refueling was started in November and was completed 134 days later. As noted in Table X-1, seed 2 had a 20% heavier uranium loading than the first seed and also contained some natural boron as burnable poison. The replacement of the 32 depleted seed fuel assemblies was performed under water, one fuel assembly at a time, through penetrations in the vessel

head. To gain necessary access, the control drive mechanisms and core instrumentation had to be removed and then replaced. This accounted for a large part of the refueling time. The second refueling was started in August 1961 and was completed in 44 days. The increase in speed was attributed to the experience gained in the first refueling, to detailed planning and scheduling, and to thorough personnel training. The estimate in reference 2 is that the refueling time could be reduced to about 30 days if the core instrumentation could be reduced to that characteristic of a nondevelopmental plant.

Because of the special concern with the use of 17-4-PH stainless steel in reactors, a general review of this material was conducted by the Commission. Accordingly, a detailed investigation of the 17-4-PH stainless-steel material used in the Shippingport reactor for two seed lifetimes was undertaken. It was concluded that the components made of this material were suitable for continued operation at Shippingport. This conclusion was based on the carefully controlled procedures used in the manufacture of these components and on the following:

1. At operating temperature the minimum safety factor on the maximum working tensile stress in the assembly is 2, after application of a conservative stress concentration factor.

2. The residual tensile stresses measured in the irradiated components were less than 30,000 psi. Samples of the material removed from the reactor were subjected to stress corrosion tests for 1000 hr at stress levels up to 60,000 psi and indicated no tendency toward stress corrosion cracking.

3. Irradiated tie rods, lead screws, and spline shafts were impact tested to produce nominal stresses of twice the value developed in operational full-height scrams without inducing defects detectable by liquid penetrant or magnetic particle inspections.

4. Destructive metallurgical evaluation of material from the lead screws that were in the reactor indicated no change in the tensile properties compared to materials that had not been in the reactor. The hardness had increased from Rockwell C 43 to about Rockwell C 47. However, this had no adverse effect on the performance of the material as indicated by the engineering test results.

5. A complete inspection of all lead screws was made during the seed 2 and seed 3 refueling. Dye check inspection disclosed a small defect in only one lead screw, which was replaced and examined. It was determined that the defect was not a service-induced consequence.

6. No permanent damage to the core would result from failure of a scram shaft assembly.

There has been a loss in ductility in the pressure vessel as described in the following paragraph from reference 2:

> Pressure vessel steels have been found to suffer a loss in ductility reflected in an increase in the ductile-brittle transition temperature as a function of the integrated fast neutron flux dosage. The magnitude of this increase in transition temperature for the Shippingport reactor vessel does not limit operation at normal operating temperatures and will not do so throughout core 2 life based on present materials data. However, at temperatures below 200°F the increase in transition temperature as a result of fast neutron dosage does place a limit on the permissible stress levels in the reactor

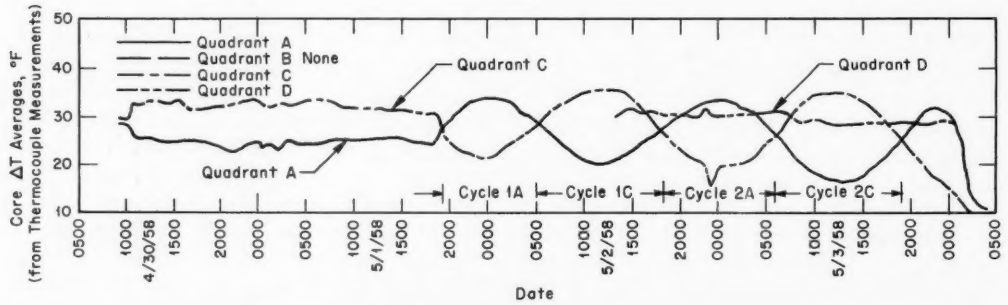

Fig. X-7 Shippingport PWR core 1 power oscillations,[2] seed 1.

vessel. Accordingly, to ensure vessel integrity, operating procedures have been established and are rigorously followed to control the pressure-temperature relationships during all plant startups and periodic hydrostatic testing such that the resultant stresses are well below the allowable values, taking into account the irradiation-induced effects on the transition temperature of the material.

Experience with Major Equipment

The operation of core structure, reactor-vessel closure, and control drive mechanisms has been very satisfactory. However, some items of equipment in the primary coolant circuit and in the steam-plant circuit have required modification or replacement. These problems have accounted for the majority of operating difficulties that have been experienced.

The four canned-motor pumps for primary coolant circulation are of the two-speed, vertical, single-stage, centrifugal design. There have been three incidents of pump failure. The first involved collapse of the can that separates the stator coils from the reactor coolant. This could have been caused either by operation at low primary system pressure or by a pinhole in the can. The minimum system pressure during pump operation has been increased from 100 to 300 psig above saturation to reduce the probability of such failures. A second incident involved failure of the upper and lower radial bearings due to overheating because of restrictions in the internal cooling system of the pump. These restrictions are believed to be due to a mixture of free hydrogen and steam entering the pump cooling system by way of a vent header that was common with the pressurizer. The condition was corrected by rerouting the pressurizer vent line to the blowdown tank. A third incident occurred after a period of hot standby service when the pump failed to start due to distortion and binding of the shaft and impeller resulting from a temperature differential believed to result from inadequate heat removal from around the shaft. The pump was replaced with another pump.

Of the four steam generators, two were supplied by one manufacturer and two by another. Early in the plant operation, some of the tubes failed by caustic stress corrosion on the secondary side which was caused by formation of a steam pocket due to insufficient circulation. To correct the condition, two additional steam risers were added to the equipment, and the water chemistry was improved. Monosodium, disodium, and trisodium phosphate are now used for pH control to assure the complete absence of "free" alkalinity in the boiler water. The phosphate concentration is maintained in the range of 100 to 300 ppm, and the pH value is maintained between 10.6 and 11.0.

The feedwater heaters have been particularly troublesome owing to leaking tubes. Defective tubes have been periodically plugged, and two of the heaters have been completely retubed. The principal causes of the trouble have been identified as inadequate venting and lack of stress relieving in the tube bends. These deficiencies have been corrected, and stress-relieved Arsenic-Admiralty tubes in lieu of the original Admiralty tubes have been installed.

Two turbine components have given trouble. A governor valve stem failed, and subsequently all the governor valves were replaced with redesigned units. The turbine interstage moisture separator failed early in its life. After more difficulties the separator was completely redesigned, and it has performed well since that time.

Radiation and Contamination Control

The reactor and the primary coolant circuit are completely enclosed within four pressure vessels that are interconnected. The multivessel container is designed and sized to hold the steam pressure resulting from a major rupture of the primary coolant system together with a rupture on the secondary side of one boiler. Conservative calculations indicate that an internal pressure of 52.8 psig and an internal temperature of 280°F would result under such unlikely circumstances.

Operation of the plant has provided operating data on the effectiveness of specific systems and methods of controlling radioactive contamination and monitoring personnel radiation exposure. Definite patterns of radiation and contamination control have been developed. Places in the plant in which personnel could receive high radiation exposure with the plant at power have been designated exclusion areas.

Access to exclusion or contaminated areas is carefully controlled, and periodic surveys of radiation levels are made in all areas of the facility. The surrounding area of the plant is monitored continuously, and the data so far have indicated no measurable increase in activity due to the operation of the plant.

The background radiation in the offices and other occupied areas of the plant has thus far shown no increase during operation. The shutdown radiation levels in the limited-access areas of the reactor plant have remained essentially the same as measured during seed 1 operation. The radiation level of the main coolant loops, at 2 hr after shutdown from prolonged 100% power operation, appears to be building up at a slow rate. The radiation was 70 to 80 mr/hr near the end of seed 2 operation compared to values at a comparable time during seed 1 operation of 60 to 70 mr/hr.

Because of the presence of tritium and radioactive corrosion products in the primary coolant system, it is important to minimize the leakage. The leakage rate was about 35 to 50 gal/hr during the operation of seeds 1 and 2. This leakage is principally due to leakage from six primary relief-valve seats. During the second refueling, four of these relief valves were repaired, and the leakage rate has been reduced to approximately 10 gal/hr. The leakage is collected and discharged to the waste-disposal system.

In the four years of operation at Shippingport, the waste-disposal system has performed adequately over a wide range of conditions. The criteria for the discharge of radioactive wastes are contained in a permit granted to Duquesne by the Commonwealth of Pennsylvania. Under the terms of the permit, a maximum of 6200 μc/day and a yearly average of 1590 μc/day of radioactivity may be discharged into the Ohio River. Tritium has an individual discharge limit of 10 curies/day averaged over 365 consecutive days and a maximum of 50 curies/day. In all cases the concentration of radioactivity in the final effluent discharged to the river or atmosphere must not be more than one-tenth of the maximum permissible concentration as given in the *National Bureau of Standards Handbook No. 69*. The radioactivity release from the Shippingport station has always been well within these limits.

The average discharge of tritium over a four-year period was only one-sixtieth of the average allowable tolerance level under the terms of the waste-disposal permit. In December 1960, isotopically pure lithium (99.99% Li^7) was made available as lithium hydroxide for pH control of the reactor coolant. Since the primary source of tritium in the reactor coolant is Li^6, the resulting concentration has been greatly reduced since that time. A maximum concentration of tritium of 280 μc/liter was reached during the seed 1 operations; at the present time the concentration in the coolant is only 2 μc/liter.

The operation of the Shippingport reactor has thus far been characterized by coolant fission-product activity levels considerably lower than what the waste-disposal system was designed to handle. The primary coolant purification system and the waste-disposal system were designed to operate with as many as 1000 defected blanket fuel elements in the core. Based on the performance of the waste-disposal system to date, it has been concluded that adequate margin exists in the waste-disposal system to meet any anticipated processing requirements at Shippingport.

Second Core

Future plans for the Shippingport facility are concentrated upon reactor-core development with the objectives of long life and high power density. These plans call for the replacement of core 1 by a second core, which will also be of the seed and blanket type. Reference 2 gives the following reasons for continuing with the seed and blanket concept:

1. The continued intrinsic worth and importance of obtaining a large fraction of the total energy from natural uranium in a light water reactor nuclear power station.
2. The achievement of a very long life core without the heavy inventory of enriched fuel that would otherwise be required.
3. The demonstration during four years of operation in the Shippingport station that the seed and blanket core concept possesses the performance characteristics, with respect to dynamic load response, operating stability, and simplicity of control, that make the plant well suited to integration with an electric utility system.
4. The reduction in the number of movable control elements required in a large, high power, long life core inherently afforded by using a relatively small, highly enriched core as the driving element.

5. The absence of any clear-cut technical or economic reasons for changing to a different core type.

The principal effects of changing to the new core will be an increase in power from 231 to 505 Mw(t) and an increase in fuel lifetime expectancy (see Table X-2). Both seed and blanket fuel elements are redesigned, and the core height is to be increased from 6 to 8 ft. Substantial changes will also be made in the pressure-vessel closure and its internal components, as indicated in Fig. X-8. The vessel will have a new head. A support flange, through which the core instrumentation leads will be brought out, will be installed between the vessel and the head. The internal components will be all new. The cooling water will flow in a two-pass arrangement over the blanket fuel and in a single-pass arrangement over the seed fuel. The head will be penetrated by 20 control-rod drives and a single refueing port.

As in core 1, the seed will be in an annular form and will consist of 20 highly enriched fuel clusters, each containing a cruciform, hafnium control rod. The blanket, part within and part surrounding the seed annulus, will consist of 77 fuel clusters of natural uranium oxide. The mean core diameter will be about 7 ft.

The seed fuel elements are compartmented plates having a total thickness of about 0.076 in. The wafers of fuel, ZrO_2-UO_2, are 0.036 in. thick, and the cladding is 0.020-in. Zircaloy-4. Three different enrichments of wafers are used, and the wafers are arranged in a particular manner within the cross section of a fuel subassembly to reduce power peaking. Lumped burnable poison, B^{10} in a stainless-steel matrix, is also compartmented. Reference 2 states that the ZrO_2-UO_2 material differs from UO_2 in three major respects:

(1) The initial porosity in ZrO_2-UO_2 has been observed to disappear completely at irradiation exposure less than 6×10^{20} fissions/cc, in contrast to porosity retention in UO_2 wafers even at 34×10^{20} fissions/cc;

(2) Defected ZrO_2-UO_2 fuel elements show no evidence of corrosion attack in either in-pile or out-of-pile tests in high temperature water or steam and for very high fissioning rates including rates which induced corrosion attack on UO_2; and

(3) The thermal conductivity of ZrO_2-UO_2 remains unchanged with irradiation.

The blanket fuel elements are also of the compartmented-plate type, with a total thickness

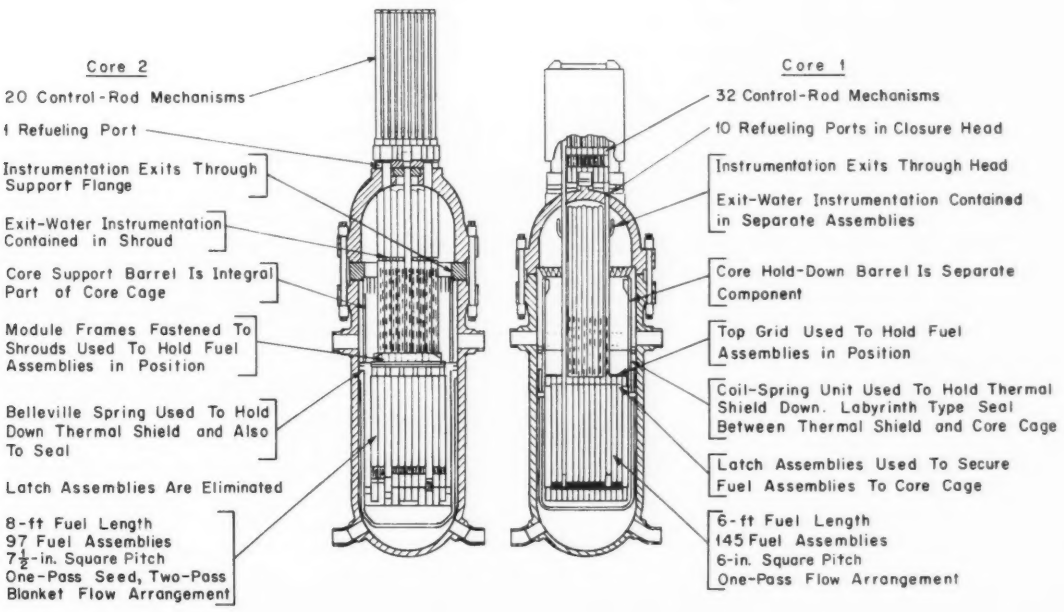

Fig. X-8 Comparison of core 1 and core 2, Shippingport PWR.[2]

of about 0.140 in. The fuel wafers are UO_2 and are 0.100 in. thick. The cladding is 0.020-in. Zircaloy-4. The reference[2] states that the rod type element is being replaced (in order to attain higher power density) because of its higher UO_2 temperature, its limited heat-flux capability, its poor transient thermal response, and its low heat-transfer surface per unit of reactor-core volume. It is expected that the compartmented plate type will contain the small amount of fission gas that is released without bulging.

An extensive amount of experimental work, both in pile and out of pile, has been performed to perfect the fabrication of the compartmented fuel. Tests indicate that the new cladding material, Zircaloy-4, is much less susceptible to hydrogen pickup than Zircaloy-2. Experience with Zircaloy-2 as a cladding material has indicated that it is capable of long-term service in high-temperature water with excellent corrosion resistance and mechanical stability. However, zirconium alloys do tend to absorb hydrogen from the water or from the water-metal corrosion reaction, and the hydrogen migrates in the zirconium and concentrates in the colder regions of the material. Experiments have shown that a hydrogen content of about 200 to 250 ppm in the cladding could create sufficient embrittlement to cause cracking. Zircaloy-4 was basically derived from Zircaloy-2 by eliminating the 0.05% nickel.

To accommodate the increased power from the second core, other components of the plant must be modified. Only three of the four primary coolant pumps are normally used for full-power operation with core 1; with core 2 all four loops will be used. The water circulation per loop is about the same, but the pressure-drop requirement is about 45% higher; therefore new pumps are being purchased. The same type of pump will be used—the canned-motor, two-speed, vertical, single-stage, centrifugal design. The core 1 pump volutes will be retained and machined in place to accept the new impellers.

The present steam generators will be modified to handle the increased duty. The size and number of the risers and downcomers will be increased, and larger steam drums will be installed. The existing turbine-generator set will be used to its full capacity of 100 Mw(e). A heat-dissipation system is being installed to condense the remaining steam, which could generate another 50 Mw(e) if the turbine capacity were available. On the basis of an economic study, the heat-dissipation system was selected over the alternative of increasing the generating capacity. Most of the refueling facilities provided for core 1 will also be used with core 2. The main exception is a fuel-cluster installation and extraction tool of new design suitable for use through the central port in the core 2 reactor-vessel closure. The current schedule is to complete the installation of core 2 and resume operation by the summer of 1964.

References

1. Westinghouse Electric Corp., Bettis Atomic Power Laboratory, The Shippingport Pressurized Water Reactor Project Catalog of Document Abstracts, USAEC Report WAPD-PWR-1606(Rev.), December 1961.
2. P. A. Fleger et al., Shippingport Atomic Power Station Operating Experience, Developments, and Future Plans, USAEC Report WAPD-T-1429, Westinghouse Electric Corp., Bettis Atomic Power Laboratory, December 1961.
3. *The Shippingport Pressurized Water Reactor*, Addison-Wesley Publishing Co., Inc., Reading, Mass., 1958.
4. Westinghouse Electric Corp., Bettis Atomic Power Laboratory, Description of the Shippingport Atomic Power Station, USAEC Report WAPD-PWR-970, June 1957.
5. Westinghouse Electric Corp., Bettis Atomic Power Laboratory, Pressurized Water Reactor (PWR) Project. Technical Progress Report, August 24, 1961, to October 23, 1961, USAEC Report WAPD-MRP-94.
6. H. Feinroth and T. D. Sutter, Jr., The First Refueling of the Shippingport Atomic Power Station, USAEC Report WAPD-233, Westinghouse Electric Corp., Bettis Atomic Power Laboratory, July 1960.

Section

XI

Power Reactor Technology

Sodium-Cooled Reactors

Corrosion and Activity Transfer

An evaluation over a two-year period, Apr. 15, 1957, to Apr. 17, 1959, has been made to determine, under reactor operating conditions, the corrosion and radioactivity transfer within the SRE primary sodium system.[1] This study was made by exposing type 304 stainless steel, zirconium, and beryllium specimens in the hot and cold legs of a bypass loop, in parallel with the SRE primary piping system. The bypass loop contained two identical vertical standpipes, each holding up to 48 metal tabs and provided with a sodium sampler. One leg received hot sodium from the primary sodium outlet line prior to passage through the primary heat exchanger, and the other received cold sodium after its passage through the heat exchanger. After passing through the bypass loop, the sodium was recycled into the main primary system.

The significant conclusion on corrosion, from evaluation of the metal specimens, was that no deleterious effects could be predicted for the stainless-steel components of the SRE primary system. The zirconium tab data indicated that moderate hydriding of the zirconium moderator cans had taken place. The data also indicated that some heavy localized hydriding, which would subsequently reduce the ductility and tensile strength, might have occurred. The relatively low weight gain observed for polished zirconium specimens was indicative of a low oxide pickup on the zirconium moderator cans. Extrapolation of the weight-change data for the polished zirconium specimens to the hot moderator can temperature indicated that an oxide surface formation of 0.40 mg/cm^2 had been reached. It was concluded, on the basis of other studies of the effects of oxidation, that further oxidation will result in essentially no further reduction in the fatigue life of the moderator can.

The first indication of fission-product activity in the SRE primary system was obtained in October 1958 from sodium sampling. The activity was 8.4×10^{-3} $\mu c/g$. The fission-product activity between Oct. 2, 1958, and Apr. 14, 1959, varied between 0.001 and 0.1 $\mu c/g$ of sodium. The mixed fission products transferred to metal specimens in the hot leg of the bypass loop showed an increase from an average of 0.011 $\mu c/cm^2$ to 0.30 $\mu c/cm^2$ between Oct. 13, 1958, and Apr. 17, 1959. The stainless-steel specimen showed no long-lived activated constituent until Apr. 17, 1959. At this time Co^{60} and Mn^{54} were detected at levels up to 5.2×10^{-4} $\mu c/cm^2$ and 7.8×10^{-3} $\mu c/cm^2$, respectively. The transfer of Co^{60} and Mn^{54} occurred about five times faster in the hot leg than in the cold leg. This suggests[1] that the mass transfer is dependent on the diffusion rate rather than the temperature differential.

During the recovery procedure following the fuel-element damage that occurred in the SRE in July 1959, fission-product release and distribution data were obtained.[2] The data indicated that the release fraction of the various fission products had some degree of volatility preference and that the sodium coolant formed an effective trapping agent for all but the rare-gas isotopes. Appreciable deposition of fission-product contamination was found throughout the primary piping system. The deposition involved a plating type mechanism, and the deposit could not be removed by simple flushing. A review of the fuel-element damage that occurred in the SRE in 1959 was given in the December 1961 issue of *Power Reactor Technology*, Vol. 5, No. 1, pages 84 to 87.

Removal of Carbon from Sodium

The removal of the element carbon from the liquid-sodium system is a subject of primary importance in sodium graphite technology. Carburization of austenitic stainless steels, such as those used in fuel cladding and other core components, occurs readily from carbon-bearing liquid sodium at temperatures of 1000°F and higher.[3] The surface of austenitic stainless steel subjected to carbon-saturated liquid sodium reaches an equilibrium content of 2.7 to 3.35 wt.% carbon at 1000 to 1300°F after less than 1 hr of exposure.[4] After carburization, thin austenitic sheets or tubes, such as the clad tubes of fuel elements, become brittle and will tolerate little or no plastic deformation.

The investigation of carbon removal was concentrated on two methods.[5] One method consisted of precipitating the carbon from solution by the introduction of metallic calcium into the sodium. The solid compound formed by the metallic calcium and carbon would then be removed from the sodium by mechanical means. The second method, "gettering," consisted of introducing metal surfaces that would remove the carbon from solution by carburization and diffusion into the material. The getter material would require replacement as its effectiveness deteriorated.

The conclusions reached[5] were that the removal of carbon from the sodium system by a carbon trap which contains a gettering agent is practical and that the choice of gettering material, carbon trap temperature, and geometry must be made on the basis of the particular sodium system for which the carbon trap is designed. It was also concluded that carbon could be removed from sodium systems by maintaining the calcium content at a minimum of 555 ppm. This method also serves to prevent further solution of carbon from solid graphite by the formation of a calcium carbide layer. However, an additional investigation of the behavior of calcium carbide-bearing sodium within a reactor system would be needed before this method could be adopted as a means of removing carbon.

Control Elements for Sodium Graphite Reactors

Reference 6 cites three of the newer methods for control of sodium graphite reactors. The first concept (wire rope-actuated control rods) was fabricated and tested out of pile, and plans

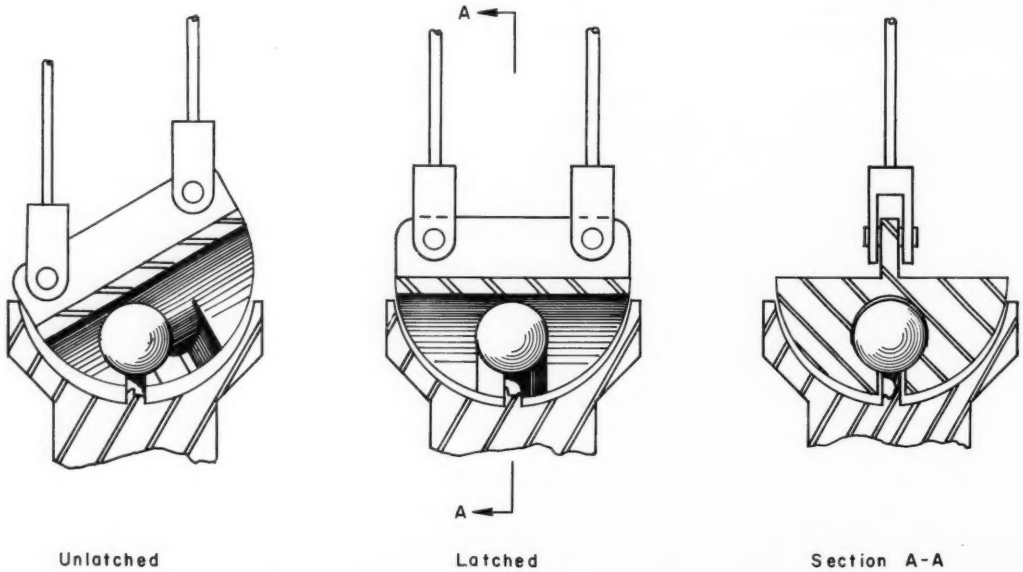

Fig. XI-1 Principle of the ball-latch mechanism.

were made to carry the testing on to the SRE. The second (fuel-and-poison rod) was explored to the extent of a conceptual design. The third (neutron-absorbing gas) was given a preliminary investigation only.

Two variations of the first concept are presented in the report along with a discussion of the relative advantages of each. One of these variations, which is more advanced in development, fabrication, and testing than the other, is a two-piece device that incorporates a ball-latch mechanism which utilizes a ball hook supported by two wire ropes (Fig. XI-1). The hook is essentially a hemisphere, with a slot milled in to engage the ball, which is supported by two wire ropes. Relaxation of one of the ropes allows the latch to tilt and the ball to slide out of the slot. The other half of the device is the ball, which is attached to the upper end of the absorber-material column. The two wire ropes are wound on two separate drums that are operated together to raise or lower the rod. When a scram is called for, a solenoid is deenergized, and this allows one drum to lower its wire rope about 2 in. below the other. This action tilts the ball latch, unlatches the rod, and allows the rod to fall. To restore the original condition, the ball latch must be lowered until the rod can be relatched to the hoisting mechanism and returned to operating position.

As a parallel effort, a brake-clutch control element was developed. Essentially this is a one-drum and one-rope arrangement. For scram a solenoid is deenergized, and the clutch is disengaged through a system of linkages, allowing the rod to fall by gravity. This system has the advantage that the hoisting mechanism need not be lowered to relatch the rod; the clutch can be reengaged and the rod withdrawn at once.

A method of snubbing the rod as it fell was also required. Since the snubbing device must operate in a high-temperature area, springs or pneumatic devices were ruled out. The basic approach adopted was to snub the rod in a bed of granular material, but the provision of a suitable high-temperature granular material was found to be difficult. Sand and other refractory materials were tried with little success. A bed of small balls (0.017 to 0.050 in. in diameter) made of Haynes Developmental Alloy No. 8157 was tested and appeared to be satisfactory.

Commercially available wire ropes were determined not to be suitable for application in the high-temperature environment. Therefore a rope made of a heat-resisting alloy (Elgiloy) was developed, tested, and determined to be strong and flexible after exposure at 1200°F for 1100 hr.

The fuel-and-poison rod concept consists of a series of cones assembled on the rod in such a way that either the fuel cones or the poison cones can be covered by the others. It is intended that in this way the rod can be adjusted to act as either a fuel rod or a poison rod. Achievement of effective action of this kind probably requires that the fuel sections be quite "black" to neutrons. The power generation in the rod would probably be very high.

In the neutron-absorbing gas concept, the gas is conceived as being introduced into the pores of the graphite moderator. It was necessary to limit the gases considered to inert gases that would not combine with the graphite moderator or the cladding. Helium-3 appears to be the only likely possibility.

Several unexplored problems that might affect this system are cited in the reference.[6]

References

1. H. E. Johnson, Corrosion and Activity Transfer in the SRE Primary Sodium System, USAEC Report NAA-SR-5363, Atomics International, Oct. 30, 1961.
2. R. S. Hart, Distribution of Fission Product Contamination in the SRE, USAEC Report NAA-SR-6890, Atomics International, Mar. 1, 1962.
3. W. C. Hayes and O. C. Shepard, Corrosion and Decarburization of the Ferritic Chromium-Molybdenum Steels in Sodium Coolant Systems, USAEC Report NAA-SR-2973, Atomics International, Dec. 1, 1958.
4. W. J. Anderson and G. V. Sneesby, Carburization of Austenitic Stainless Steel in Liquid Sodium, USAEC Report NAA-SR-5282, Atomics International, Sept. 1, 1960.
5. W. J. Anderson, Removal of Carbon from Liquid Sodium Systems, USAEC Report NAA-SR-6386, Atomics International, Dec. 1, 1961.
6. P. F. Shaw, Control Elements for Sodium Graphite Reactors, USAEC Report NAA-SR-5398, Atomics International, Aug. 15, 1961.

Section

XII

Power Reactor Technology

Gas-Cooled Reactors

Helium Technology

Reference 1 is a discussion of the use of helium as a reactor coolant. At present helium is scheduled for use in four major reactor projects: the Dragon at Winfrith Heath, the EGCR at Oak Ridge, the High-Temperature Gas-Cooled Reactor (HTGR) near Philadelphia, and the Turret at Los Alamos. The reference cites the well-known advantages of chemical inertness and high thermal conductivity and specific heat; problem areas are also considered.

The purification of helium in power reactors is the subject of reference 2, in which the impurities are divided, for discussion, into fission-product impurities and chemical impurities. The discussion, although it treats fundamental concepts, directs its interest toward the impurity problems in the Dragon reactor.

The Dragon reactor uses fuel elements that do not have metallic jackets; consequently the escape of a variety of fission products to the recirculated helium coolant is expected. Most varieties of the fission products are expected to condense either on surfaces inside the fuel elements or, at room temperature, in pipes outside the core. The coolant will, however, accumulate the noble gases krypton and xenon and perhaps some bromine and iodine vapor unless special provisions are made for removal. The discussion of fission-product removal in the reference[2] is directed toward the removal of krypton and xenon; the method considered is adsorption on charcoal.

Two stages of adsorption in charcoal beds are required. The first of these is a delay process that occurs in a large charcoal bed operating at approximately room temperature. It is stated that the adsorption of krypton and xenon on charcoal is entirely reversible and that incoming atoms displace adsorbed atoms progressively through a bed of charcoal until breakthrough occurs. These atoms which break through are consequently the oldest; therefore the bed serves to hold up xenon and krypton atoms until radioactive decay has reduced appreciably the rate of heat generation. It is stated that a bed of charcoal having a volume of 5000 liters can delay the krypton isotopes from the 20-Mw(t) Dragon reactor for about 15 hr and can delay the xenon for about 200 hr at 25°C. During this holdup, more than 99% of the beta-decay power (about 100 kw for the maximum possible release of gases from the reactor) is lost.

Once the generation rate of radioactive power has been substantially reduced, it is feasible to trap the xenon and krypton in low-temperature charcoal beds (−196°C). In general, two or more such beds would be provided, and they would be alternately reactivated by allowing them to heat up while the gases released at the higher temperature were pumped off to containers or to some other means of storage or ultimate disposal.

The reference summarizes the known characteristics of charcoal beds, both at room temperature and at low temperatures, and indicates how design procedures are arrived at.

The chemical impurities in helium may come from a variety of sources, and, although helium is a noble gas, the impurities may react with graphite and/or metals present in the reactor. Air and water vapor may be contained in the first charge of helium to the reactor, and the graphite itself may liberate carbon monoxide and hydrogen upon heating, the quantities released depending on the thermal history of the material during fabrication. The steel com-

ponents of the reactor system also can release carbon monoxide and hydrogen.

The corrosion of the graphite-clad fuel element is illustrated by the following reactions:

$$O_2 + 2C = 2CO \quad (1)$$

$$CO_2 + C = 2CO \quad (2)$$

$$H_2O + C = H_2 + CO \quad (3)$$

$$CO + H_2 = C + H_2O \quad (4)$$

$$CO + 3H_2 = CH_4 + H_2O \quad (5)$$

$$C + 2H_2 = CH_4 \quad (6)$$

Reactions 2 and 3 are reversible, suggesting that mass transport to the cooler portions of the loop is possible. Reaction 6 is also reversible, although it has the opposite temperature dependency of reaction 2 and provides a mechanism for transporting carbon from the cold to the hot regions of the fuel element. In the permeable-cladding reactors such as HTGR and Dragon, impurities that are relatively nonreactive with graphite can diffuse through the cladding and attack the fuel. Carbon monoxide and nitrogen are the most important examples of these impurities and form oxides and nitrides, respectively. Steels are susceptible to oxidation-reduction reactions.

The above discussion has neglected the effects of irradiation, and the reference[2] concludes that "...little or no information has been obtained on the effects of irradiation." Some data on the effects of irradiation have been reviewed in the December 1961 issue of *Power Reactor Technology*, Vol. 5, No. 1, page 80.

Since it is evident that the impurities in the helium can enter into a relatively large number of reactions with materials present in the reactor system, methods of controlling the concentrations of the impurities are necessary. In principle it should be possible to allow for the corrosion due to impurities initially present in the system and to make some further allowance for the introduction of impurities by leaks, etc. This technique has the disadvantage of not being able to cope with unexpected sources of impurities, and on-stream processing of the helium coolant is recommended.[2]

Several methods are available to remove chemical impurities from helium: gettering, oxidation and absorption, and freezing. These will be discussed in turn. Useful metals for the gettering purification of helium are given in Table XII-1.* Each of the metals listed in

Table XII-1 USEFUL METALS FOR THE PURIFICATION OF HELIUM[2]

Metal*	Melting point, °C	Working temperature (°C) for impurity removal				
		N_2	H_2	CO	O_2	$CO_2 \rightarrow CO$ $H_2O \rightarrow H_2$
U	1138	800	250	650	>300	>300
Th	1845	800	(250)		400	(>300)
Zr	1850	1000	(300–550)	(950)	600	(800)
Ti	1670	>1000	(300–550)	(950)	980	(800)
Zr-Ti alloy	~1610	(>1000)	300–550	950	800	(800)
La	912	800		(600)	500	
Ce	806	(800)		600	200	
Ba	850	300	(150–530)		300	
Ca	810	650	150–530		650–680	(>500)
Mg	651	640			600	(>500)
Ca-Mg alloy	445	500	450		475	450 (CO_2)
Cu	1083				400–600	
Na-K alloy	Liquid at 25				25	

* Figures in parentheses are assumed by analogy with a similar metal or from data on the reaction of the metal with the undiluted impurity gas. The absence of a figure for the temperature of a particular metal does not necessarily mean that no reaction takes place but rather that no data are available.

Several methods are available to remove chemical impurities from helium: gettering, oxidation and absorption, and freezing. These will be discussed in turn. Useful metals for the gettering purification of helium are given in Table XII-1.* Each of the metals listed in

* Tables XII-1 and XII-2 and Fig. XII-1 are reprinted here by permission from the *Journal of Nuclear Energy: Part B.*[2]

Table XII-1 is discussed in reference 2, but the state of the art appears to require extensive experimental work on a system prototype.

The chemical oxidation and absorption systems are limited to nonaqueous processing since the water vapor introduced into the helium by aqueous processing would be intolerable. Carbon monoxide, hydrogen, and methane can be oxidized by various reagents (e.g., copper oxide), and the resulting water vapor and carbon dioxide can be absorbed by materials such as activated alumina and soda lime, respectively; oxygen can be absorbed by manganous oxide. Table XII-2 shows that quite low outlet water concentrations can be obtained with commercially available absorbents.

Impurity removal by freezing is especially useful in the cases of water and carbon dioxide. Concentrations can be reduced to the vapor pressure of the solid at the refrigerant temperature. The Dragon reactor utilizes a freezer consisting of a heat exchanger operating near liquid-nitrogen temperature. It is regenerated by warming while another freezer takes over.

Additional details on the Dragon helium-purification system are given in Fig. XII-1. The fuel-element traps, located in the lower ends of the elements, are to trap metals and halogen vapors. The helium temperature at this point is about 350°C, but it is expected that a significant delay in the release of iodine vapor may occur even at this temperature. These are charcoal traps and are removed with the fuel elements. The precooler reduces the temperature to about 100°C to facilitate adsorption of xenon and krypton in the charcoal delay beds. The CuO bed oxidizes hydrogen and carbon monoxide for removal in the freezer. The cold charcoal beds are a final cleanup for krypton and xenon and are cooled by liquid nitrogen. The effluent helium is then pumped through the freezer and is circulated back to the reactor.

Table XII-2 COMPARISON OF THE EFFICIENCIES OF ACTIVATED ALUMINA, MOLECULAR SIEVE, AND ANHYDRONE IN A 2-cm-DIAMETER BED[2]

Material, 10 g	Water concentration, ppm		Bed length, cm	Time to p_1 not exceeding 10 ppm, hr	Grams of H_2O removed per 10 g of dry material	Activation conditions		
	Inlet, p_0	Outlet, p_1				Temp., °C	Pressure, μ	Time, hr
Activated alumina	130–140	7	5.2	105	0.34	230	3	30
Molecular sieve*	190	0.7	4.7	384	2.0	600	20	2
Anhydrone†	180	0.2–0.6	4.5	750	3.3	200	40	2.5

* Zeolitic alumina silicates.
† Magnesium perchlorate.

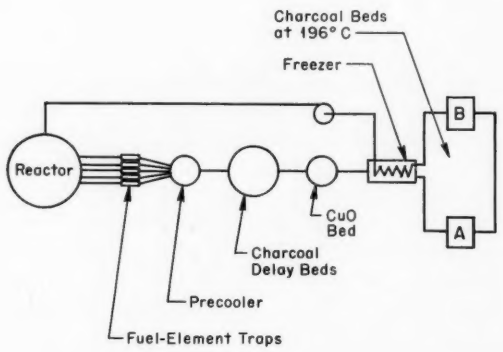

Fig. XII-1 Simplified flow sheet for Dragon coolant cleanup plant.[2]

Prestressed Concrete Pressure Vessels

Since 1955 prestressed concrete pressure vessels have been considered in the United Kingdom as alternates for the steel vessels of the gas-cooled graphite-moderated reactors. The importance of this alternate consideration has increased with the steady increase in the size of gas-cooled nuclear-power stations that are being designed and built in England and on the Continent.

The original concept of the concrete pressure vessel was considered by the United Kingdom Atomic Energy Authority (UKAEA) in the middle

1950's; they examined its feasibility and cost and decided at that time that it had no significant advantage.[3] During 1958 and 1959 Simon-Carves, Ltd., was assigned the job of re-examining the scheme and developing it on a different basis to establish its practicability, increased safety, and economic promise. During this period of development, a model was designed, constructed, and successfully tested.

Meanwhile, independent development on radically different designs had been conducted by the French and was applied to the construction and operation of the prototype, horizontal core, prestressed concrete pressure vessels for the G2 and G3 reactors at Marcoule. Successful operation at Marcoule of the world's first reactor using a concrete pressure vessel began in 1959. Experience has confirmed that the earlier stress analysis and the values for ultimate load factors compare favorably with those commonly accepted for steel pressure vessels. As a result of the operating success, the French have selected concrete for the 400-Mw EDF-3 in preference to the steel vessels used in EDF-1 and EDF-2.

Some of the characteristics of the prestressed concrete pressure vessel are unusual in that the thick prestressed concrete structure serves as both the pressure vessel and the radiation shield.

Under pressure and temperature the behavior of the prestressed concrete pressure vessel is fundamentally different from that of the steel pressure vessel. The concrete in the former acts merely as a matrix to support and separate the high-tensile-steel prestressing cables that form the pressure-resisting elements. The initial prestressing force applied by the wires places the concrete walls of the cylindrical vessel under compression, a state of stress that is gradually relieved, up to a predetermined level, by an increase in the design value of the internal pressure.

The prestressed concrete pressure vessel is thus structurally more stable when under load than when unpressurized. At higher pressures the concrete will pass into a state of tension and will subsequently crack. The level at which such cracking will occur can be governed within reasonably close limits by adjusting the prestressing load in the cables. This is a normal characteristic of prestressed concrete structures. Ultimately, it is theoretically possible for higher pressures to cause the prestressing cables to fail. A characteristic mode of failure under excessive overload has been determined by tests to be common to a variety of configurations. The gastight lining, fitted to the inside face of the concrete cylinder, is generally of mild steel. When subjected to pressures in excess of the working and design pressures of the vessel, the mild steel tends to yield and rupture locally by the time the prestressed concrete has developed cracks across its thickness. Gas is thus allowed to escape, and the internal pressure would normally decrease, enabling the concrete cracks to close under the influence of the prestressing steel. The design can be arranged for the yielding of the mild steel and the cracking of the concrete to take place below the rupture stress of the high-tensile-steel cables, which then would retain their integrity under many of the conceivable overpressure accidents, preventing failures of an explosive nature and inhibiting the large-scale escape of radioactive gases and fission products.

The prestressing cables are installed around the circumference of the vessel and are prestressed to a value higher than they will ever encounter during operation of the vessel so as to allow for subsequent losses in prestress due to creep of the steel, creep and shrinkage of the concrete, and other possible causes. The large number of cables, the wires within each cable, and the small relative strains induced in the concrete by high cable strains ensure that the cables are held in a nearly constant strain condition and that any local failure, in a single cable, of one wire, several wires, or even all the wires would induce a negligible rise of stress in the other cables.

When the prestressing cables are left ungrouted and accessible within their steel sheaths, the operator can check cable stresses, adjust tension, or renew cables, thus correcting any cable deficiency in the pressure-retaining system. Irradiation and temperature tests on the cables have not shown that appreciable physical changes occur; in current designs the cables are protected against any such effects by being located outside the thick concrete layer. Vessel heads can be either domes or flat slabs of the required structural and biological shielding thickness. They can be either prestressed in their own plane or reinforced by an externally applied prestressing force.

Two basic schemes are being studied by the British for the employment of concrete pressure vessels. One scheme, the "all-in" design, contains the whole circuit of boiler, ducts, and core within a single concrete vessel. The second scheme, the "planetary" design, contains the boilers in one or more concrete vessels that are separated or partially separated from the core concrete vessel.

The advantages and disadvantages of the all-in design and the advantages of the planetary design are summarized below:[3]

All-in Design

Advantages:
- Structural design of this single vessel is simpler
- Wall thicknesses are greater for this large vessel
- Simpler foundation conditions are required

Disadvantages:
- Inaccessibility of boiler tubes
- Radiolysis of the water in the boiler tubes is a problem
- Water-tube leak repair is extremely difficult
- Increased corrosion and possible embrittlement of water tubes are due to high oxygen and hydrogen concentration

Advantages of the Planetary Design

- Water tubes are shielded from core radiation by vessel walls
- Leak detection, maintenance, and repair are possible
- Radiolysis ceases to be a problem
- Flexibility in construction and membrane programs
- Separate smaller vessels allow the various contractors greater freedom and independence

It is stated[3] that satisfactory layouts can be achieved for either scheme. The planetary design is favored from the construction standpoint and is considered to be a less radical change than the all-in scheme; however, a final selection will not be made until further experimental work and study have been conducted.

The reference[3] discusses also the need for suitable design and safety criteria for the concrete vessels and stresses the basic differences between such vessels and conventional steel vessels. With a steel vessel, within the elastic range, a pressure rise is accompanied by a proportionate increase in steel stress. Hence load factors have a direct significance. With concrete, a pressure increase up to the point of concrete cracking gives rise to a small disproportionate increase in steel cable stress which is of little significance. The concrete stress change will be a reduction of precompression and later an increase in tensile stress. Under ideal working conditions a very small residual compressive stress would remain in the concrete. If, however, an unrealistically high test pressure or ultimate pressure is specified in the design, ideal stresses under working conditions will not be achieved, the concrete stress being considerably in excess of its optimum. Hence load factors not only have little bearing on the working conditions but also, if set too high, may be downright harmful.

References

1. A. P. Fraas, Helium as a Reactor Coolant, *J. Nucl. Energy: Pt. B*, 2: 53 (February 1962).
2. J. E. Antill et al., The Purification of Helium in High Temperature Reactors, *J. Nucl. Energy: Pt. B*, 2: 63 (February 1962).
3. S. Gill and I. W. Hannah, Prestressed Concrete Pressure Vessels, *Nucl. Power*, 7(71): 48–50 (March 1962).

Section

XIII

Power Reactor Technology

Spectral Shift Reactor

References 1 and 2 present the results of a study in which plant designs, operating characteristics, and power costs were prepared for several nuclear-power plants employing the spectral shift control reactor (SSCR) concept. The work was performed jointly by the Babcock and Wilcox Company and Stone and Webster Engineering Corporation under AEC contracts. The principle of spectral shift control is to compensate long-term reactivity changes by changing the proportions of the reactor's D_2O-H_2O moderator mixture and thereby changing the neutron-energy spectrum.

Now that the experience with UO_2 fuel elements in water-cooled reactors has indicated that quite long exposure lifetimes are feasible, the method of achieving reasonably low fuel costs in such reactors seems quite clear: it consists simply of designing for a long exposure lifetime—perhaps in the range of 20,000 Mwd/ton and above. Since the neutron-multiplication properties of a fuel element change radically over an exposure of that magnitude, the problem of coping with the reactivity changes during a core lifetime can be a difficult one. If the entire core is exposed as a unit, i.e., if a single-batch reloading scheme is used, the initial excess reactivity must be very high. If the excess is compensated by absorbing control rods, a serious wastage of neutrons will result, and so will, usually, very troublesome distortions of the spatial power distribution. One well-known method of avoiding or reducing these problems is by reloading the core in small batches; this fractional reloading scheme is often supplemented by a reshuffling of the partially exposed fuel elements during the reloading procedure to improve the spatial power distribution. A disadvantage of the method is the necessity for several refueling shutdowns during an average fuel-element lifetime. The spectral shift control scheme is intended to make possible single-batch reloading without sacrificing neutrons to control-rod absorption and without introducing large distortions of the power distributions by the reactivity-control scheme.

Spectral shift control requires a close-packed core lattice, as is typical of pressurized-water reactors that are somewhat undermoderated. A change in the concentration of the D_2O-H_2O moderator or moderator-coolant mixture affects the reactivity of such a core principally because the neutron slowing-down power of D_2O is less than that of H_2O. Thus the greater the concentration of D_2O in the D_2O-H_2O mixture, the greater will be the intermediate- and fast-neutron densities relative to the thermal-neutron densities and the greater will be the number of neutrons absorbed in the resonances of U^{238} relative to those causing fission of U^{235} (Fig. XIII-1).* Changes in the D_2O-H_2O proportions will also cause other changes in the neutron balance, such as the relative number of neutrons absorbed in the moderator-coolant mixture and in structural materials and the fractional neutron leakage. However, these effects in a sufficiently undermoderated reactor are considerably smaller than the effect of the change in U^{238} resonance absorption, which alters the division of neutron absorption between fissile and fertile material but does not change appreciably the utilization of neutrons.

The spectral shift control concept is then applied. The moderator-coolant mixture for a reactor with a new core loading has a high concentration of D_2O (78 mole % for the reference design of the study[1]). As the reactor is operated and as its reactivity decreases owing to fuel burnup and fission-product buildup, the

*Figure XIII-1 is reprinted here by permission from the American Society of Mechanical Engineers.[2]

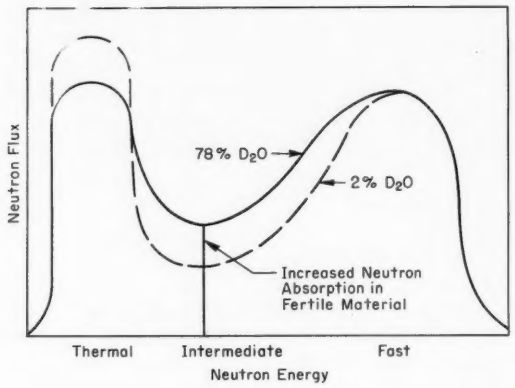

Fig. XIII-1 Schematic of change in neutron-energy spectrum with D_2O-H_2O concentration.[2]

proportion of D_2O to H_2O in the moderator is decreased by diluting the mixture with H_2O. The neutron spectrum is thereby shifted to increase the population density of low (thermal) energy neutrons and to reduce the resonance absorption in U^{238}. In this manner the effects of burnup and fission-product buildup can be counteracted, and the reactivity of the core can be maintained. The process of diluting the moderator mixture with H_2O continues throughout the life of the core until the final D_2O concentration is reduced to the economic optimum as determined by the relative value of additional reactivity that could be obtained and by the cost of reconcentrating the D_2O. The economic optimum concentration of D_2O was determined to be about 2 mole % by this study.

The basic advantages anticipated[1,2] for spectral shift control are most pronounced when considered in relation to a conventional water-moderated reactor utilizing single-batch reloading. These advantages are considered here under the headings "Neutron Economy," "Power Density," and "Core Life."

Neutron Economy

In the SSCR, long-term control is accomplished primarily by varying the neutron absorption in fertile material. No large fraction of neutrons is "wasted" by being absorbed in control rods, burnable poisons, or soluble poisons, and improvements in conversion ratio are therefore expected. The calculated integrated conversion ratio, over the life of a core, is quoted,[1] for the reference design, as 0.73.

Power Density

Since most of the control rods are removed from the SSCR core during full-power operation, it should experience less of the local power perturbations caused by poison control rods than a conventional water reactor that uses absorbing rods for long-term reactivity control, and the distribution will vary less with exposure. It is therefore expected[1] that zone loading of different enrichments will be more effective in eliminating power peaking. The flattened power distribution predicted for the reference-design SSCR has an overall maximum-to-average power ratio of 1.92. This low value results from subdividing the core into 33 zones and subzones containing 16 different uranium enrichments. The improved power distribution obtained by this extensive application of zone loading results, of course, in a high design value for the average power density.

Core Life

An improvement in the "metallurgical" core life is expected[1] for the SSCR because the lower power peaking means that the average burnup of the core will more nearly approach the maximum allowable burnup. The spectral shift scheme provides, of course, for the desired reactivity lifetime.

Work that was done under the contract for the design and economic study included[1] the preparation of SSCR plant designs and cost data for the following seven plants:

1. A reference-design nuclear-power plant with a reactor core of uranium oxide clad in Zircaloy. This design utilizes current technology, and the plant has an electrical capacity of 330 Mw(e).

2. An alternate reference-plant core of uranium oxide clad in stainless steel. Fuel-cycle costs were computed to permit comparison with those of the Zircaloy-clad core. The capital costs and the operating and maintenance costs for the reference plant were essentially unaffected by substituting the stainless-steel-clad core.

3. Nuclear-power plants of 154 and 458 Mw(e) net, based on current technology, and using Zircaloy-clad cores of uranium oxide similar to the reference-design core.

4. Alternate nuclear-power plants of 154 and 458 Mw(e) net, essentially identical to those

mentioned in item 3 above, but using stainless-steel cladding.

5. A "potential" nuclear-power plant with a reactor core of thorium oxide and recycled U^{233} oxide clad in Zircaloy. This plant has an electrical capacity of 333 Mw(e) net and is based on anticipated advances in reactor-core technology resulting from the successful completion of a six-year research and development program.

The reference-design plant of 330 Mw(e) net capacity with Zircaloy-2 fuel cladding receives by far the most extensive coverage in the report. The other plant designs are treated as variations of this reference design.

The core of the reference design consists of 109 fuel elements containing a total of 40,325 kg of uranium, at an average U^{235} enrichment of 3.33 wt.%. These are assembled to form a lattice as shown in Fig. XIII-2. Fuel elements are of three types: (1) 72 fuel elements, each containing 220 fuel rods arranged in approximately an 8-in. square; (2) 25 control-rod elements, each containing 188 fuel rods arranged in an 8-in. square with the centerline rows of fuel rods omitted to accept a cruciform control-rod blade, as shown in Fig. XIII-3; and (3) 12 triangular partial elements, each containing 130 fuel rods, which are used to fill out the octagon shape at the periphery of the reactor core. The fuel rods consist of slightly enriched UO_2 powder in Zircaloy-2 tubes that have a 0.436-in. outside diameter and a 0.025-in. wall thickness. The oxide is loaded into the tubes by vibratory compaction, and the rods are then swaged to the final outside diameter and to an oxide density that is 92% of the theoretical density.

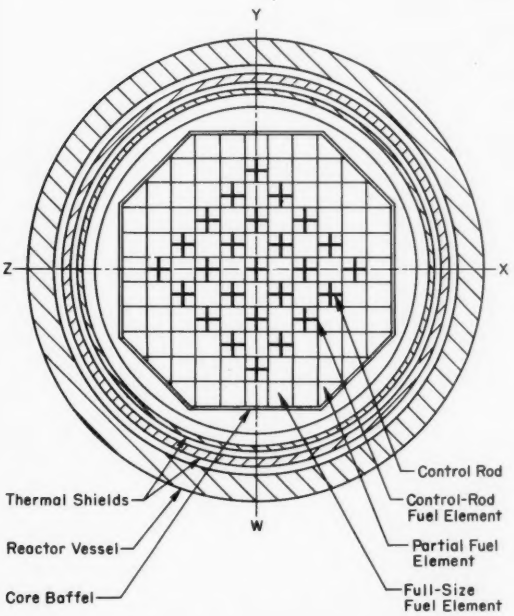

Fig. XIII-2 Cross section of SSCR reference-design reactor vessel and core.[1]

The design calls for zone loading the core radially, axially, and locally to achieve a maximum total instantaneous power-peaking factor of 1.92. The four radial and three axial zones, and the average enrichment of each of these zones, are shown in Fig. XIII-4. Each of these zones is further subdivided into two or three local zones of enrichment as shown in Fig. XIII-5. This results in 33 different zones and subzones, containing 16 different uranium enrichments. As a result, there are no more than 12 of any one kind of fuel element, and in several cases there are only four of a kind. Some elements contain portions of 12 of these zones and subzones and may therefore contain as many as 8 different uranium enrichments. Every individual fuel rod must contain two different uranium enrichments to provide the three axial zones. Most of the elements must be positioned in their respective core lattice locations in a particular rotational orientation so that zone and local enrichments are properly located. Refueling is to take place every 790 calendar days. At that time the plant is shut down, and the entire core is replaced with fresh fuel elements.

As shown in Fig. XIII-2, the SSCR incorporates 25 poison rods for control. Of these, 21 are normally completely out of the core during full-power operation. These rods are to compensate for xenon build-in and that portion of the Doppler reactivity effect resulting from the change in fuel temperature with reactor power, to provide shutdown margin, and to serve as safety rods. Four of the control rods function as shim rods and are inserted in the core to a depth of from 25 to 50% at all times during operation. The D_2O-H_2O moderator-coolant mixture is diluted intermittently rather than continuously, and it is the position of these four shim rods that tell the operator when dilution with H_2O is required. When the group of four shim rods must be withdrawn to the 0.25 posi-

tion in order to attain full power, H_2O is added to the mixture under manual control until the change in concentration requires inserting the four shim rods to the 0.5 position. Additional control is provided in the SSCR design to permit operation in the 0 to 20% of full-power range, and during startup and shutdown, by a system that adds and removes boric acid from the moderator-coolant system.

The total control available in all 25 control rods is 0.08 k_{eff}. Another 0.08 k_{eff} is available in the soluble poison boric acid system, for a total of 0.16 k_{eff}. Since the k_{eff} of the hot clean core with 100% H_2O moderator-coolant is 1.28, it is very important that all precautions be taken to prevent the unintentional dilution of the D_2O-H_2O mixture with H_2O. Interlocks and alarms are provided to prevent this, and the

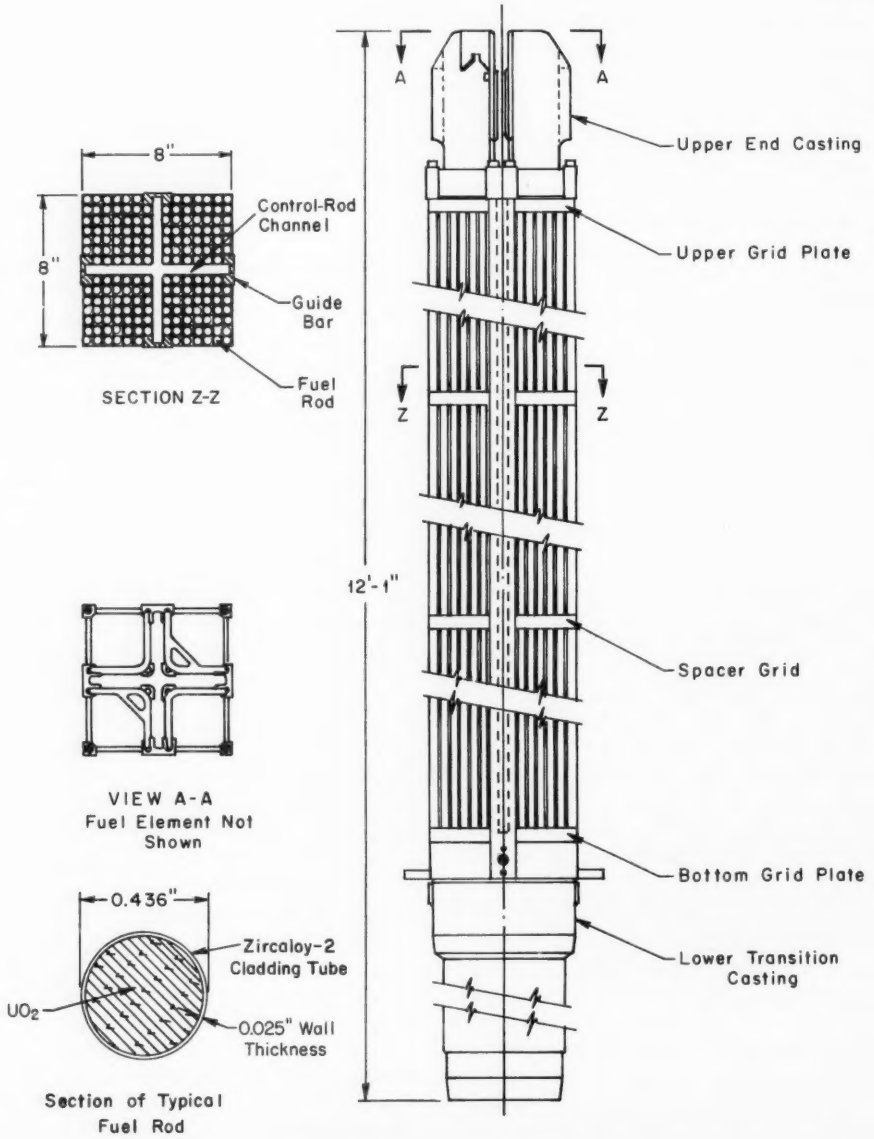

Fig. XIII-3 SSCR control-rod type fuel element.[1]

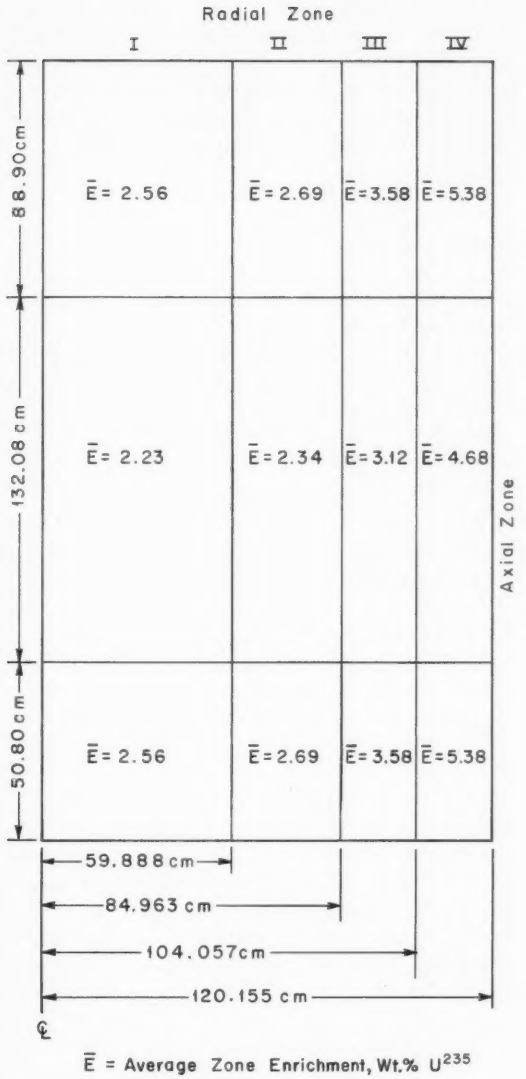

Fig. XIII-4 SSCR reference-design core radial and axial enrichment zones.[1]

dilution pipeline is provided with two valves in series which are interlocked to shut off automatically to prevent a light-water accident. In the event that all these precautions should fail, an emergency borated-water injection system is provided. This safety injection system would also be used to shut down and cool the core in the event of a large primary system rupture.

The 1074 Mw(t) of power produced by the SSCR reference-design reactor is transported by the D_2O-H_2O moderator-coolant through three parallel loops to three vertical steam generators. Here, 800-psia saturated light-water steam is produced for use in the conventional steam plant. This plant employs moisture separation, reheat, and four stages of feedwater heating. The net plant electric power output is 330 Mw, giving a net electric generating efficiency of 30.7%. Equipment in the primary coolant system, the auxiliary systems, and the turbine-generator section of the SSCR plant are essentially the same as those of conventional pressurized-water reactor plants. The one exception is a distillation plant that is used to reconcentrate the diluted D_2O-H_2O moderator-coolant mixture. This distillation plant consists of two towers, each 4 ft in diameter and 86 ft high, which fractionate the diluted moderator-coolant bled from the reactor into the 78 mole % D_2O required at the startup of a fresh core and into a dilute stream of 0.5 mole % D_2O.

The generating cost estimated in the reference[1] for this 330-Mw(e) SSCR reference de-

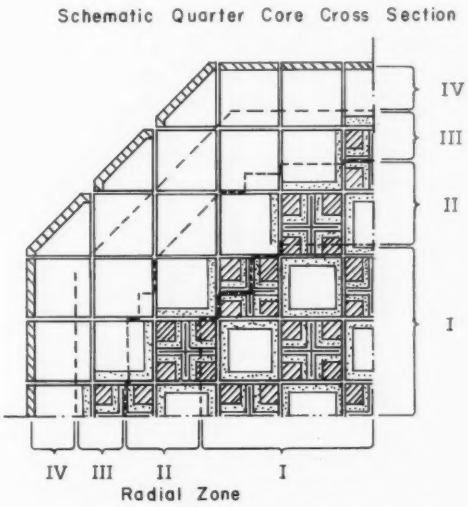

Local Enrichment, Ratio $E/\bar{E}$

E = Local Enrichment

$\bar{E}$ = Average Zone Enrichment

	Zone I	Zone II	Zone III	Zone IV
	0.82	0.80	0.70	— — —
	0.95	0.93	0.88	0.90
	1.12	1.06	1.01	1.01

Fig. XIII-5 Local enrichments within zones of SSCR.[1]

sign plant is 6.37 mills/kw-hr, compared with 6.7 mills/kw-hr estimated for a conventional (fossil fuel) plant of the same capacity in the same New England area.

The spectral shift concept represents an effective method of compensating large reactivity changes without compromising neutron economy and without introducing large distortions of the power distribution. These are real advantages to be weighed against the expenses connected with this novel use of D_2O and against whatever practical problems the system may exhibit. The importance of the latter may depend rather strongly on whether there is reasonable assurance that a core will, in fact, operate for its entire lifetime without requiring the replacement of some fuel assemblies. There are other questions stemming from the highly undermoderated condition of the fresh core. It seems probable, for example, that the removal of fuel from the interior of the lattice of the fresh core would increase reactivity. Such a situation is not obviously a troublesome one, but it is one that may illustrate the unusual character of the reactor.

References

1. D. Mars and D. Gans, Jr., Spectral Shift Control Reactor Design and Economic Study, USAEC Report BAW-1241, Babcock and Wilcox Co. and Stone and Webster Engineering Corp., December 1961.
2. J. Coughlin, Spectral Shift Control Reactor, Paper No. 61-PWR-6, presented at the National Power Conference, American Society of Mechanical Engineers, San Francisco, Calif., Sept. 24–27, 1961.

Section

XIV

Power Reactor Technology

Power-Reactor Experiments

In October 1961 the International Atomic Energy Agency (IAEA) sponsored a symposium on power-reactor experiments which was held in Vienna. The symposium was devoted to discussions on the technical features, present experience, and future potential of power-reactor concepts that are in the experimental stage of development, particularly the concepts for which an integrated reactor experiment is either under way or contemplated. The papers presented and the resulting discussions have been collected and published by the Agency in two volumes.*[1,2]

Several of the papers described reactor experiments in the megawatt range, and these have been tabulated and identified in Table XIV-1. Most of the remaining papers treated specific problems of the various concepts and described the current status of development of the concepts. Although it is impractical to attempt a review of all of the papers, the scope of the conference and the range of concepts under consideration may be inferred from Table XIV-1 and from the list of papers in the references. The reactor types considered may be grouped under the headings "Gas Cooled," "Circulating Fuel," "Fast Breeder," "Nuclear Superheat," and "Miscellaneous." The conference was, of course, devoted to the more advanced concepts in these categories and did not consider prototype, demonstration, or commercial reactors which are in existence or under construction.

In the field of gas-cooled reactors, most of the attention was given to reactors employing fuel elements without metallic jackets, although the EBOR reactor is an exception, in which oxide elements (BeO plus highly enriched UO_2) with Hastelloy X jackets are being considered as the first fuel loading. Among the reactors that do not employ metallic jackets, the approach to fission-product containment within the fuel ranges from attempts to minimize the escape of fission products, as in the Dragon experiment,[1a] to the intentional promotion of fission-product release, as in the Japanese concept of the semihomogeneous reactor.[1f] The basic idea underlying the latter concept is that the fission products that do leave the fuel will be removed by suitable continuous processes during reactor operation, with resultant benefits in neutron economy.

The Dragon program appears to have made considerable progress toward selection of sealants and bearing materials. Where possible, flanged joints with silver gaskets are to be used. Silver gaskets and serrated flange faces have produced leak-rate coefficients lower than 10^{-9} atm/(cm^3)(sec) per centimeter of gasket length. Bearings and related surfaces which have been vapor etched to a finish of 15 to 20 μin. and coated with a microfine MoS_2 powder have exhibited excellent wear properties in gaseous atmospheres up to 450°C, where lubricants may not be allowed. An in-pile mass transport loop in the BR-2 (Mol, Belgium) is being constructed and will be used to obtain data concerning the oxidation of graphite, carbon resettling problems, and hydrogenation of graphite. Similar investigations will be made for the Pebble-Bed Reactor by ORNL.

In any consideration of the overall status of high-temperature gas-cooled reactors, the Peach Bottom reactor should, of course, also be considered.[4] It was not covered at the symposium, presumably because it is not considered to be a reactor experiment. In the field of advanced gas-cooled concepts which represent

*IAEA publications may be purchased at the United Nations Bookshop, United Nations Headquarters, New York City, or ordered from the International Atomic Energy Agency, Distribution and Sales Unit, Kaerntnerring, Vienna I, Austria.

Table XIV-1 TABULATION OF POWER-REACTOR EXPERIMENTS THAT ARE IN PROGRESS OR BEING CONSIDERED[1,2]

Name	Sponsor (country)	Power, Mw(t)	Fuel material	Fuel cladding	Moderator material	Coolant	Status	Remarks
Gas-cooled reactor types:[1a-1h]								
Dragon[1a,1b]	U. K. –O.E.C.D.	20	UC_2-ThC_2	Graphite	Graphite	He	Under construction	Reactor design is described; problems concerning loop containment, corrosion of graphite, coolant processing, and fuel handling are being investigated.
Experimental Beryllium Oxide Reactor (EBOR)[1c]	U. S.	10	UO_2-BeO	Hastelloy X	BeO	He	Completion March 1963	A developmental program, along with operation of a low-power reactor, is aimed toward producing a reactor that meets maritime or gas-turbine requirements.
Pebble-Bed Reactor	U. S.	10	UO_2-ThC_2	Graphite	Graphite	He	Design study	A low-power reactor is proposed to investigate fuel designs, graphite corrosion, coolant purification, and coolant containment problems.
Circulating-fuel reactor types:[1i-1l]								
Molten-Salt Reactor Experiment (MSRE)[1l]	U. S.	10	ThF_4-UF_4		Graphite	LiF-BeF_2-ZrF_4-ThF_4-UF_4	Critical in 1964	High temperatures without high pressures, under good heat-transfer conditions, are expected; problems concerning compatibility of loop and moderator materials, remote maintenance, freeze valve, and freeze flanges are recognized.
KEMA Suspension Test Reactor (KSTR)[1j,1k]	Netherlands	0.25	UO_2-ThO_2		H_2O	H_2O	Under development	UO_2-ThO_2 fuel particles in suspension in circulating H_2O; particles are small enough to allow escape of fission products by recoil; to operate at 250°C under hydrogen overpressure of 20 atm, with total pressure of 60 atm. Low-temperature zero-energy assembly already constructed.
Aqueous Homogeneous, UO_2 Suspension (HR-2)[1i]	Czechoslovakia	10	UO_2		H_2O	H_2O	Design study	Redesign of HR-1 (reference 3).
Fast-breeder reactor types:[1m-1s]								
Dounreay Fast-Breeder Reactor (DFBR)[1m]	U. K.	72	U	Nb and V		NaK	In operation	Considerable operating experience applicable to high-temperature breeding reactors is being obtained. Fuel and coolant handling, coolant purification, and cladding problems are being studied.
Experimental Fast Oxide Reactor (EFOR)[1n]	U. S.	10	PuO_2-UO_2	Stainless steel		Na	Proposed	The engineering problems, safety aspects, and economics are being investigated for fast-breeder oxide-fueled reactors.
Fast-Breeder Reactor, Rapsodie[1q,1r]	France	10	U metal or oxide			Na	Under construction	An experimental fast breeder that can use a variety of fuel-element types; sodium-cooled, with NaK intermediate system.
Fast Reactor, BR-5[1s]	U.S.S.R.	5	PuO_2			Na	Operating	An experimental fast reactor using plutonium oxide fuel. Kinetics, temperature coefficients, power coefficients, and fission distributions are discussed.

Nuclear superheat reactor types:[2a–2g]								
BORAX-V[2a]	U. S.	20	UO_2	Type 304 stainless steel	H_2O	H_2O	In operation	Both direct-cycle boiling cores and boiling-superheating cores will be tested. Objectives are to ascertain operational limitations and/or specific conditions for several cores and answer questions pertaining to operation of dual-zone reactors.
ESADA, Vallecitos Experimental Superheat Reactor (VESR)[2d]	U. S.	12.5 (later 23)	UO_2	Stainless steel	H_2O	H_2O	Operation expected by fall 1962	A separate superheat reactor type that will receive saturated steam from the VBWR, add considerable superheat and exhaust to a turbine system in which the steam will be used to produce electric power. The ESADA-VESR program is a developmental stage for a possible 300- to 500-Mw(e) nuclear-power plant.
Miscellaneous:								
Sodium Reactor Experiment (SRE) (modified)[2h]	U. S.	45	UC	Stainless steel	Graphite	Na	Reworked by 1963	The SRE facility will be modified to obtain increased power levels, high temperatures, and higher thermal performance.
Organic-Cooled Heavy-Water-Moderated Reactor (ESSOR)[2i]	Euratom	40+	Variable	Variable	D_2O	Organic	Under development	A tube type D_2O-moderated reactor having a ring of 24 D_2O-cooled MTR type fuel elements surrounding a test zone of 12 fuel elements cooled by organic liquid. Maximum power of "feeder" annulus = 40 Mw.
Plutonium Recycle Test Reactor (PRTR)[2j]	U. S.	70	PuO_2–UO_2		D_2O	D_2O	Being tested	A pressure-tube reactor cooled and moderated by D_2O. Initial tests have revealed no unsafe or unexpected problems due to PuO_2 utilization. Control by moderator-reflector level has been accomplished. More tests are scheduled. PuO_2/UO_2 ratio will be varied.
Saxton[2k]	U. S.	20	UO_2	Stainless steel	H_2O	H_2O	Testing during 1962	A pressurized-water reactor for experimental operation. Novel features include a water-soluble neutron absorber, planned bulk boiling, an oversized steam generator and pressurizer, a variable-speed coolant pump, and a multilayer core vessel. Mixtures of H_2O and D_2O may be used later for neutron spectral shift studies.
VULCAIN[2l]	Belgium	65	UO_2	Zr alloy	D_2O–H_2O	D_2O–H_2O	Design study	A mixed-moderator pressurized-water reactor, suitable for maritime applications. Coolant and moderator will be separated thermally, and H_2O-to-D_2O ratio will be increased to compensate burnup.

less drastic departures from past technology, one would consider also the Advanced Gas-Cooled Reactor (AGR)[5] and the Experimental Gas-Cooled Reactor (EGCR).[6]

The circulating-fuel concepts treated were the Molten-Salt Reactor and the Aqueous Homogeneous Suspension Reactor. The design of the Molten-Salt Reactor Experiment (MSRE) and the research and development leading to the design were discussed in considerable detail.[1m] The major contributions in the aqueous homogeneous field were descriptions of the work in the Netherlands, which has been going on for some years. The two papers covering this project describe the results of experiments with a subcritical circulating suspension system[1j] and the chemical aspects of the aqueous homogeneous suspension reactor.[1k] In addition to its use for measuring the purely neutronic characteristics of the system, the neutron multiplication of the subcritical system was used as an indicator of fuel concentration, to make possible investigations of the flow and concentration distribution of the suspension. A paper from Czechoslovakia on the hydrodynamic aspects of a suspension reactor[1i] described how the results of tests with a mockup of the HR-1 reactor, which had previously been discussed at the 1958 Geneva Conference,[3] had led to a redesign, which has been designated HR-2. A Russian paper[1p] discussed the use of fused plutonium and uranium chlorides as the circulating fuel for a fast-breeder reactor.

The papers on fast-breeder reactor experiments covered the Dounreay fast breeder (DFBR),[1m] the French fast breeder, Rapsodie,[1q,1r] and a description of operating experience with the Russian fast breeder, BR-5.[1s] The design of a proposed experimental fast oxide reactor, of 10-Mw(t) output, was also described.[1n]

The British fast-breeder program was started in 1953 and is continuing after several refinements of the DFBR facility. The paper on the DFBR described particularly those refinements and modifications which have been found desirable since criticality was first attained in late 1959. Unexpectedly high oxide and hydride concentrations have been experienced, and the entrainment of nitrogen gas in the circulating coolant has been observed. Nitrogen is used as the blanket gas and is being held at 50 psig at present. The niobium and vanadium fuel canning materials have been moderately successful and will apparently be adequate if the oxide and hydrogen content of the coolant is kept within a few parts per million. Toward this objective, very careful cleaning, purging, and filling of the coolant loop are required. A source of hydrogen previously resulted from moisture entrapment during sodium filling.

A complete account of the status of fast-reactor development should, of course, include also the EBR-II (reference 7) and the Enrico Fermi fast reactor,[8] which were not discussed at the symposium.

In the field of nuclear superheat, the papers discussing reactor experiments and in-pile experiments came from the United States and Russia. The U. S. reactor experiments reported included the BORAX-V reactor[2a] (which was reviewed in the December 1960 issue of *Power Reactor Technology*, Vol. 4, No. 1, pages 71 to 73) and the ESADA Vallecitos Experimental Superheat Reactor,[2d] which is being built by the General Electric Company under the sponsorship of the Empire State Atomic Development Associates (ESADA). Other nuclear superheat reactors, which are not reactor experiments, are the Pathfinder reactor[9] and the BONUS reactor.[10]

The results of early irradiation tests on nuclear superheat fuel elements in the SADE test loop in the Vallecitos Boiling-Water Reactor (VBWR) were also reported. These included one test in which a failure appeared to be attributable to chloride stress corrosion. Later tests have confirmed the seriousness of stress corrosion in nuclear superheat fuel elements. Some of these results are discussed in Sec. VII of this issue. A general discussion of nuclear superheat was given in the June 1961 issue of *Power Reactor Technology*, Vol. 4, No. 3, pages 71 to 85.

The Russian papers on nuclear superheat consisted of further discussions on (1) the performance of experimental superheating elements in the Russian First Atomic Power Station reactor[2b] and (2) the design of a graphite-moderated superheating reactor incorporating elements of the same general type.[2c] It is stated that experimental superheating elements have operated at steady-state conditions for more than 1000 hr and under transient cycling conditions for more than 50 superheatings. Steam temperatures as high as 370°C (697°F) at 85

kg/cm^2 (1208 psi) were obtained. It will be recalled that the early Russian concept of an integral boiling-superheating reactor[11] envisioned a graphite-moderated reactor containing internally cooled, tubular fuel elements, some of which were cooled by boiling water and others by superheated steam. Although the steam is superheated directly in this concept by passage through the superheating fuel elements, this steam is not that which was evaporated in the boiling elements but, rather, is secondary steam that has been formed by heat exchange with the boiling-water coolant. It appears that the Russian workers have now changed to a completely direct-cycle system, probably because the generation of really high-pressure steam, as would be desirable for use in conjunction with superheat, would be difficult with indirect steam generation. However, the use of direct-cycle steam in the superheater elements may accentuate the stress-corrosion problem because such steam ordinarily has a high oxygen content as a result of radiolytic decomposition in the reactor.

Other papers on nuclear superheat covered the Swedish project on a pressure-vessel type of natural-circulation boiling-D_2O reactor with integral superheat[2f] and a British investigation of the use of zirconium alloys for pressure tubes and fuel jackets in steam-cooled reactors.[2g]

A number of other reactor experiments, which do not fall under any of the categories discussed above, are listed under the "Miscellaneous" heading in Table XIV-1. The table indicates briefly their purposes and characteristics.

References

1. *Power Reactor Experiments, Vol. I, Proceedings of a Symposium, Vienna, October 23–27, 1961*, International Atomic Energy Agency, Vienna, 1962.
   - *a.* L. R. Shepherd and P. J. Marien, Research and Development Aspects of the Dragon Reactor Experiment, page 13.
   - *b.* G. E. Lockett, Engineering Aspects of the Dragon Reactor Experiment, page 49.
   - *c.* W. C. Moore, Experimental Bases for the Design of the EBOR, page 79.
   - *d.* A. P. Fraas, Pebble-Bed Reactor Problems To Be Investigated in a 10-Mw(t) Reactor Experiment, page 103.
   - *e.* Z. P. Zarie, Rhombohedrally Packed Pebble Bed Reactor, page 125.
   - *f.* E. E. Nishibori et al., Concept of the Semi-homogeneous Reactor (SHR) and Present Status of Research, page 149.
   - *g.* F. Barth et al., In-Pile Measurements of the Release of Fission Products from Uranium Dioxide in a Graphite Matrix, page 155.
   - *h.* J. B. Sayers and J. H. Worth, Comparison of the Irradiation Behaviour of 1% PuO_2 in UO_2 and Stoichiometric UO_2, page 171.
   - *i.* P. Noratny and V. Khamrad, Hydrodynamical Aspects of a Homogeneous Suspension Reactor, page 187.
   - *j.* J. A. H. Kersten et al., Physical Aspects of an Aqueous Homogeneous Suspension Reactor, page 197.
   - *k.* M. E. A. Hermans et al., Chemical Aspects of an Aqueous Homogeneous Suspension Reactor, page 225.
   - *l.* A. L. Boch et al., The Molten-Salt Reactor Experiment, page 247.
   - *m.* J. L. Phillips and A. G. Frame, The Dounreay Fast Breeder Reactor Experiment, page 295.
   - *n.* M. J. McNelly et al., Experimental Fast Oxide Reactor, page 317.
   - *o.* S. A. Hasnain, Fuel Cycles in Fast Reactors, page 345.
   - *p.* M. Taube, Fused Plutonium and Uranium Chlorides as Nuclear Fuel for Fast Breeder Reactors, page 353.
   - *q.* C. P. Zaleski and L. Vautrey, The Fast Breeder Reactor RAPSODIE, page 365.
   - *r.* L. Vautrey and C. P. Zaleski, Experiments Prior to Construction of the RAPSODIE Reactor, page 369.
   - *s.* M. S. Pinkhasik et al., Operating Experience with the BR-5 Fast Reactor, page 375.
2. *Power Reactor Experiments, Vol. II, Proceedings of a Symposium, Vienna, October 23–27, 1961*, International Atomic Energy Agency, Vienna, 1962.
   - *a.* W. R. Wallin et al., BORAX-V Integral Nuclear Superheat Reactor Experiments, page 9.
   - *b.* V. V. Dolgov et al., Single-Pass Superheat Experimental Setup at the First Atomic Power Station Reactor, page 27.
   - *c.* N. A. Dollezhal et al., Uranium-Graphite Power Reactor with Direct Steam Supply to the Turbine, page 41.
   - *d.* D. H. Imhoff, The ESADA Vallecitos Experimental Superheat Reactor, page 53.
   - *e.* S. A. Skvorutsov and S. M. Feinberg, Application of Supercritical Steam Parameters to Pressurized Water Power Reactors, page 81.
   - *f.* P. H. Margen, Current Status of Work in Sweden on a Boiling and Superheating Heavy-Water Reactor, page 97.
   - *g.* R. C. Asher et al., Investigations Relating to the Use of Zirconium Alloys in Steam-Cooled Reactors, page 135.
   - *h.* S. Siegel and R. Dickinson, The Modified Sodium Reactor Experiment, page 159.
   - *i.* C. Chassignet et al., Description of a Specific Test Reactor for Studying the ORGEL System, page 183.

j. J. R. Triplett and R. E. Peterson, Measured Physics Parameters, Design Features and Operating Characteristics of the PRTR, page 213.

k. W. E. Shoupp et al., The Saxton Experimental Power Reactor, page 229.

l. P. E. Maldague, The VULCAIN Reactor, page 253.

3. V. Zajic et al., Design of an Experimental 10-Mw Homogeneous Reactor Fueled with Circulating Uranium Oxide Suspension in Light Water, *Proceedings of the Second United Nations International Conference on the Peaceful Uses of Atomic Energy, Geneva, 1958,* Vol. 9, p. 441, United Nations, New York, 1958.
4. Philadelphia Electric Co., Application of Philadelphia Electric Company for Construction Permit and Class 104 License, Part B, Preliminary Hazards Summary Report, Peach Bottom Atomic Power Station, Vol. I—Plant Description and Safeguards Analysis, USAEC Docket No. 50-171, Report NP-9115, July 1960.
5. AGR, *Nucl. Eng.,* 6(59): 151–158 (April 1961).
6. Kaiser Engineers and Allis-Chalmers Manufacturing Co., Experimental Gas Cooled Reactor; Preliminary Hazards Summary Report, USAEC Report ORO-196, May 1959.
7. L. J. Koch et al., Experimental Breeder Reactor II (EBR-II); Hazard Summary Report, USAEC Report ANL-5719, Argonne National Laboratory, May 1957.
8. Revised License Application, Technical Information and Hazards Summary Report, Section I: Reactor and Plant Design, Power Reactor Development Co., June 1961.
9. C. B. Graham et al., A Controlled Recirculation Boiling Water Reactor with Nuclear Superheater, *Proceedings of the Second United Nations International Conference on the Peaceful Uses of Atomic Energy, Geneva, 1958,* Vol. 9, p. 74, United Nations, New York, 1958.
10. A. S. Jameson, Design Features of the BONUS Nuclear Power Station, ASME Paper 61-WA-235, August 1961.
11. N. A. Dollezhal et al., Uranium-Graphite Reactor with Superheated High Pressure Steam, *Proceedings of the Second United Nations International Conference on the Peaceful Uses of Atomic Energy, Geneva, 1958,* Vol. 8, p. 398, United Nations, New York, 1958.

Index

Power Reactor Technology

Volume 5

Included in this issue is the index for Volume 5 of *Power Reactor Technology*. An index for this quarterly is prepared annually and appears in the final (Number 4) issue. A cumulative index for Volumes 4 to 6 will appear in the September 1963 issue. Here the bold numbers denote issues, and the other numbers denote pages.

D

E

F

G

H

I

K

L

M

N

O

P

R

S

T

U

V

W

X

Y

Z

NUCLEAR SCIENCE ABSTRACTS

The U. S. Atomic Energy Commission, Division of Technical Information, publishes *Nuclear Science Abstracts (NSA)*, a semimonthly journal containing abstracts of the literature of nuclear science and engineering.

NSA covers (1) research reports of the U. S. Atomic Energy Commission and its contractors; (2) research reports of government agencies, universities, and industrial research organizations on a world-wide basis; and (3) translations, patents, books, and articles appearing in technical and scientific journals.

Complete indexes covering subject, author, source, and report number are included in each issue. These are cumulated quarterly, semiannually, and annually providing a detailed and convenient key to the literature.

Availability of *NSA*

SALE *NSA* is available on subscription from the Superintendent of Documents, U. S. Government Printing Office, Washington 25, D. C., at $22.00 per year for the semimonthly abstract issues and $15.00 per year for the four cumulated-index issues. Subscriptions are postpaid within the United States, Canada, Mexico, and all Central and South American countries, except Argentina, Brazil, British and French Guiana, Surinam, and British Honduras. Subscribers in these Central and South American countries, and in all other countries throughout the world, should remit $27.50 per year for subscriptions to semimonthly abstract issues and $17.50 per year for the four cumulated-index issues.

EXCHANGE *NSA* is also available on an exchange basis to universities, research institutions, industrial firms, and publishers of scientific information. Inquiries should be directed to the Division of Technical Information Extension, U. S. Atomic Energy Commission, P. O. Box 62, Oak Ridge, Tennessee.

TECHNICAL PROGRESS REVIEWS may be purchased from Superintendent of Documents, U. S. Government Printing Office, Washington 25, D. C. for $2.00 per year for each subscription or for $0.55 per issue. The use of the coupon below will facilitate the handling of your order.

POSTAGE AND REMITTANCE: Postpaid within the United States, Canada, Mexico, and all Central and South American countries except as hereinafter noted. Add $0.50 per year, or $0.15 per single issue, for postage to all other countries, including Argentina, Brazil, British and French Guiana, Surinam, and British Honduras. Payment should be by check, money order, or document coupons, and MUST accompany order. Remittances from foreign countries should be made by international money order, or draft on an American bank, payable to the Superintendent of Documents, or by UNESCO book coupons.

order form

SUPERINTENDENT OF DOCUMENTS
U. S. GOVERNMENT PRINTING OFFICE
WASHINGTON 25, D. C.

Enclosed:
document coupons ☐ check ☐ money order ☐

Charge to Superintendent of Documents No._____

Please send a one-year subscription to

☐ REACTOR MATERIALS
☐ POWER REACTOR TECHNOLOGY
☐ NUCLEAR SAFETY
☐ REACTOR FUEL PROCESSING

(Each subscription $2.00 a year; $0.55 per issue.)

SUPERINTENDENT OF DOCUMENTS
U. S. GOVERNMENT PRINTING OFFICE
WASHINGTON 25, D. C.

(Print clearly)

Name_____

Street_____

City_____ Zone____ State_____